

DRAFT
for
Public Comment

GUIDELINE FOR FLUID MODELING
OF ATMOSPHERIC DIFFUSION

June 1979

U.S. ENVIRONMENTAL PROTECTION AGENCY
Office of Air, Noise, and Radiation
Office of Air Quality Planning and Standards
Research Triangle Park, North Carolina 27711

DRAFT

DRAFT

GUIDELINE FOR FLUID MODELING
OF ATMOSPHERIC DIFFUSION

by

William H. Snyder

Meteorology and Assessment Division
Environmental Sciences Research Laboratory

U.S. ENVIRONMENTAL PROTECTION AGENCY
Office of Air, Noise, and Radiation
Office of Air Quality Planning and Standards
Research Triangle Park, NC 27711

June 1979

DRAFT

DISCLAIMER

Mention of trade names or commercial products does not constitute endorsement or recommendation for use.

The author, William H. Snyder, is a physical scientist in the Meteorology and Assessment Division, Environmental Sciences Research Laboratory, U.S. Environmental Protection Agency, Research Triangle Park, North Carolina. He is on assignment from the National Oceanic and Atmospheric Administration, U.S. Department of Commerce.

PREFACE

The U.S. Environmental Protection Agency is charged by Congress with establishing and enforcing air pollution control standards to protect the public health and welfare. To accomplish its mission, it is essential to be able to describe and predict the transport and diffusion of pollutants in the atmosphere. Present mathematical models are not yet adequate for calculating concentrations of contaminants when the plume is affected by obstructions such as hills and buildings. Field programs to obtain adequate data are very expensive and time consuming. Small scale models immersed in the flow of wind tunnels and water channels, i.e., fluid models, can frequently be of use in simulating atmospheric transport and diffusion in a timely and relatively inexpensive manner.

It is the aim of this guideline to point out the capabilities and limitations of fluid modeling and to recommend standards to be followed in the conduct of such studies. The guideline is intended to be of use both to scientists and engineers involved in operating fluid modeling facilities and to air pollution control officials in evaluating the quality and credibility of the reports resulting from such studies.

The fundamental principles of fluid modeling are well-established, but when decisions must be made concerning a particular model study, the fundamental principles frequently do not provide specific guidance. There is a need for basic and systematic modeling studies to provide more specific guidance. This guideline will be periodically revised as more specific experience is gained, new techniques are developed, and old ones refined.

TABLE OF CONTENTS

	<u>Page</u>
PREFACE	iii
LIST OF FIGURES	vii
NOMENCLATURE.	x
ACKNOWLEDGEMENTS.	xiv
1. INTRODUCTION	1
2. FUNDAMENTAL PRINCIPLES	3
2.1 The Equations of Motion	3
2.2 The Dimensionless Parameters.	7
2.2.1 The Rossby Number.	8
2.2.2 The Reynolds Number.	14
2.2.2.1 The Laminar Flow Analogy.	14
2.2.2.2 Reynolds Number Independence.	17
2.2.2.3 Dissipation Scaling	27
2.2.3 The Peclet Number and the Reynolds-Schmidt Product	29
2.2.4 The Froude Number.	31
2.3 Boundary Conditions	34
2.3.1 General.	34
2.3.2 Jensen's Criterion and Fully Rough Flow.	36
2.3.3 Other Boundary Conditions.	38
2.4 Summary and Recommendations	39
3. PRACTICAL APPLICATIONS	41
3.1 Plume Rise and Diffusion	41
3.1.1 Near-Field Plume Behavior	43
3.1.2 Summary and Recommendations on Modeling Near Field	56
Plumes	57
3.1.3 Far-Field Plume Behavior	58
3.1.3.1 Ignoring the Minimum Reynolds Number.	60
3.1.3.2 Raising the Stack Height.	60
3.1.3.3 Distorting the Stack Diameter	63
3.1.4 Summary and Recommendations on Modeling Far-	65
Field Plumes	67
3.2 The Atmospheric Boundary Layer	68
3.2.1 Characteristics of the Atmospheric Boundary	80
Layer.	82
3.2.1.1 The Adiabatic Boundary Layer.	105
3.2.1.2 Summary of the Adiabatic Boundary	107
Layer Structure	120
3.2.1.3 The Diabatic Boundary Layer.	121
3.2.1.4 Summary of the Diabatic Boundary	124
Layer Structure.	124
3.2.2 Simulating the Adiabatic Boundary Layer	
3.2.3 Simulating the Diabatic Boundary Layer.	
3.2.4 Summary on Simulating the Atmospheric Boundary	
Layer	
3.3 Flow Around Buildings.	
3.3.1 Discussion.	

3.3.2	Recommendations	130
3.4	Flow Over Hilly Terrain.	133
3.4.1	Neutral Flow.	133
3.4.2	Stratified Flow	136
3.4.3	Recommendations	139
3.5	Relating Measurements to the Field	141
3.6	Averaging Times and Sampling Rates in the Laboratory	143
4.	THE HARDWARE.	147
4.1	Visual Observations.	147
4.2	Quantitative Measurements.	148
4.3	Producing Stratification	149
4.4	Air Versus Water	152
4.5	Summary.	154
5.	CONCLUDING REMARKS.	155
6.	REFERENCES.	158

LIST OF FIGURES

<u>NUMBER</u>	<u>TITLE</u>	<u>PAGE</u>
1	Schematic of diffusion in the Ekman Layer.....	9
2	Turbulent jets illustrating Reynolds number independence.....	18
3	Shadowgraphs of the jets shown in Figure 2.....	18
4	Filter function in Equation 2.12.....	20
5	Spectrum of wind speed at 100m.....	21
6	Form of turbulence spectrum.....	22
7	Change of spectrum with Reynolds number.....	23
8	Plume downwash in the wake of a stack.....	44
9	Variation of plume rise with Reynolds number.....	55
10	Laminar plume caused by low Reynolds number effluent.....	59
11	Effects of wind shear on the flow round a building.....	65
12	The depth of the adiabatic boundary layer according to the geostrophic drag law compared with other schemes.....	70
13	Typical wind profiles over uniform terrain in neutral flow.....	75
14	Variation of power law index, turbulence intensity, and Reynolds stress with roughness length in the adiabatic boundary layer.....	75
15	Shear stress distributions measured at various downwind positions in a wind tunnel boundary layer.....	76
16	Variation of longitudinal turbulence intensity with height under adiabatic conditions.....	78
17	Variation of integral length scale with height and roughness length.....	79

<u>NUMBER</u>	<u>TITLE</u>	<u>PAGE</u>
18	Empirical curves for spectra and cospectrum for neutral conditions.....	80
19	Typical nonadiabatic boundary layer depths from the geostrophic drag relations.....	89
20	Variation of friction velocity with stability from the geostrophic drag relations.....	89
21	Theoretical variation of the power-law exponent as a function of z_0 and L for z equal to 100m.....	91
22	Variation of the power-law exponent, averaged over layer from 10 to 100m, as a function of surface roughness and Pasquill stability class.....	92
23	Typical surface layer velocity profiles under nonadiabatic conditions.....	95
24	Typical temperature profiles in the surface layer.....	95
25	The relationship between Ri and z/L	98
26	Variation of ϕ_w and ϕ_θ with z/L in the surface layer.....	98
27	Variation of ϕ_u with z/L in the surface layer.....	100
28	Variation of ϕ_v with z/L	100
29	Universal spectral shape.....	101
30	Location of spectral peak for u, v, w and θ plotted against z/L	101
31	Upstream view of a long wind tunnel.....	109
32	Vortex generators and roughness in a short wind tunnel..	110
33	Schematic representation of the counter-jet technique...	111
34	Development of boundary layer in a long wind tunnel.....	111
35	Development of mean velocity profiles along the smooth floor of a long tunnel.....	114
36	Thickness parameters for boundary layer of Figure 35....	114

<u>NUMBER</u>	<u>TITLE</u>	<u>PAGE</u>
37	Spectrum of the longitudinal component of velocity.....	116
38	Velocity profiles above crest of triangular ridge indicating effect of blockage.....	131
39	Contour map of three-dimensional hill showing inappropriate choice of area to be modeled.....	138
40	Averaging time requirements for wind tunnel measurements.....	145

NOMENCLATURE

A	constant or area
B	constant
c	constant
C	constant or concentration
C_{uw}	cospectrum of Reynolds stress
d	zero-plane displacement
D	stack diameter
E	spectrum function
f	nondimensional frequency or arbitrary function
f_c	Coriolis parameter
f_m	nondimensional frequency corresponding to spectral peak
F_L	Lagrangian spectrum function
Fr	Froude number
g	acceleration due to gravity
G	geostrophic wind speed
h	hill, building or obstacle height
h_r	roughness element height
H	stack or building height
I	turbulence integral scale
k	von Karman constant
K	eddy viscosity or diffusivity
λ_B	buoyancy length scale
λ_m	momentum length scale
L	characteristic length scale or Monin-Obukhov length

Lu_{α}	integral length scale of longitudinal velocity in α - direction
Lw_{α}	integral length scale of vertical velocity in α -direction
n	frequency
p	pressure or power-law index
Pe	Peclet number
Q	pollutant emission flow rate
Re	Reynolds number
Ri	Richardson number
Ri_B	bulk Richardson number
Ri_f	flux Richardson number
Ro	Rossby number
S	spectrum function
Sc	Schmidt number
t	time
T	averaging time, time of travel from source, or fluid temperature
u	fluctuating velocity in x-direction (streamwise)
u_{*}	friction velocity
U	mean wind speed
U_i	instantaneous flow velocity in i-direction
v	fluctuating velocity in y-direction (cross-streamwise)
w	fluctuating velocity in z-direction (vertical)
W	effluent speed
x	Cartesian coordinate (streamwise)
x_i	coordinate in i-direction
y	Cartesian coordinate (cross-streamwise) or particle displacement

z	Cartesian coordinate (vertical)
z_0	roughness length
α	molecular mass diffusivity
β	blockage ratio (area)
δ	boundary layer depth
δ_{ij}	Kronecker's delta
δP	deviation of pressure from that in neutral atmosphere
δT	deviation of temperature from that in neutral atmosphere
Δh	plume rise
$\Delta \rho$	density difference
ϵ	dissipation rate of turbulence, roughness element height, or fractional error
ϵ_{ijk}	alternating tensor
η	Kolmogoroff microscale
θ	potential temperature
κ	thermal diffusivity or wavenumber
λ_m	wavelength corresponding to spectral peak
\bar{u}	stability parameter
ν	Kinematic viscosity
ξ	time separation
ρ	fluid density or Lagrangian autocorrelation function
σ	Standard deviation (x, y, z subscripts refer to puff or plume widths; u, v, w to velocity fluctuations)
τ	fluctuating temperature (deviation from mean)
u	Kolmogoroff velocity
ϕ_h	nondimensional potential temperature gradient
ϕ_H	nondimensional horizontal (u plus v) turbulence intensity

ϕ_m	nondimensional wind speed gradient
ϕ_u	nondimensional longitudinal turbulence intensity
ϕ_v	nondimensional lateral turbulence intensity
ϕ_w	nondimensional vertical turbulence intensity
ϕ_θ	nondimensional intensity of temperature fluctuations
χ	nondimensional concentration
ω	earth's rotation rate

Subscripts and Special Symbols

$()_a$	ambient value
$()_{eq}$	equilibrium value
$()_f$	field value
$()_g$	geostrophic value
$()_L$	Lagrangian value
$()_m$	model value
$()_{mx}$	maximum value
$()_o$	value of quantity in neutral atmosphere, except as noted
$()_p$	prototype value
$()_r$	reference quantity
$()_s$	stack value
$()_x$	value of quantity in x-direction
$()_y$	value of quantity in y-direction
$()_z$	value of quantity in z-direction
$()_\infty$	freestream value
$()'$	nondimensional quantity
$\overline{(\)}$	average value
$\underline{(\)}$	vector quantity

1. INTRODUCTION

The present mathematical models of turbulent diffusion in the lower atmospheric layer tend to ignore the fundamental fluid-dynamical processes involved in the dispersion of materials. This results from the fact that the memory size of the latest computer is far too small to keep track of the large number of "eddies" in a turbulent flow. Corrsin (1961a), in speculating on the future role of large computing machines in following the consequences of the Navier-Stokes equations under random initial conditions, estimated a required memory size of $\sim 10^{13}$ bits, then asked if "the foregoing estimate is enough to suggest the use of analog instead of digital computation; in particular, how about an analog consisting of a tank of water?" (emphasis added). In spite of the tremendous advances in computer memories in the past two decades, Corrsin's remark is still appropriate.

Fluid models of various aspects of atmospheric motion have been described in the literature many times. The necessity of studying the dispersion of atmospheric pollutants, especially in urban areas, has further directed thoughts of meteorologists towards fluid modeling.

Many factors affect the dispersion of pollutants in the atmosphere; thermal effects, the topography, the rotation of the Earth, etc. Fluid modeling studies are desirable mostly because essential variables can be controlled at will, and the time and expense are greatly reduced from that required in full-scale studies. It is not usual, however, for all the factors influencing atmospheric dispersion to be included in a model. Normally, the similarity cri-

teria are conflicting in some sense; it may be necessary to model one physical process at the expense of not being able to model another.

For correct modeling, certain nondimensional parameters in the prototype must be duplicated in the model. Almost invariably, duplication of these nondimensional parameters is impractical or impossible. Hence, a decision must be made as to which parameters are dominant. The less important ones must be ignored. This decision will generally depend upon the scale in which the investigator is interested. For example, when studying the upper air flow above a city, the waffle-like topography may be treated as surface roughness. The heat island effect may be modeled by using a heated plate. If the city is large enough, Coriolis forces may be important. If, however, the interest is in dispersion in the immediate vicinity of buildings, the topography cannot be treated as surface roughness. The heat-island effect would require a detailed distribution of heat sources, and Coriolis forces could be ignored because the aerodynamic effects of the flow around the buildings would dominate.

Chapter 2 reviews the fundamental principles for fluid modeling relevant to air pollution meteorology and evaluates the usefulness of such models from both scientific and engineering viewpoints. Because many detailed decisions must be made during the design and execution of each model study, and because the fundamental principles frequently do not provide enough guidance, discussions of the details of the most common types of modeling problems are provided in Chapter 3. Air and water are most commonly used as media for the simulation of atmospheric motions. The potentials of both of these fluids are reviewed in Chapter 4.

2. FUNDAMENTAL PRINCIPLES

A discussion of the fundamental principles for fluid modeling of atmospheric phenomena is presented here. The dynamics of the flow in the fluid model must accurately simulate those in the field. Similarity criteria are derived through analysis of the equations of motion. This analysis shows that various nondimensional parameters must be matched between the model and field flows. The significance of each of these parameters is discussed in detail. Additionally, effects in the field upstream of the modeled area must be accounted for in the fluid model by developing appropriate boundary conditions. Hence, some discussion of boundary conditions is included at the end of the chapter.

2.1 THE EQUATIONS OF MOTION

The equations of motion are the starting point for the similarity analysis. With the Earth as a reference frame rotating at an angular velocity Ω , the fluid motion is described by the following equations (Lumley and Panofsky, 1964):

Conservation of Momentum

$$\frac{\partial U_i}{\partial t} + \frac{U_j \partial U_i}{\partial x_j} + 2\varepsilon_{ijk} U_k \Omega_j = -\frac{1}{\rho_0} \frac{\partial \delta P}{\partial x_i} + \frac{g}{T_0} \delta T \delta_{3i} + \frac{\nu \partial^2 U_i}{\partial x_k \partial x_k} \quad (2.1)$$

Continuity

$$\frac{\partial U_i}{\partial x_i} = 0 \quad (2.2)$$

Energy

$$\frac{\partial \delta T}{\partial t} + \frac{\partial \delta T}{\partial x_i} U_i = \kappa \frac{\partial^2 \delta T}{\partial x_i \partial x_i} \quad (i = 1, 2, 3) \quad (2.3)$$

where the x_3 axis is taken vertically upward, U_i is instantaneous velocity, δP and δT are deviations of pressure and temperature from those of a neutral atmosphere, ρ_0 and T_0 are density and temperature of a neutral atmosphere (functions of height), ν is kinematic viscosity, κ is thermal diffusivity, ε_{ijk} is the alternating tensor (if any two of the indices i, j, k , are equal,

the component is 0; if i , j , and k are all unequal and are in cyclic order, the component is +1; if not in cyclic order, the component is -1), δ_{ij} is Kroneker's delta ($\delta_{ij} = 1$ if the two indices are equal and 0 if unequal), and the summation convention is used here (whenever a suffix is repeated in a term, it is to be given all possible values and the terms are to be added for all).

Equation 2.1 shows that the vector sum of the forces per unit mass acting on a parcel of fluid must balance the acceleration of that parcel. The first term represents the unsteady acceleration of the fluid element. The second represents the advective acceleration. The remainder are, respectively, the Coriolis force, the pressure gradient force, the buoyancy force, and the frictional force per unit mass.

Equation 2.2 is, of course, the continuity equation, which expresses the conservation of mass in an incompressible fluid. Equation 2.3 expresses the conservation of thermal energy; the time rate of change of thermal energy (first term) equals the convection (or advection) of energy by the flow (second term) plus the conduction of energy (third term).

The assumptions made in deriving the above equations are:

- (1) The atmosphere is composed of a perfect gas of constant composition,
- (2) the deviations of pressure, temperature, and density are small compared with the neutral (adiabatic) values,
- (3) the density is independent of the fluctuating pressure (small Mach number),
- (4) variations of ν and κ are negligible,
- (5) the generation of heat through viscous stresses is negligible, and
- (6) there are no sources of any kind.

The second step in the similarity analysis is to nondimensionalize the

equations of motion through the use of appropriate reference quantities.

Reference quantities assumed to be supplied through the boundary conditions are: L , length; U_R , velocity; ρ_R , density; δT_R , temperature deviation; and Ω_R , angular velocity. The dimensionless variables are

$$\begin{aligned} x'_i &= \frac{x_i}{L} & U'_i &= \frac{U_i}{U_R} \\ t' &= \frac{U_R}{L} t & \varrho' &= \frac{\varrho_0}{\varrho_R} \\ \delta P' &= \frac{\delta P}{\varrho_R U_R^2} & \delta T' &= \frac{\delta T}{\delta T_R} \\ \Omega'_j &= \frac{\Omega_j}{\Omega_R} \end{aligned}$$

Using these definitions to nondimensionalize Eqs. 2.1 to 2.3 yields

$$\frac{\partial U'_i}{\partial t'} + U'_i \frac{\partial U'_i}{\partial x'_j} + \frac{2}{Ro} \varepsilon_{ijk} U'_i \Omega'_j = - \frac{1}{\varrho'} \frac{\partial \delta P'}{\partial x'_i} + \frac{1}{Fr^2} \delta T' \delta_{3i} + \frac{1}{Re} \frac{\partial^2 U'_i}{\partial x'_j \partial x'_j} \quad (2.4)$$

$$\frac{\partial U'_i}{\partial x'_i} = 0 \quad (2.5)$$

and

$$\frac{\partial \delta T'}{\partial t'} + U'_i \frac{\partial \delta T'}{\partial x'_i} = \frac{1}{Pe} \frac{\partial^2 \delta T'}{\partial x'_i \partial x'_i} \quad (2.6)$$

where $Ro \equiv U_R / L \Omega_R$ is the Rossby number,

$Fr \equiv U_R / (gL \delta T_R / T_0)^{1/2}$ is the densimetric Froude number,

$Re \equiv U_R L / \nu$ is the Reynolds number,

and $Pe \equiv U_R L / \kappa$ is the Peclet number.

Concerning the philosophy of modeling, Eqs. 2.4 to 2.6 with appropriate boundary conditions completely determine the flow. The question of uniqueness

of solutions of the Navier-Stokes equations is avoided here (see Lumley, 1970). These five equations contain five unknowns, U_1^i , U_2^i , U_3^i , ρ^i and T^i , so that, in principle, their solutions may be determined. Any two flows within the same general category (i.e., in so far as they are governed by the above equations) will be similar if and only if they are described by identical solutions to the given set of Eqs. 2.4 to 2.6. Solutions to this set of equations will be identical if and only if the coefficients Ro , Fr , Re , and Pe and the nondimensional boundary conditions are identical (Birkhoff, 1960; Batchelor, 1963). The final statement, then, as it applies to laboratory modeling of atmospheric motions becomes: any atmospheric flow which can be described by Eqs. 2.4 to 2.6 may be modeled by any other flow which can also be described by the same set of equations, provided that the Rossby, Froude, Reynolds, and Peclet numbers are identical, and provided that the nondimensional boundary conditions (to be discussed later) are identical. Equations 2.4 to 2.6 apply to both laminar and turbulent flows. It is not necessary to determine a priori whether the flow is laminar or turbulent.

Thus far, only the requirements for similarity of flow patterns have been discussed. The dispersion of a pollutant within the system will now be considered. The contaminant is assumed to be completely passive in the sense that it is without effect on the governing equation and undergoes no transformations in the fluid.

Prediction of the dispersion of this contaminant in space and time is desired. Since a passive contaminant is specified, its dynamic behavior must be the same as that of the air; hence, the similarity criteria describing its dynamic behavior have already been specified. The additional parameter, however, remains to be specified. This is obtained through nondimensionalization of the molecular diffusion equation:

$$\frac{\partial y}{\partial t} + U \frac{\partial y}{\partial x} = \alpha \frac{\partial^2 y}{\partial x^2} \quad (2.7)$$

where y represents the instantaneous concentration and α is the molecular mass diffusivity. Nondimensionalization of this equation requires $x' = x/L_0$, and yields

$$\frac{\partial y}{\partial t} + U \frac{\partial y}{\partial x'} = \frac{1}{ReSc} \frac{\partial^2 y}{\partial x'^2} \quad (2.8)$$

where $Sc = \nu/\alpha$ is the Schmidt number.

To summarize, Equations 2.4 to 2.6 and 2.8 form a complete set of equations which govern the dispersion of a dynamically passive contaminant in the atmosphere and in a model. If and only if the nondimensional coefficients in these equations and the boundary conditions are identical, the dispersion of the contaminant in a model will be identical to that in the atmosphere.

2.2 THE DIMENSIONLESS PARAMETERS

It is generally impossible to simultaneously match all of the dimensionless parameters when the ratio of the length scales (i.e., prototype to model) is greater than about 10. As an example, consider the Reynolds and Froude numbers

$$Re = \frac{U_\infty L}{\nu}, \quad Fr = \frac{U_\infty}{\sqrt{gL_0 T_0/T_\infty}}$$

If one models in a wind tunnel, the values of ν and g are identical to values in the atmosphere, and T_0 is roughly the same. Thus, decreasing the length scale by 10 requires an increase of 10 in the velocity to satisfy the Reynolds number criterion. Considering the Froude number, if decreased by 10 and U_∞

increased by 10 implies that δT_R must be increased by a factor of 1000, which is, of course, highly impractical. In general, a length scale reduction much greater than 10 is desired.

A factor of 15 in the Reynolds number may be gained by modeling with water as the fluid medium, but then the Peclet number and Reynolds number criteria cannot be satisfied simultaneously. The Peclet number can be written as the product of the Reynolds number and the Prandtl number. Even if the Reynolds number can be matched, the Prandtl number cannot, because it is a fluid property and differs by a factor of 10 between air and water. The Prandtl number is not, however, a critical parameter (see later discussion).

Many examples of this type can be shown. All modelers recognize that rigorous modeling with significant reduction in scale is impossible. Under certain circumstances, however, some of the criteria may be relaxed. In the first example, if the atmospheric flow were of neutral stability, the Froude number would be infinite. This is easily accomplished by making the model flow isothermal. (The vertical dimension of a typical wind tunnel is small enough that the temperature differences between isothermal and strictly neutral conditions is extremely small. Hence, "neutral" and "isothermal" are used interchangeably when referring to wind tunnel flows.) Hence, both Reynolds number and Froude number criteria may be satisfied simultaneously.

It is instructive now to examine the nondimensional parameters in detail.

2.2.1 The Rossby Number, $U_R/L\Omega_R$

The Rossby number represents the ratio of advective or local accelerations (U_R^2/L) to Coriolis accelerations (proportional to $U_R\Omega_R$). Local accel-

erations may result from unsteadiness or non-uniformities in the velocity field. Coriolis accelerations, of course, result from the fact that the earth rotates. The importance of the Rossby number criterion for modeling of atmospheric diffusion is described as follows.

In the planetary boundary layer, or "Ekman" layer, which extends from the Earth's surface to a height of one to two kilometers, the combined effects of the Coriolis acceleration, the pressure gradient, and surface friction cause the wind vector to change direction or spiral with increasing height from the surface. The geostrophic wind is parallel to the isobars, whereas the surface wind blows to the left across the isobars, typically at an angle of 20° to 40° . The maximum rate of change of wind direction with height occurs at the surface.

Imagine a cloud of material released at ground level in an Ekman layer. Its transport and dispersion are illustrated in Figure 1. The surface wind is directly into the paper. The crosswind velocity profile is as shown. The ini-

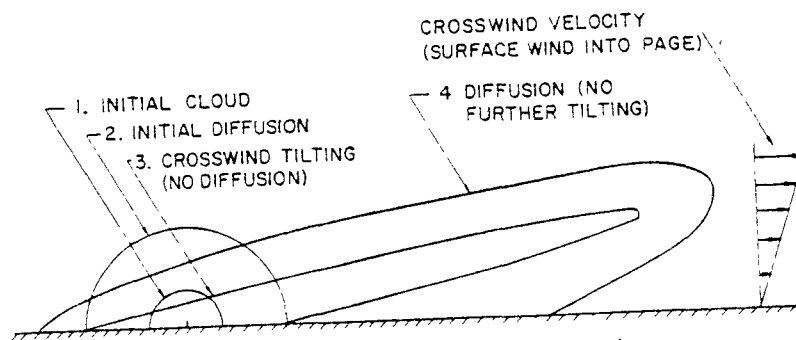


Fig. 1. Schematic of diffusion in the Ekman layer.

tial cloud (Step 1), being small, is transported mainly by the surface wind. Its size increases mainly by turbulent dispersion (Step 2). At this point, the upper levels of the cloud will be advected in a different direction from that of the surface wind. Conceptually, the tilting of the cloud is imagined to occur independently of diffusion, whereas, in reality, tilting and diffu-

sion occur simultaneously. The cloud is tilted by the crosswind (Step 3), and the simultaneous turbulent diffusion (Step 4) increases the width of the cloud at ground level over what it would have been by turbulent diffusion alone. In fact, the center of gravity of a slice of the cloud at ground level will not follow the surface wind.

The Rossby number describes the relative importance of the Coriolis accelerations when compared with advective, or local accelerations. If the Rossby number is large, Coriolis accelerations are small, so that enhanced dispersion due to directional wind shear may be ignored. Equivalently, a near infinite Rossby number is automatically matched in a model.

To date, all wind and water tunnel modelers have assumed the Rossby number to be large and discarded the terms involving it in the equations of motion, or, equivalently, ignored that particular parameter as a criterion for modeling. Cermak et al. (1966) made the rather broad statement that, provided the typical length in the horizontal plane is less than 150 km, the Rossby number can generally be eliminated from the requirements for similarity. Hidy (1967) made similar statements. McVehil et al. (1967) ignored the Rossby number when modeling atmospheric motions on the scale of one kilometer in the vertical and several tens of kilometers in the horizontal. Ukeguchi et al. (1967) claimed that the cut-off was 40 to 50 km. Mery (1969) claimed that the Coriolis force may be neglected if the characteristic length is less than 15 km. The present discussion shows that the cut-off point is on the order of 5 km for modeling diffusion under appropriate atmospheric conditions (i.e., neutral or stable conditions in relatively flat terrain).

The criterion is based on a length scale rather than on the Rossby number itself because the angular rotation of the Earth, ω_0 , is a constant

($Ro = U_R/L_0^{\Omega}$), and the characteristic velocity of the atmospheric flow does not vary by more than an order of magnitude, so that the characteristic length is primarily responsible for determining the Rossby number.

Several papers have examined the effect of crosswind shear on dispersion. Pasquill (1962a) measured horizontal spread both in the longitudinal and crosswind directions for medium-range dispersion. His data, however, were insufficient to allow firm conclusions to be drawn about the relative importance of turbulence and shear in promoting horizontal spread.

Corrsin (1953) showed that $\sigma_x \propto t^{3/2}$ in a uniform shear flow (σ_x is streamwise puff width), by considering Lagrangian particle motions. Saffman (1962) applied the concentration-moment (von K rm n integral) method to the classical diffusion equation (he did not consider turning of wind with height, although similar considerations are involved). For a semi-infinite flow, ground-level source (puff), and linear velocity profile, he also found $\sigma_x \propto t^{3/2}$. For a completely unbounded flow, Smith (1965) showed that $\sigma_x \propto t^{3/2}$, using statistical techniques.

Since the contribution to the spread from the turbulence alone is $\sigma_x \propto t^{1/2}$, it is clear that the shear effect will eventually dominate the dispersion process. These solutions are valid only for constant diffusivity and large times; they do not provide any indication of the early development. Hence, they are of no help in determining at what distance the shear effect becomes dominant.

Tyldesley and Wallington (1965) used a numerical scheme and an analog computer to study the effect of crosswind shear on dispersion. They used an 8-step Ekman spiral except with the surface wind $22\frac{1}{2}^\circ$ from the geostrophic wind. They claimed that the 3/2 power law does not apply because the cross-

wind shear is not constant with height. Their estimates indicate that the wind shear becomes dominant around 4 to 6 km from the source. For much larger distances, the turbulence will again dominate because the shear goes to zero for large heights.

Högström (1964) and Smith (1965) used statistical approaches to the crosswind shear problem. A homogeneous field of turbulence, a mean wind speed which was constant with height, and a crosswind component which varied linearly with height were assumed. They obtained expressions valid for all times of travel, but did not estimate times or distances at which the shear would dominate.

Csanady (1969) attempted to confirm analytically the numerical results of Tyldesley and Wallington. Because of analytical difficulties, he confined his investigation to a slice at ground level of a cloud released from a source at ground level. He found that, indeed, the centroid of the slice at ground level did not follow the surface wind. By the time the cloud occupied 1/3 of the Ekman layer (~600m), its distance from a line parallel to the surface wind was of order 10 km. The contribution to the spread from the turbulence and from the shear were found to be equal at one kilometer from the source. He estimated that, in the actual atmosphere, the shear effect would overtake the turbulence effect at 3 to 4 km from the source. He showed that for small times, $\sigma_y \propto t^{1/2}$ (i.e., turbulent diffusion dominates). For intermediate times, $\sigma_y \propto t^{3/2}$ (i.e., shear-induced diffusion dominates). For large times, $\sigma_y \propto t^{1/2}$ again, because the cloud height is the same as the Ekman layer depth, and the flow is, in effect, bounded (σ_y is cross-streamwise puff width).

Thus far, no diffusion experiments have been reported that have been specifically designed to examine the relative effects of turbulence and shear,

but Pasquill (1969) reexamined two independent studies which contain information of interest in this connection. He looked at Högström's (1964) data on the behavior of smoke puffs released from an elevated source under neutral and stable atmospheric conditions. The data for the crosswind spread show the onset of a more rapid than linear growth at 2.5 km. These data are somewhat misleading because they indicate the total puff width rather than the width at a given level. Hence, they indicate the bodily distortion (tilting) of the puff but do not show directly the enhanced spread at a given level. In accounting for this, Pasquill concluded that the enhanced spread at a given level as a result of shear becomes important around 5 km from the source.

In analyzing the Hanford data of Fuquay, Simpson, and Hinds (1964) (continuous ground release of a tracer), Pasquill concluded that the effect on spread at ground level under stable atmospheric conditions appeared to have set in significantly at about 12.8 km. He summarized:

...a bodily crosswind distortion of the plume from a point source (either elevated or on the ground) sets in between 2 and 3 km. However, the form of the crosswind growth curves suggests strongly that the contribution of the distortion to the spread at a given level was not of practical importance below about 5 km in the case of the elevated source and about 12 km in the case of the ground level source. Thereafter the implication is that the shear contribution is dominant.

It is evident that, if it is desired to model diffusion in a prototype with a length scale greater than about 5 km, under neutral or stable atmospheric conditions, in relatively flat terrain, the Rossby criterion should be considered. One encouraging note is that Harris' (1962) high wind (neutral stability) results show no systematic variation in wind direction with height over flat terrain up to $z=200\text{m}$.

2.2.2 The Reynolds Number, $U_R L / \nu$

The physical significance of the Reynolds number becomes apparent by noting that it measures the ratio of inertial forces (U_R^2/L) to viscous or frictional forces ($\nu U_R/L^2$) in the equations of motion. It imposes very strong limitations on rigorous simulation; it is the most abused criterion in models of atmospheric flows. The scale reductions commonly used result in model Reynolds numbers three to four orders of magnitude smaller than found in the atmosphere. The viscous forces are thus relatively more important in the model than they are in the prototype. If strict adherence to the Reynolds number criterion were required, no atmospheric flows could be modeled.

Various arguments have been presented which attempt to justify the use of smaller Reynolds numbers in a model (i.e., to justify the neglect of the Reynolds number criterion). These arguments may be divided into three general categories; the laminar flow analogy, Reynolds number independence, and dissipation scaling. Each of these is discussed below.

2.2.2.1 The Laminar Flow Analogy

Abe (1941) was the first to introduce this concept. If the instantaneous velocity, temperature, and pressure in Eq. 2.1 are written as the sum of mean and fluctuating parts ($U_i = \bar{U}_i + u_i$), and the equation is then averaged, the following equation is obtained (after minor manipulation):

$$\frac{\partial \bar{U}_i}{\partial t} + \bar{U}_j \frac{\partial \bar{U}_i}{\partial x_j} + 2\varepsilon_{ijk} \bar{\Omega}_j \bar{U}_k = -\frac{1}{\rho_0} \frac{\partial \bar{\delta P}}{\partial x_i} + \frac{g}{T_0} \delta \bar{T} \delta_{3i} + \nu \frac{\partial^2 \bar{U}_i}{\partial x_j \partial x_j} + \frac{\partial \overline{u_i u_j}}{\partial x_j}. \quad (2.9)$$

An eddy viscosity is defined to relate the Reynolds stress to the mean velocity, $-\overline{(u_i u_j)} = K(\partial \bar{U}_i / \partial x_j)$. The nondimensional equation is then

$$\frac{\partial \bar{U}_i'}{\partial t'} + U_j' \frac{\partial \bar{U}_i'}{\partial x_j'} + \frac{2}{Ro} \epsilon_{ijk} \bar{U}_k' \Omega_j' = -\frac{1}{\rho'} \frac{\partial \bar{P}'}{\partial x_i'} - \frac{1}{Fr^2} \bar{\delta T}' \delta_{3i} - \frac{1}{Re} \frac{\partial^2 \bar{U}_i'}{\partial x_j' \partial x_j'} - \frac{1}{Re_K} \frac{\partial^2 \bar{U}_i'}{\partial x_j' \partial x_j'} \quad (2.10)$$

where $Re_K = U_R L / K$ is called a "turbulent" Reynolds number. Now if K/ν is of order 10^3 , the term containing the turbulent Reynolds number is much larger than the term containing the ordinary Reynolds number. If the nondimensional equation for laminar flow were now written, it would appear identical to Equation 2.10, with the exception that the term containing the turbulent Reynolds number would be absent. Assuming that the prototype flow is turbulent and that the model flow is laminar, the scale ratio is of the order $1:10^3$, and U_R is the same order of magnitude in model and prototype, then,

$$(Re)_{\text{model}} \approx (Re_K)_{\text{prototype}}.$$

Hence, similarity may be established by modeling a turbulent prototype flow by a laminar model flow when the scale ratio is of the order of $1:10^3$, all else being equal in a nondimensional sense.

This scheme is fundamentally incorrect for the same reasons that K-theories are fundamentally incorrect. Eddy sizes scale with distance from the ground, with the size of the obstacle, or, generally, with the scale of substantial variation in the mean flow. Turbulent diffusion is a flow property, not a fluid property. The laminar flow analogy assumes unrealistically that eddy sizes are very small compared with the scale of variation of the property being diffused. Perhaps under very restrictive conditions, when there exists a small upper bound to the sizes of atmospheric eddies (i.e., extremely stable conditions), there may be some realistic modeling possibilities, but

the chances of that being the case without any doubt are small.

Perhaps qualitative use of this technique is the answer to those (non-diffusive) problems where the spread of a contaminant is controlled primarily by advective transport (mean flow). Two previous experimental studies give guidance here. Abe (1941) attempted to model the flow around Mt. Fuji, Japan, at a scale ratio of 1:50,000 using this analogy. Cermak et al. (1966) claimed that "the model flow patterns obtained were not even qualitatively close to those observed in actual field tests" (the original paper was not available for verification). Cermak and Peterka (1966) made a second study of the wind field over Point Arguello, California (a peninsula jutting into the Pacific Ocean). Cermak et al. (1966) claimed that:

Comparison of the surface flow directions and smoke traces for neutral and inversion flows established an excellent agreement in wind flow patterns over the Point Arguello area for flows approaching from the northwest.

After careful study of the figures presented, the present author is not convinced of the validity of this statement. Large scatter of concentration levels in the field data prevented firm conclusions concerning diffusion characteristics of the two flow fields. Rather surprisingly, a logarithmic plot of concentration versus downwind distance showed that rates of decrease of concentration with distance were grossly similar in model and prototype. In view of the dissimilarity in surface flow patterns, this agreement is regarded as fortuitous.

Since kinematic viscosity is a fluid property, it is not an adjustable parameter. Turbulent eddy viscosity varies strongly with height, stability, and direction. This severely limits the use of this laminar-turbulent analogy for fluid modeling. Mathematical modeling techniques are superior to fluid modeling techniques in the sense that K is a controllable variable in the math-

ematical model (e.g., a function of height, stability and direction). The quantity K is not a controllable variable in this sense in the fluid model.

2.2.2.2 Reynolds Number Independence

This approach is based on the hypothesis that in the absence of thermal and Coriolis effects and for a specified flow system, whose boundary conditions are expressed nondimensionally in terms of a characteristic length L and velocity U_p , the turbulent flow structure is similar at all sufficiently high Reynolds numbers (Townsend, 1956). Most nondimensional mean-value functions depend only upon nondimensional space and time variables and not upon the Reynolds number, provided it is large enough. There are two exceptions: (1) those functions which are concerned with the very small-scale structure of the turbulence (i.e., those responsible for the viscous dissipation of energy), and (2) the flow very close to the boundary (the no-slip condition is a viscous constraint). The viscosity has very little effect on the main structure of the turbulence in the interior of the flow; its major effect is limited to setting the size of the small eddies which convert mechanical energy to heat. One way to avoid the effects of viscosity at the boundaries is to roughen the surface of the model (see discussion of Boundary Conditions).

This hypothesis of Reynolds number independence was put forth by Townsend (1956). He called it Reynolds number similarity. There now exists a large amount of experimental evidence supporting this principle. Townsend stated it simply: "geometrically similar flows are similar at all sufficiently high Reynolds numbers." This is an extremely fortunate phenomenon from the standpoint of modeling. The gross structure of the turbulence is similar over a very wide range of Reynolds numbers. This concept is used by nearly all mod-

elers. It is graphically illustrated in Figures 2 and 3. The two jets shown in each figure are identical in every way except for the viscosity of the fluids, and therefore the Reynolds numbers, which differ by a factor of 50.

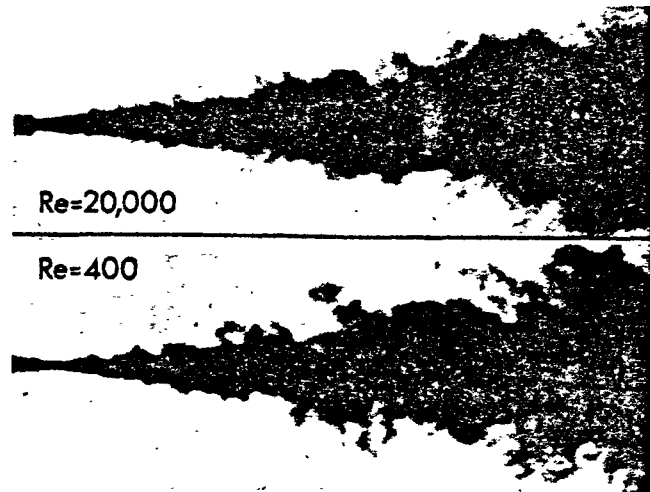


Figure 2. Turbulent jets showing that the Reynolds number does not much affect the large scale structure, so long as it is sufficiently large that the jet is indeed turbulent. The upper jet has a Reynolds number 50 times that of the lower. (Courtesy of National Committee for Fluid Mechanics Films and R.W. Stewart).

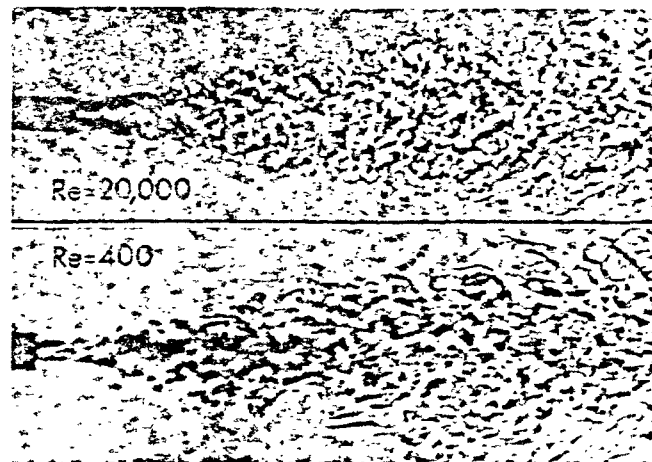


Figure 3. Shadowgraphs of the jets shown in Fig. 2. Note how much finer grained is the structure in the high Reynolds number jet than that in the low Reynolds number jet. (Courtesy of National Committee for Fluid Mechanics Films and R. W. Stewart).

To obtain a better idea of the contributions to dispersion from the various scales of turbulence, it is convenient to examine the spectral form of the Taylor (1921) diffusion equation. Taylor's expression for the mean-square fluid particle displacement in a stationary homogeneous turbulence is given by

$$\overline{y^2(T)} = 2\overline{v^2} \int_0^T \int_0^t \rho(\xi) d\xi dt \quad (2.11)$$

where $\overline{v^2}$ is the variance of particle velocities, $\rho(\xi) \equiv \overline{v(t)v(t+\xi)}$ is the Lagrangian autocorrelation of particle velocities with time separation ξ , and T is the time of travel from the source. Kampé de Fériet (1939) and Batchelor (1949) applied the Fourier-transform between the autocorrelation and the corresponding Lagrangian spectrum function, $F_L(n)$,

$$F_L(n) \equiv \int_0^T \rho(t) \cos(2\pi nt) dt,$$

to obtain

$$\overline{y^2(T)} = \overline{v^2} T^2 \int_0^\infty F_L(n) \left[\frac{\sin(\pi n T)}{\pi n T} \right]^2 dn, \quad (2.12)$$

where n is the frequency. The squared term under the integral, illustrated in Figure 4, is very small when $n > 1/T$ and virtually unity when $n < 0.1/T$. Thus, for very small travel times, the filter function is virtually unity, so that all scales of turbulence contribute to the dispersion with the same weight that they contribute to the total energy. For larger travel times, the larger scales of turbulence progressively dominate the dispersion process. This means that eddies with diameter smaller than about one-tenth the plume width do not significantly affect the spread of the plume; only those eddies with diameter about the same size as the width of the plume and larger substantial-

ly increase its width.

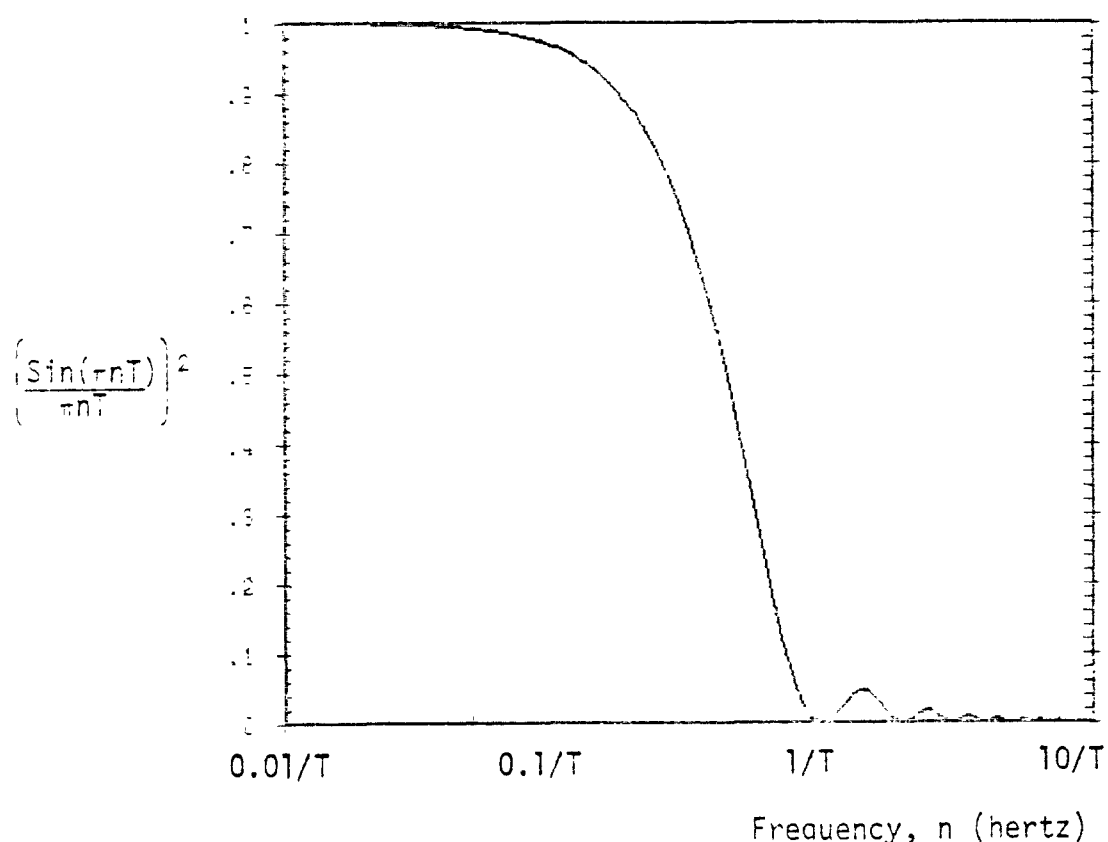


Figure 4. Filter function in Eq. 2.12: As the travel time T increases, the contribution of small scale (high frequency) motions to dispersion diminishes rapidly.

It may be helpful here to examine typical energy spectra so that 1) "weather" and "turbulence" may be defined as separate and distinct entities, and 2) the influence of Reynolds number upon the shape of the spectrum will be more easily understood.

Figure 5 shows a spectrum

$$S_u(n) = 4 \int_0^\infty \overline{u(t) u(t+t')} \cos 2\pi n t' dt'$$

of wind speed near the ground from a study by Van der Hoven (1957). It is evident that wind effects can be separated roughly into two scales of motion:

large scale (low frequency) motions lasting longer than a few hours, and small scale (high frequency) motions that last considerably less than an hour. The large scale motions are due to diurnal fluctuations,

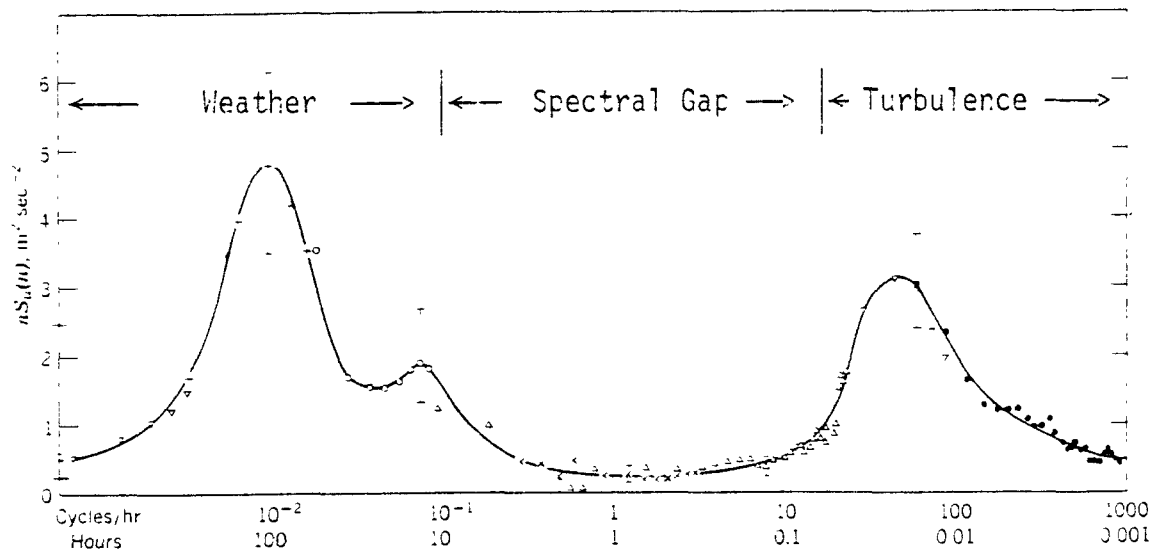


Figure 5. Spectrum of wind speed at 100m, from a study by Van der Hoven (1957).

pressure systems, passage of frontal systems, seasonal and annual changes, etc., and are generally called weather. The small scale motions are associated with roughness elements, topographical features, and differential surface heating in the boundary layer and are called turbulence. The spectral gap (low energy region) separating weather from turbulence is a very fortunate occurrence, both from an analytical viewpoint and from a fluid modeling viewpoint. Because of this gap, it is possible to consider these regions independently and to execute proper mathematical operations to determine the statistical properties of the two regions. It is the smaller scales of motion, the turbulence, which are simulated in a fluid modeling facility. Steady state averages of fluctuating quantities in the model atmosphere correspond to approximately one-hour time periods in the real atmosphere (during which the mean wind is steady in speed and direction). From results of model ex-

periments conducted at different mean wind speeds and directions, the low frequency contribution can be constructed analytically from distribution charts of wind speed and direction (wind roses).

Figure 6 is a definition sketch of a turbulent energy spectrum from Wyngaard (1973), which will be helpful in understanding future discussions. (It is not intended here to present a detailed discussion of turbulent energy spectra. Only those features of direct interest will be covered. The ardent student should consult Batchelor, 1953a, Hinze, 1975, or Tennekes and Lumley, 1972.) In Figure 6, we have used wave number κ instead of frequency n so that

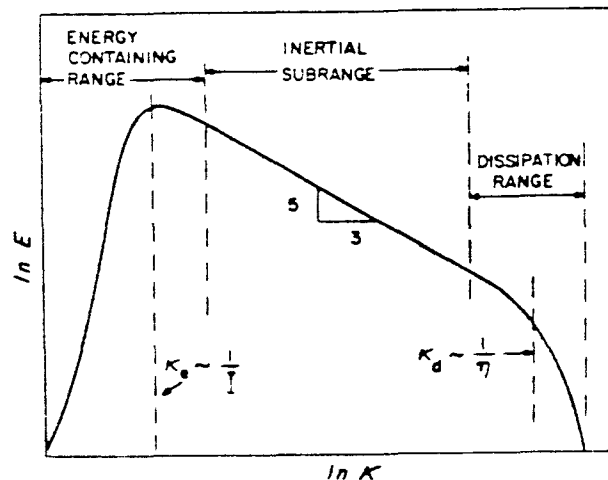


Fig. 6. Form of Turbulence spectrum.

we will be more inclined to think in terms of length scales. The relationship is $\kappa = 2\pi n / \bar{U}$. (The spectrum function S_u in Figure 5 is one-dimensional, whereas that of Figure 6, E , is three-dimensional. The differences need not concern us here.) Note that an integral scale I and a microscale η are defined. The integral scale may be thought of as the characteristic size of the

energy containing eddies and is located at the peak of the three-dimensional spectrum. The microscale may be thought of as characteristic of the smallest eddies in a turbulent flow. They are the ones primarily responsible for the dissipation of turbulent kinetic energy. The ratio of the integral scale to the micro scale, then, is a measure of the width of the spectrum or the range of eddy sizes in the turbulence.

A pertinent question at this point is: how does the spectrum of turbulence in a simulated atmospheric boundary layer in, say, a wind tunnel compare with that in the real atmospheric boundary layer?

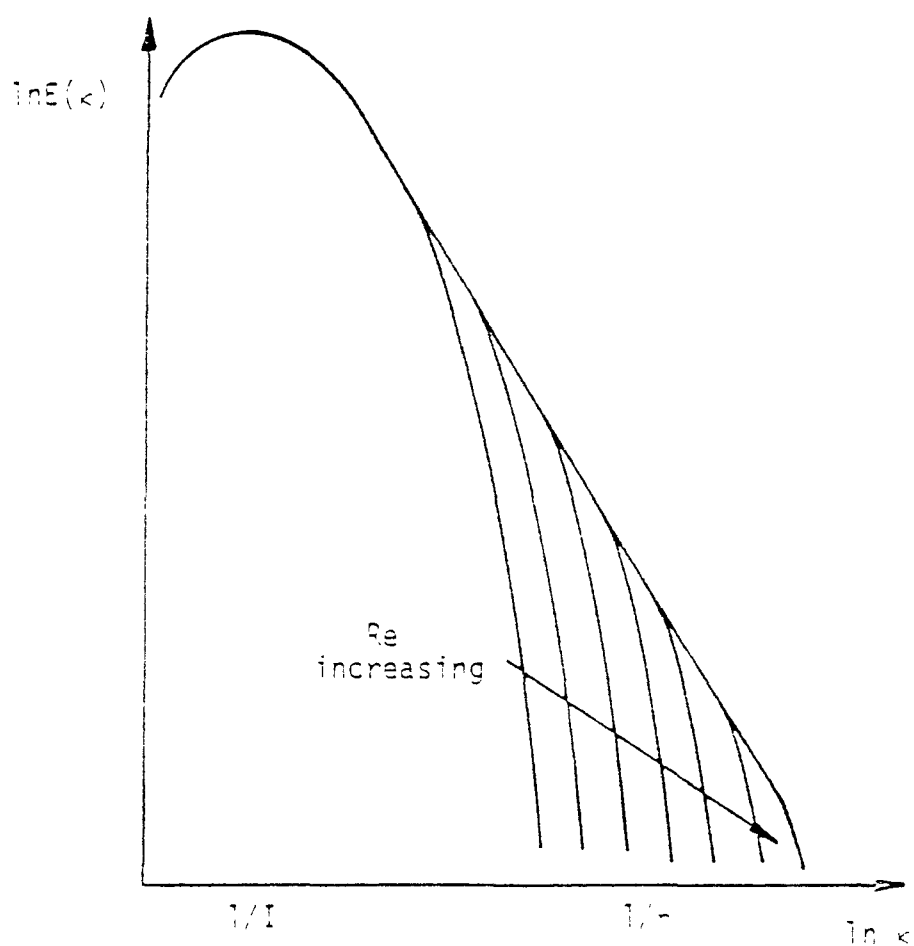


Figure 7. Change of spectrum with Reynolds number.

Figure 7 shows how the spectrum shape is affected by changing the Reynolds

number. For a given class of turbulent flow, a decrease of the Reynolds number decreases the range of the high-frequency end of the spectrum, whereas the size of the energy-containing eddies changes only very slowly with Reynolds number.

To be somewhat more quantitative, it is useful to examine the trends observed experimentally and theoretically in grid-generated turbulence. A good measure of the width of a turbulent energy spectrum is the ratio of the integral scale, I , to the Kolmogoroff microscale, η . It may be shown, through arguments presented by Corrsin (1963), that this ratio is

$$\frac{I}{\eta} \approx Re^{3/4}, \quad (2.13)$$

where Re is the grid Reynolds number (based upon upstream velocity, U , and mesh size, M). Ideally, both I and η would be reduced in the same proportion in a model (i.e., the geometrical scale ratio), so that the width (number of "decades") of the spectra would be identical in model and prototype. It is clear, however, that this would require identical Reynolds numbers in model and prototype. Eq. 2.13 may be used to estimate the comparative widths of model (m) and prototype (p) spectra:

$$\frac{(I/\eta)_m}{(I/\eta)_p} = \frac{(Re_m)^{3/4}}{(Re_p)^{3/4}} = \left(\frac{L_m}{L_p}\right)^{3/4}, \quad (2.14)$$

assuming that the ratio of flow speed to viscosity is roughly the same in model and prototype. (L is a characteristic length in the flow, for example, the mesh size or the height of a building.) Hence, at a scale ratio of 1:1000, a seven-decade-wide atmospheric spectrum is "modeled" by a 4½-decade-wide laboratory spectrum. This appears to be a drastic reduction in spectral width, but observations of grid-generated flows show that only the high-frequency end of the

spectrum is cut out, so that this reduction in spectral width has insignificant effects. It is found empirically that I/L at a fixed distance x/M downstream from a grid is nearly independent of Reynolds number (Corrsin, 1963). Similarly, it may be expected in other flow geometries that I/L at corresponding geometrical locations will be roughly independent of Reynolds number, i.e.,

$$\frac{I_p}{L_p} \approx \frac{I_m}{L_m}. \quad (2.15)$$

Indeed, the integral scale is found to be roughly half the size of the characteristic length and independent of Reynolds number in a wide variety of classes of flows.

Combining Eqs. 2.13 and 2.15 yields

$$\frac{\eta_p}{\eta_m} \approx \frac{I_p}{I_m} \left(\frac{L_m}{L_p} \right)^{3/4} \approx \left(\frac{L_p}{L_m} \right)^{1/4}. \quad (2.16)$$

In summary, integral scales reduce with the first power of the geometrical scale ratio (as desired), whereas Kolmogoroff microscales reduce with only the one-fourth power of the geometrical scale ratio. As we have seen in our previous discussion, the largest eddies contribute to the spread of a plume and the ones smaller than the plume width have little dispersive effect; hence, the mismatch of Reynolds number between the model and the prototype is insignificant.

A practical example here will make the point clear. The Kolmogoroff microscale in the atmosphere is about one millimeter between 1 and 100 m above ground (Lumley and Farofsky, 1964). As indicated by Eq. 2.14, at a scale ra-

ratio of 1:500, the spectral width in a model would be approximately two orders of magnitude smaller than desired. The Kolmogoroff microscale in the model would be about 100 times larger than required by rigorous similarity. This would correspond to a Kolmogoroff microscale of 10 cm in the atmosphere. It is difficult to imagine a practical atmospheric diffusion problem where eddies smaller than 10 cm would contribute significantly to the spread of a contaminant.

It should be noted that the arguments beginning with Eq. 2.13 have been concerned with Eulerian scales and spectra, whereas they would best have been posed in terms of Lagrangian coordinates, as required in Eq. 2.12. However, it is reasonable to assume that if the Eulerian spectra and scales of model and prototype are similar, then so will be the Lagrangian spectra and scales; more appropriately, if Eulerian spectra differ in certain respects between model and prototype, then the Lagrangian spectra will be dissimilar in like fashion. Hence, conclusions drawn in the Eulerian framework are expected to be valid in the Lagrangian framework (to at least within the same order of magnitude).

Concerning puff (relative) diffusion, the problem is somewhat different. Corrsin (1961b) has argued that the principal contribution to two-particle relative diffusion comes from eddies of roughly the same size as the particle pair separation. This contrasts with single particle diffusion, where the principal contribution comes from eddies of the same size and larger. Hence, puff diffusion in a model will depend somewhat more strongly upon the model Reynolds number. Intuitively, it appears that reasonable results would be obtained if the Kolmogoroff microscale were small compared with the initial puff width.

The discussion of the Reynolds number criterion in the modeling literature normally centers around sharp-edged geometry where it is usually stated that the mean flow patterns will not be much affected by changing the Reynolds number. While this is true, it does not make full use of the concept. Most mean-value functions, including those describing the main turbulence structure, will be nearly independent of Reynolds number, providing it is sufficiently high; the only exceptions are those two discussed at the beginning of this section.

The question is: how high must the Reynolds number be to be high enough? A precise answer would depend upon the geometrical shape of the boundaries, the roughness of the model surface, the accuracy desired, the type of information desired from the model, and possibly other effects (e.g., those characterized by the Rossby and Froude numbers). The answer to this question is reasonably well known for simple flow classes such as jets and cylinder wakes, but is largely unknown for models of atmospheric motions. Specific recommendations on minimum Reynolds numbers to be achieved in various classes of flows will be made in Section 3, Practical Applications.

2.2.2.3 Dissipation Scaling

A hypothesis on the similarity of the detailed turbulence structure of model and prototype flows was proposed by Memoto (1968). Again, a basic assumption is that thermal and Coriolis effects are negligible. He reasoned that mean flow patterns of both the model and prototype would be similar if the turbulent structure of the two flows were geometrically similar. Two assumptions were made:

- (1) the turbulence of both model and prototype flows was 'locally isotropic' (Kolmogoroff, 1941),

(2) the Kolmogoroff velocity, u , and microscale, η , characterize the turbulence at each point in the flow.

Assumption 1 is satisfied if the Reynolds number is very large (Hinze, 1975). Using assumption 2, Nemoto reasoned that the turbulence structures of model and prototype flows would be similar when

$$\frac{\eta_m}{\eta_p} = \frac{L_m}{L_p} \quad (2.17)$$

and

$$\frac{u_m}{u_p} = \frac{U_{Rm}}{U_{Rp}} \quad (2.18)$$

where the subscripts m and p refer to model and prototype, respectively.

From the definitions of η and u , the following equation may be established:

$$\varepsilon = \frac{u^3}{\eta} \quad (2.19)$$

From Eqs. 2.17, 2.18 and 2.19, it may be deduced that:

$$\frac{U_{Rm}}{U_{Rp}} = \left(\frac{\varepsilon_m}{\varepsilon_p} \right)^{1/3} \left(\frac{L_m}{L_p} \right)^{1/3} \quad (2.20)$$

Eq. 2.20 is the similarity criterion proposed by Nemoto. He has also shown how the above relationship may be obtained from a special nondimensionalization of the turbulent energy equation.

It is agreed that the turbulence structures of model and prototype flows would be similar if Eqs. 2.17 and 2.18 could be satisfied. However, it is impossible to satisfy Eq. 2.17 using typical length scale reductions (i.e., 1:300 to 1:1000). As mentioned previously, the Kolmogoroff microscale in the lower layer of the atmosphere is about 1mm. Typical values of η in laboratory flows are 0.075mm (Wyngaard, 1967), and 0.5mm (Snyder and

Lumley, 1971). Measurements in very high Reynolds number laboratory flows (Kistler and Vrehalovich, 1966) show that the smallest Kolmogoroff microscale which can reasonably be generated in the laboratory is 0.05mm. Thus, the largest ratio of microscales is of order 20, which is far short of the typical ratio required (i.e., 300 to 1000).

Generally speaking, the satisfaction of Eq. 2.17 requires identical Reynolds numbers of the model and prototype flows, as shown in the discussion of Reynolds number independence. This is also easily shown by the usual nondimensionalization of the turbulent energy equation (Cermak et al., 1966).

2.2.3 The Peclet Number and the Reynolds-Schmidt Product

The Peclet number is most easily discussed by writing it as

$$Pe = \frac{U_R L}{\kappa} = \frac{U_R L}{\nu} \frac{\nu}{\kappa} = Re \cdot Pr$$

where Pr is the Prandtl number.

The Reynolds-Schmidt product may be written as

$$\frac{U_R L}{\alpha} = \frac{U_R L}{\nu} \frac{\nu}{\alpha} = Re \cdot Sc.$$

Both of these dimensionless parameters have the same form (i.e., the product of a Reynolds number and a ratio of molecular transport coefficients). Both the Prandtl and Schmidt numbers are fluid properties and not flow properties. The Prandtl number is the ratio of the momentum diffusivity (kinematic viscosity) to the thermal diffusivity. The Schmidt number is the ratio of the momentum diffusivity to mass diffusivity.

For air, the Prandtl number does not vary strongly with temperature. When air is used as the medium for modeling, the Prandtl number is nearly the same in model and prototype, and, if the Reynolds numbers were the same, the

Peclet number criterion would be nearly satisfied. However, if water is used as the medium for modeling, the Prandtl number at ordinary room temperatures is a factor of about 10 larger than it is in air, and it varies rather greatly with temperature. Thus, from the standpoint of rigorous similarity, it does not appear that water would be a suitable medium in which to do model studies.

The Schmidt number for most gases in air is about one. Thus, the Schmidt number for an effluent plume (which contains only minor fractions of gases other than air) diffusing in the atmosphere is about one. If air is used as the medium for modeling, the Schmidt number (for nearly any foreign gas introduced) will be nearly the same in model and prototype. If, at the same time, the Reynolds number were the same, the Reynolds-Schmidt product criterion would be nearly satisfied.

When water is used as the medium for modeling, salt water or alcohol are typically used to simulate the buoyancy of a plume. The Schmidt number for sodium chloride or alcohol in water is approximately 800. Thus, it appears that strict similarity using water as the modeling medium would be difficult to obtain.

The basic problem, however, in matching of the Peclet number or Reynolds-Schmidt product, is not in the Prandtl or Schmidt numbers, but rather in the Reynolds number. Arguments similar to those constructed for Reynolds number independence may be used to justify the neglect of the Peclet number and Reynolds-Schmidt product as modeling criteria. The term on the right-hand side of Eq. 2.6 represents the molecular diffusion of heat. The term on the right-hand side of Eq. 2.8 represents the molecular diffusion of mass. In this connection, both heat and mass are regarded as passive scalar contaminants.

If the flow is of a sufficiently high Reynolds number, then the main structure of the turbulence will be almost totally responsible for the transport of the contaminant (heat or mass). Molecular diffusion will contribute very little to the bulk contaminant transfer; its main function is to smooth out the very small-scale discontinuities of concentration or temperature (i.e., it acts as a low-pass filter on the concentration or temperature fluctuations). Indeed, arguments of this nature have been used to postulate the form of concentration or temperature spectra at large wave numbers (see Corrsin, 1964; Pao, 1965). The main effect of the diffusivities is confined to setting the high wave-number cutoff of the temperature or concentration spectrum. Since turbulent diffusion strongly dominates molecular diffusion in turbulent air flows, especially at high Reynolds numbers, and since molecular diffusion is even less important for Prandtl or Schmidt numbers larger than unity, the effect of not matching the Prandtl or Schmidt numbers of the prototype in the model is unimportant. Generally speaking, the Peclet number and Reynolds-Schmidt product may be neglected as modeling criteria if the flow exhibits Reynolds number independence. Both air and water are suitable media for modeling, from this standpoint. Further discussions of air versus water are given in Chapter 4.

2.2.4 The Froude Number, $U_R/(gL\delta T_R/T_0)^{1/2}$

The square of the Froude number represents the ratio of inertial forces to buoyancy forces. A large value of the Froude number implies that buoyancy forces are small compared to inertial forces. Thus, thermal effects become important as the Froude number approaches unity. Batchelor (1953b) has shown how this parameter is related to the Richardson number. In the absence of a clearly defined length in the atmospheric boundary layer, it is convenient to

replace U_R^2/L by a representative velocity gradient and $\delta T_R/L$ by a representative temperature gradient. Substitution of these gradients into the expression for the Froude number yields,

$$Fr^2 = \frac{T_0}{g} \frac{U_R^2}{L^2} \frac{L}{\delta T_R} = \frac{T_0}{g} \frac{(\partial \bar{U} / \partial z)_R^2}{(\partial \delta T / \partial z)_R}.$$

Thus, the Froude number may be regarded as the inverse square root of a Richardson number. It is also related to the Monin-Obukhov (1954) length. Although any of these parameters may be used as similarity criteria, the Froude number is used here because it appeared naturally through the non-dimensionalization of Eq. 2.1. Batchelor (1953b) has also discussed the conditions under which this parameter is the sole governing criterion for dynamical similarity of motions of a perfect gas atmosphere.

A different interpretation of the Froude number is quite useful in considering stably stratified flow over hilly terrain. Suppose the flow approaching an isolated hill has a uniform velocity profile and a linear density gradient. The appropriate form of the Froude number is then

$$Fr^2 = \rho U_R^2 / (gh\Delta\rho),$$

where the characteristic length L has been replaced by the height h of the hill and the density difference $\Delta\rho$ is that between the base and top of the hill. The square of the Froude number represents the ratio of kinetic to potential energy, i.e., it represents the ratio of the kinetic energy in the approach flow to the potential energy required to raise a fluid element from the base to the top of the hill. It is clear that if the Froude number is much less than unity (very strong stratification), there is insufficient kinetic energy in the approach flow to raise fluid from the base to the top of the hill. With a two-dimensional hill perpendicular to the wind direction, this would result

in upstream blocking of the flow below the hill top (Long, 1972). For a three-dimensional hill, the fluid, rather than being blocked, can go round the hill (Hunt and Snyder, 1979). Hunt et al. (1978) and Snyder et al. (1979) have shown in more quantitative terms how the streamline patterns (hence, plume trajectories) change drastically with changing Froude number. It is thus evident that the Froude number is an essential parameter to be matched when modeling stably stratified flow over hilly terrain (see further discussion in Section 3.4).

The Froude number is not, by itself, a difficult parameter to duplicate in a fluid model. It is likely to be the most important individual parameter to be matched when the model is to simulate atmospheric diffusion. When the modeling medium is air, provisions must be made for heating or cooling of the air stream to obtain the temperature stratification. However, in order to match small Froude numbers of the prototype in a model with a typical scale reduction (i.e., 1:300 to 1:1000), and in order to maintain reasonable temperatures (i.e., maximum temperature difference of 200°C) in the model, it is necessary to decrease the mean flow speed. To match the Reynolds number between the model and the prototype requires that the mean flow speed be increased. This conflict is resolved by matching the Froude number while insuring that a Reynolds-number-independent flow is established. This is not always possible.

When considering water as the medium for modeling, it is necessary to define the Froude number in terms of density, rather than temperature, i.e.,

$$Fr = \frac{U_R}{(gL\Delta\rho/\rho)^{\frac{1}{2}}}$$

where ρ represents density. The common method of producing stable density stratification in water is by producing thin layers of various concentrations of salt in water. In view of the very small mass diffusivity of salt in water, an undisturbed stable mass of salt water will remain that way for several weeks before the density gradient is changed substantially by molecular diffusion. Maximum density differences are limited (about 20% in the dimensionless density difference), so that flow speeds must be reduced as was the case with air as the modeling medium. Recirculating systems using this technique have been impractical because of resulting mixing within a pump. However, Odell and Kovaszay (1971) have recently designed a rotating disk pump which maintains the gradient; this device may permit the use of recirculating salt water systems, although thus far it has only been used in very small channels. An interesting technique is reported by Homma (1969) wherein fresh and saline water are mixed to produce stable density gradients at the entrance of a once-through open water channel. This technique offers the possibility of providing the proper boundary conditions of turbulent flow (see next section), which is quite difficult in the still tank.

2.3 BOUNDARY CONDITIONS

2.3.1 General

A statement was made earlier that it was not necessary to determine a priori whether the flow was laminar or turbulent in order to apply Eqs. 2.4 to 2.6 to the determination of the similarity parameters. It is certainly necessary to determine whether or not the flow is turbulent in order to specify the boundary conditions. It is assumed here that the atmospheric flow is always turbulent. Furthermore, it was stated that the model flow would be identical to the prototype flow if, among other things, the

non-dimensional boundary conditions were identical.

Batchelor (1953b) points out:

Regarding the boundary conditions, we do not know enough about the differential equations concerned to be able to say with certainty what conditions must be specified to make the problem determinate, but it is a plausible inference from physical experience that \underline{u}' and ρ' must be given as functions of t' at all spatial boundaries and u' , ρ' , p' must be given as functions of x' at an initial value of t' ; it seems certain that such a set of boundary conditions is sufficient, although in some circumstances the conditions may well be over-sufficient.

(The prime here indicates a nondimensional quantity and the underline signifies a vector.) In the problem considered in the present paper, it is clear that sT' and x' also must be specified at an initial value of t' at all values of x' and at all spatial boundaries as functions of t' . This information is never available; even if it were, it could not be applied to the physical model. In the same sense, such detail is not required nor even desired as the output from the model. What is desired are quantities characteristic of the ensemble of realizations of turbulent flow. Evidently, what is required are properties characteristic of the ensemble of realizations of boundary conditions. This would require the specification of all the statistical properties (all of the moments) of the velocity, temperature, pressure, and density fields both initially everywhere and on the boundaries for all times. Even this much information is not available.

The most complete information which can be supplied at the present time are the first few moments, at least the mean and the variance. It is not known if the specification of only the first few moments is sufficient; it is plausible, from physical experience, that such a specification is sufficient. Indeed, it is dubious that any moments above the first two could be controlled at will.

Nearly all modelers have considered the specification of boundary conditions from a different viewpoint, that is, through the spectrum of turbulence in the approach flow. Armitt and Counihan (1968) have given qualitative arguments which suggest that, for the study of plume dispersal, not only must the turbulence intensity components be properly modeled, but also the spectrum of each component is required, particularly the low-frequency end of the spectrum. This idea is in agreement with the previous discussion on the contributions of the various scales of turbulence to the dispersal of contaminants. Some control of the turbulence spectra in the approach flow is possible (see Section 3.2).

2.3.2 Jensen's Criterion and Fully Rough Flow

The specification of the velocity on solid boundaries is simple; it is zero, and all of its moments are zero. Hence, geometrical similarity of model and prototype is required. This raises another question; how much detail is necessary? From the standpoint of rigorous similarity, of course, every detail of the prototype must be duplicated in the model. However, in view of the fact that the Reynolds number will not be duplicated, the fine detail is unnecessary. Jensen (1958) has suggested that, if the roughness length of the prototype, z_0 , may be determined (or at least estimated), then it should be scaled according to

$$\frac{z_{0m}}{z_{0p}} = \frac{L_m}{L_p} .$$

(the roughness length is a fictitious length scale characterizing flow over a rough surface. For uniformly distributed sand grains of size ϵ , the roughness length is typically $\epsilon/20$.)

This equation is known as Jensen's criterion, and has been widely used. It implies that elements or details smaller than δ will have very little effect on the overall flow; hence they need not be matched in the model. Details about the same size as δ need to be matched only approximately (for example, randomly distributed grains of sand). It may be necessary, with large reductions in scale, to abandon Jensen's criterion, as discussed below.

The flow of fluid close to a smooth boundary is not Reynolds number independent. The no-slip condition at the surface is a viscous constraint. A viscous sublayer exists immediately adjacent to the wall where viscous stresses dominate. If the surface is roughened such that the irregularities are larger than the thickness of the viscous sub-layer which would have existed on a smooth surface under otherwise identical flow conditions, viscous stresses become negligible. The irregularities then behave like bluff bodies whose resistance is predominantly form drag, i.e., the resistance is due to the pressure difference across the obstacle rather than to viscous stresses. Such a rough surface is said to be aerodynamically rough; the flow over an aerodynamically rough surface is Reynolds-number independent. The criterion which insures that the flow is aerodynamically rough is $u_* z_0 / \nu \geq 2.5$ (Sutton, 1949), where u_* is the friction velocity.

This is extremely fortunate from a modeling standpoint, because atmospheric flows are almost always aerodynamically rough (Sutton, 1949). If model flow conditions are chosen such that $u_* z_0 / \nu \geq 2.5$, one can be certain that the boundary layers are turbulent, so that such things as separation 'bubbles' and wakes behind obstacles and transition, separation, and reattachment of boundary layers on topographical surfaces will change very little with Reynolds number. The critical roughness Reynolds number, then, is that at which the boundary layer on the model becomes qualitatively comparable to that on the proto-

type.

For large reductions in scale, the simultaneous satisfaction of Jensen's criterion and the critical Reynolds number may not be possible. The critical Reynolds number criterion is undoubtedly the more important of the two criteria, because it controls the quality of the flow. Over-roughening of the model surfaces, thereby ignoring the Jensen criterion, will merely limit the resolution of the flow over the model (details about same size as ϵ will not be capable of being resolved), but, since the Reynolds criterion is met, the over-all flow patterns will most likely be matched.

2.3.3 Other Boundary Conditions

Specification of the detailed temperature distributions at the solid boundaries is rarely discussed from the modeling standpoint. In current practice, the solid boundary is maintained at constant temperature. It is plausible that the amount of detail in the temperature distribution should be determined on the same basis as the amount of detail in the geometrical boundaries. This has never been done, although elementary attempts have been made by Chaudhry and Cermak (1971). Similar considerations apply to the specification of the boundary conditions of the density distributions when the modeling medium is salt water.

Specification of boundary conditions on concentration distributions is, in principle, easy. In practice, the difficulty would depend on the type of problem to be studied. For example, if the problem were to determine the effect of a single source, the boundary conditions could be $x'=0$ initially everywhere and $x'=\text{constant}$ at the location of the source for all time thereafter.

Very little is known about the boundary specification of the pressure, p' . Normally, the mean pressure gradient in a wind tunnel is adjusted to zero.

Fluctuating pressures are, in any event, not controllable parameters in a model flow.

In current practice, the upstream boundary conditions on velocity and temperature are specified to be reasonably similar to some theoretical formula such as the logarithmic velocity distribution. Cermak et al. (1966) argue that boundary layers (kinetic and thermal) grown naturally over long lengths of rough ground must be inherently similar to those in the atmosphere. Others (Ludwig and Sundaram, 1969; Armitt and Counihan, 1968; Mery, 1969) use artificial techniques for generating thick boundary layers over short distances. Only Mery (1969) has attempted to model both the velocity and temperature profiles using artificial techniques. Any of the present techniques for boundary-layer generation appears to be suitable; all of them come reasonably close to matching the first two moments of the velocity and temperature distributions. Boundary-layer heights must, of course, correspond with the geometrical scale ratio. Practical goals and techniques for simulating the atmospheric boundary layer are discussed in Section 3.2.

2.4 SUMMARY AND RECOMMENDATIONS

Similarity criteria for modeling atmospheric flows in air and water have been derived. Rigorous similarity requires that five nondimensional parameters plus a set of nondimensional boundary conditions must be matched in both model and prototype. It has been determined that the Rossby number should be considered when modeling prototype flows with a length scale greater than about 5 km, under neutral or stable atmospheric conditions, in relatively flat terrain. It is concluded that more work needs to be done to determine under what conditions the prototype length scale may be extended while still ignoring the Rossby number criterion. It is recommended that study be started on

methods for simulating Coriolis forces in a model.

The concept of Reynolds number independence has been found to be extremely useful and powerful. Heuristic arguments have been given through the use of this concept that it is not necessary to match Reynolds number, Peclet number or Reynolds-Schmidt product between model and prototype, provided the model Reynolds number is sufficiently large. Current practice indicates that sufficiently large Reynolds numbers are attainable at least for sharp-edged geometrical structures in ordinary meteorological wind tunnels. More work needs to be done to determine if sufficiently high Reynolds numbers may be obtained in the laboratory for the simulation of flow over more streamlined surfaces. The Froude number is the most important single parameter describing the prototype flow which must be duplicated in the model. The specification of boundary conditions was found to be nebulous both in terms of how many variables are necessary and sufficient and also in terms of the type of statistical information required (i.e., is the specification of only a few lower order moments of each variable sufficient?) Geometrical similarity (nondistorted models) is required from the specification of zero velocity at the solid boundaries. It was decided that details of the prototype of size smaller than the roughness length need not be reproduced in the model. Objects about the same size as the roughness length need not be reproduced in geometrical form but an equivalent roughness must be established. Over-roughening may be required to satisfy the roughness Reynolds number criterion.

Boundary conditions in the fluid model are set by simulating the atmospheric boundary layer. Practical goals and techniques for simulating the atmospheric boundary layer are summarized in Section 3.2.4.

3. PRACTICAL APPLICATIONS

The fundamental principles of fluid modeling have been discussed in the previous chapter. When it comes to the particular details of a model study, however, many decisions must be made, and the fundamental principles frequently do not provide enough guidance. It is the aim of this chapter to cover the most common types of problems encountered by a modeler when designing a particular model study, and to provide rational guidelines where possible or to cite common practice where there is no rationale.

The following sections discuss in detail the special problems encountered in modeling plume rise, the atmospheric boundary layer, flow around buildings, and flow over complex terrain. Each of these sections is summarized with a set of recommendations.

3.1 PLUME RISE AND DIFFUSION

Numerous investigators have studied the rise of plumes from model stacks. Many different kinds of facilities, including wind tunnels, water tanks, towing tanks, water channels, and even the calm stably-stratified environment of an ice-skating rink, have been used. The water tanks and the ice-skating rink have been used to study the behavior of plumes in calm environments, both

stratified and unstratified. The wind tunnels, water channels and towing tanks have been used to study the behavior of plumes issuing from stacks into crosswinds. The effluent has ranged from pure jets to strongly buoyant plumes. The crosswinds have ranged from neutrally stratified with uniform velocity profiles to simulated atmospheric boundary layers (stable and unstable stratification with, for example, logarithmic velocity profiles).

The historical development of modeling techniques concerning plume rise is analogous to the historical development of theoretical formulas for the prediction of plume rise, i.e., the effluent buoyancy was thought to be negligible in comparison with its momentum. Sherlock and Stalker (1940) appear to have done the first wind tunnel study relating to plume behavior. Specifically, their experiments established the rule that the effluent speed must exceed one-and-one-half times the wind speed in order to avoid downwash in the lee of the stack. This "one-and-one-half-times" rule is still widely applied today. They worked with a 1:300 scale model, but chose to use essentially identical model and full-scale values of wind speed and effluent temperature. One of their conclusions was "...the temperature of the [stack] gas is relatively unimportant as a means of controlling the downwash...". At the present time, it is still not clear exactly what effect buoyancy does have on the one-and-one-half-times rule, but it is evident that the buoyancy was not properly scaled in the Sherlock and Stalker experiments. Their experiments, even with the very hot (400° F) effluent, were highly momentum-dominated plumes (effectively, jets), and corrections were made only for the change of momentum due to change in temperature (density). More recent work (cf. Huber et al. 1979) indicates that the buoyancy per se of the lighter effluent is ineffectual in preventing downwash; instead, the decrease in density alone contributes to

downwash because it reduces the effluent momentum.

Numerous model studies have been conducted since those of Sherlock and Stalker, but very few of the results have been compared with atmospheric data or even with other model results. Much worse, there has not been a uniform application of similarity criteria. Each investigator appears to apply a different set of rules which ensure that his experiment models the rise of a plume in the atmosphere. It is evident after only a little study that some of the rules are conflicting and that all of them cannot be correct.

3.1.1 Near-Field Plume Behavior

Let us consider the simplest conceivable problem of a plume downwashing in the lee of a stack because the effluent contains insufficient momentum to overcome the low pressure suction due to the crosswind (See Figure 8). We will suppose that the stack walls are thin, the stack is tall and the effluent has the properties of air at the same temperature as the surroundings, i.e., $D_o/D_i=1$, $H_s/D \gg 1$, $\rho_s/\rho_a=1$, $\Delta p=0$ and $Fr=\infty$. Further, since we are concerned only with the local flow field near the top of the stack, we have purposely omitted shear in the crosswind ($\partial u/\partial z \ll U/D$) as well as stratification and turbulence in the approach flow. To model this problem, we must match only two parameters, the ratio of effluent speed to wind speed and the Reynolds number:

$$W_s/U, \quad W_s D/\nu.$$

As discussed in Section 2.2.2.2, provided the Reynolds number is larger than some critical value, its precise magnitude is irrelevant. There appears, however, to be considerable disagreement concerning the particular value of this "critical" Reynolds number. Ricou and Spaulding (1961) have shown that the entrainment rate of momentum-dominated jets in calm surroundings is essentially constant for Reynolds numbers in excess of 25000. Only minor variations were

observed between 15,000 and 25,000. Substantial variations were observed below 10,000; the entrainment rate was increased by more than 20%. Hence, if minor errors are acceptable, the critical Reynolds number is 15,000. This simplified problem would be relatively easy to model even in a fairly small wind tunnel (say, 0.5m square test section) with moderate wind speeds (~20 m/s) and a small stack (1cm dia.). We will shortly see, however, that if the effluent is buoyant, the problem becomes much more complicated. It will not be so easy to obtain such a large Reynolds number, and we must look harder to determine if the 15,000 value for the critical Reynolds number can be reduced. We will return to our discussion of critical Reynolds numbers later in this section.

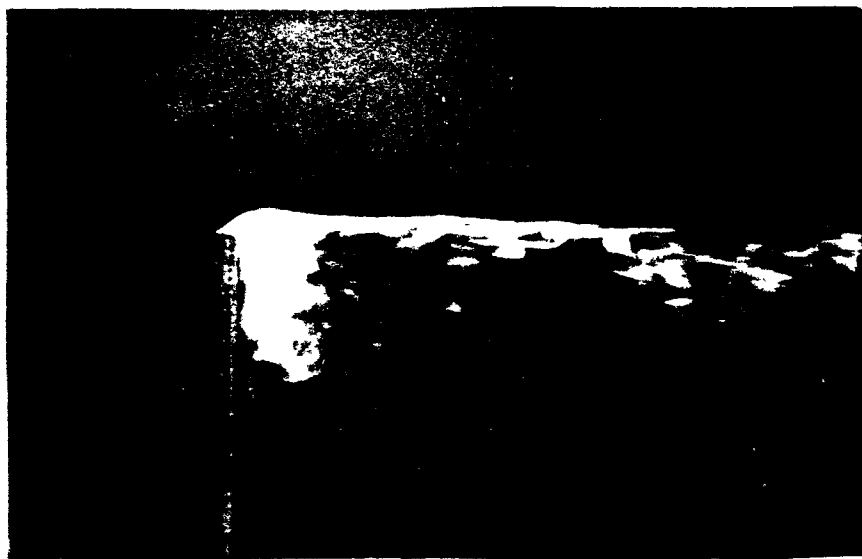


Figure 8. Plume downwash in the wake of a stack.

Notice that, provided the Reynolds number exceeds 15,000, there is only one parameter of importance, W_s/U . Since full scale stacks and effluent speeds (even fairly small stacks and low speeds) result in huge Reynolds numbers (a typical small value might be 10^6), the full scale flow is Reynolds number independent. This implies that the size and shape of the wake behind

the stack and the amount of downwash depend on only one parameter, W_s/U , and not on wind speed per se. Similarly, provided the Reynolds number is large enough, the flow structure in a model in a wind tunnel is similar to that of the prototype and is independent of wind speed per se. (This discussion may appear obvious and therefore trivial, but in demonstrating wind tunnel experiments to novices, or even frequently to accomplished experimentalists, the inevitable question is: to what full scale wind speed does this flow correspond? The correct answer, i.e., all wind speeds above the barest minimum, invokes puzzled glances and disbelief!)

Let us now complicate the problem, one step at a time, to see what additional issues arise in the modeling. There are really two Reynolds numbers in this problem, corresponding to two different classes of flow: one for the flow inside the stack $W_s D/\nu$ and one for the flow around the outside of the stack UD/ν . The critical Reynolds numbers may differ because the classes of the flows differ. The critical Re for pipe flow assuredly differs from that of a two-dimensional wake.

It is useful here to consider the changes that occur in the flow pattern around a circular cylinder as the Reynolds number is increased (for additional details, see Goldstein, 1965). At very low Re (<1), the streamline patterns are symmetrical fore and aft of the cylinder. As Re is increased (~ 10), two symmetrical standing vortices are formed at the back; they grow in size and are stretched farther and farther downstream until at $Re \sim 100$, they break down and are shed alternately at regular intervals from the sides of the cylinder. This type of flow persists over a very wide range of Re ($10^2 \leq Re \leq 10^5$). Townsend (1956, p 134-5) showed that various mean quantities such as the velocity defect, the turbulence intensity, and the width of the wake of a two-dimensional circular cylinder were invariant with Re in the range of 800 to 8000, but they

are most likely invariant over a much wider range. At an Re of about 10^5 , the boundary layer on the cylinder becomes turbulent and leaves the cylinder farther back on the surface, reducing the drag coefficient from a nearly constant value of $1.1 \pm 10\%$ in the range $10^2 < Re < 10^5$ to about 0.36. Hence, we might say there are two critical Reynolds numbers for the flow around a cylinder: one where the Kármán vortex street (shedding vortices) is formed and one where the boundary layer becomes turbulent.

If we wish to model downwash around a full scale stack where $Re \geq 10^5$, it is essential to ensure that the boundary layer is turbulent. This may be done by ensuring that the model Re exceeds the upper critical Re of about 10^5 , which would require a large and/or fairly high speed wind tunnel, but it is also possible to simulate a much higher Re using the common wind tunnel practice of tripping the boundary layer, either through use of a trip wire or fence or by roughening the surface of the cylinder, thereby forcing the boundary layer to become turbulent (Goldstein, 1965 or Schlichting, 1968).

If the full scale Re is less than about 10^5 , then it is only necessary that the model Re exceed the lower critical Re of about 100. For a rectangular stack, because of the sharp corners forcing separation, the lower critical Re would be lower still, and the upper critical Re would be much higher, possibly non-existent.

It should be noted that if we were not concerned with entrainment of the effluent into the wake, i.e., if we wanted to model a non-downwashed plume, then the cylinder Reynolds number would be relatively unimportant in any event, so that we need be concerned only with the critical Re for the effluent flow as it exits the stack under ordinary circumstances.

Suppose the effluent is of high temperature, so that its density is, say,

half the ambient air density. In a wind tunnel, it is usually easier and more practical to use a lighter gas to simulate this high temperature field effluent than it is to heat the model effluent. Similarly, in a water channel or tank, it is usually easier to use salt water or alcohol than to heat or cool the model effluent. This low density manifests itself in two opposite ways: first, at a fixed effluent speed, the effluent momentum flux is reduced, tending to make the plume more easily bent-over, thus promoting downwash, and second, the buoyancy of the effluent is increased, tending to inhibit the downwash. It is not clear which is the more important effect. Overcamp and Hoult (1971) showed rather convincingly that the effect of the increased buoyancy was to inhibit downwash of cooling tower plumes, where the Froude number $W_s / (gD\Delta\rho/\rho_a)^{1/2}$ ranged from 0.2 to 2. Huber et al. (1979), however, observed enhanced downwash as the effluent density was decreased. The Froude numbers in their experiments were greater than 4, which is more typical of power plant plumes. It would appear that the crossover point where the effect of the lower density switches from inhibiting downwash to enhancing it occurs at a Froude number around 3; however, it is likely also to be a function of the effluent momentum to crosswind momentum ratio.

Most investigators would agree that the following set of parameters to be matched for this more complex problem are sufficient (although, perhaps, not all are necessary):

$$\frac{W_s}{U}, \frac{\rho_s}{\rho_a}, Re, \frac{W_s}{(gD\Delta\rho/\rho_a)^{1/2}} \quad .$$

Since products of similarity parameters are themselves similarity parameters, the following set is fully equivalent to that above:

$$\frac{\rho_s W_s^2}{\rho_a U^2}, \frac{\rho_s}{\rho_a}, Re, \frac{W_s}{(gD\Delta\rho/\rho_a)^{1/2}} \quad (3.2)$$

The first parameter expresses the ratio of effluent momentum flux to cross-wind momentum flux, and must be matched if the initial bending or the rise due to the initial momentum of the plume is important. The last parameter is the Froude number, which expresses the ratio of inertial to buoyancy forces in the effluent. (Note the different interpretation of Fr here as opposed to its characterizing the stratification in the approach flow as it was introduced in Section 2.2.4.)

A questionable parameter is the density ratio ρ_s/ρ_a per se. As mentioned previously, the density difference manifests itself through its effects on the effluent momentum and the effluent buoyancy, which are expressed in the first and last parameters of Eq. 3.2. Of course, it is perfectly acceptable to match the density ratio between model and prototype, but if it is not an essential parameter, then the full capabilities of modeling facilities will not be realized. It is frequently advantageous to exaggerate the density differences in the model in order to achieve low Froude numbers. Ricou and Spalding (1961) showed very convincingly that the rate of entrainment dm/dx in a highly momentum-dominated jet (no crosswind) obeys the relation

$$\frac{1}{\rho_a} \frac{dm}{dx} = C \left(\frac{\rho_s}{\rho_a} \right)^{1/2} W_s D, \quad (3.3)$$

where C is a constant. Hence the entrainment rate is a direct function of the density ratio. For small density differences, the entrainment rate is not much affected. However, if helium (S.G.=0.14) were used as the buoyant effluent from a stack in a wind tunnel, maintaining geometric similarity and the

ratio of effluent to wind speed W_s/U , to simulate a full scale effluent with specific gravity of 0.7, then the entrainment rate would be halved. Hence, its rise due to initial momentum would not be correctly modeled. Considerations such as these are evidently what lead Hault (1973) to state that the density difference $\Delta\rho/\rho_a$ must not exceed 0.4. But such a statement cannot be made unequivocally. If the density difference in the field were 0.5, as might be the case for a gas turbine exhaust, then it would certainly be desirable to exceed 0.4 in the model. More importantly, as shown by Eq. 3.3, it is certainly possible to exaggerate the density difference to 0.8 by using essentially pure helium as the model effluent and still maintain the same entrainment rate by increasing the effluent flow rate W_s . But Eq. 3.3 of Ricou and Spalding applies only beyond a few diameters beyond the stack exit (say $>10D$). In order to avoid an "impedance mismatch" in our downwash problem, where we are concerned with the flow behavior right at the top of the stack, it is necessary to match the density ratio. Beyond a few diameters, it is only essential to match the momentum flux ratio.

A major point of disagreement among investigators concerns the definition of the Froude number. Approximately half the investigators define the Froude number with the effluent density as the reference density, Fr_s ; the other half define it with the ambient density (at stack top) as the reference density, Fr_a . Yet, nowhere is any reason given for the particular choice. It might appear at first glance that the choice is completely arbitrary. However, given that two plumes have the same Froude number based on effluent density, it is not necessarily so that they have the same Froude number based on ambient density. Consider the following example of a typical power plant plume being modeled at a scale of 1:400 using helium as the buoyant effluent in a wind tunnel:

TABLE 1: Typical Parameters for Modeling Plume Downwash.

Parameter	Prototype Value	Model Value
W_s	20m/s	1.67m/s
g	9.8m/s^2	9.8m/s^2
D	10m	2.5cm
$\rho_a(T_a)$	1.2g/l(20°C)	1.2g/l(20°C)
$\rho_s(T_s)$	0.83g/l(150°C)	0.17g/l(20°C)
Fr_a	3.6	3.6
Fr_s	3.0	1.37
Re	13×10^6	360

The Froude numbers differ by a factor of the square root of the density ratios, i.e., $Fr_a = (\rho_a/\rho_s)^{1/2} Fr_s$, so that unless ρ_s/ρ_a is the same in model and prototype, the choice of the definition of the Froude number is not arbitrary. Yet, almost all investigators exaggerate the density differences in the model in order to obtain large enough buoyancy in the plumes (low Froude numbers). They do not match ρ_s/ρ_a as required by Eq. 3.2, so that it is not possible to match both Froude numbers simultaneously.

This is a particularly vexing problem because most plume rise theories are founded on the assumption of small density differences, so that the two Froude numbers are essentially equivalent. There are only two places in the literature providing guidance on which Froude number is the most appropriate. Hoult et al. (1977) state that two complete, independent wind tunnel tests were run, one using the ambient density, the second using effluent density, as the reference density. The tests involved the modeling of gas turbine exhausts, which generally involve large effluent velocities and high effluent

temperatures. They claim (unfortunately, without presenting any data to support their claim) that the better choice is ambient density and that the error between model and field observations (presumably, of far-field plume rise) when using effluent density was about 90%, which was nearly 10 times the error incurred using ambient density. It is important to note that using ambient density as a reference corresponds to using effluent temperature as a reference, i.e.,

$$\frac{T_s - T_a}{T_s} = \frac{\rho_a - \rho_s}{\rho_a} \quad (3.4)$$

due to the perfect gas law at constant pressure, $pT = \text{const.}$

A physical interpretation of the difference between the two definitions is suggested in a footnote by Briggs (1972) (his comments applied specifically to alternate definitions of buoyancy flux, but are equally applicable here): "the difference --- amounts to different approximations for the effective density (inertia per unit volume) of the fluid being driven by the buoyant force:

(1) that the effective density is approximately constant $= \rho_s$, which is reasonable very close to the stack, say within a few stack^s diameters downwind;

(2) that the effective density is approximately constant $= \rho_a$, which is a better approximation at all larger distances."

It is clear, then, that in our stack downwash problem, we should use the effluent density as the reference density in matching of Froude numbers. It is also clear that, if we were attempting to model far field plume rise, we should use the ambient density as the reference density, in agreement with Hoult et al. (1977).

A second point of disagreement among modelers has to do with whether the

relevant parameter is the ratio of effluent speed to wind speed W_s/U or the ratio of effluent momentum flux to crosswind momentum flux $\rho_s W_s^2 / (\rho_a U^2)$. This may also be thought of as a ratio of dynamic pressures. Again, if ρ_s/ρ_a is matched between model and prototype, the choice is arbitrary. As discussed above, however, most modelers drop the requirement of matching the density ratio, and the choice is no longer arbitrary. Sherlock and Stalker (1940) found that the behavior of the plume depended upon the ratio of the momenta and that the ratio of the two speeds was a close approximation, provided that both velocities were reduced to equivalent velocities at a common temperature. Their one-and-one-half-times rule was thus based on the momentum ratio, a fact not appreciated by most authors who quote the rule. The recommendation made here, then, is that the relevant parameter is the momentum ratio, and not the speed ratio per se.

A third problem is that in water tanks or channels, a heavy salt solution is commonly used to simulate a buoyant effluent by inverting the stack and exhausting the salt solution into lighter fresh water. The same principle could conceivably be used in a wind tunnel by using a heavier-than-air gas such as freon with an inverted stack. There is a subtle question here that has not been fully answered. In the field, it is a lighter effluent entraining heavier air, whereas in the water tank, it is a heavier effluent entraining a lighter ambient fluid. It is conceivable that the entrainment mechanisms could be significantly altered due to this interchange of heavier and lighter fluids. Eq. 3.3 indicates that a heavy fluid issuing from an inverted stack can be used to simulate a lighter fluid from an upright stack, if the effluent speed W_s is appropriately reduced. As argued previously, there may be a subtle effect on the entrainment very near the stack, but this disappears

quickly as the density difference is rapidly diluted. The total rise of the plume is not highly sensitive to the entrainment parameter; the forced plumes of Hoult and Weil (1972) and Lin et al. (1974), both using salt water effluent, appear to simulate field results quite well. It is clear that the problem is not yet completely answered and requires detailed systematic study. A tentative conclusion, in view of other inherent inaccuracies in modeling at small scales, is that this subtle difference may be overlooked.

It was shown in the early part of this section that a critical Reynolds number of 15,000 was not difficult to achieve per se. However, the introduction of buoyancy makes this Re_c much more difficult to attain. In order to match Froude numbers, it was essential to introduce helium as the effluent (which incidentally, has a kinematic viscosity approximately 8 times that of air) and to reduce the effluent speed by a factor of 12 (see Table 1), so that the effluent Reynolds number is only 360. Thus, we must determine whether a lower critical Reynolds number can be justified.

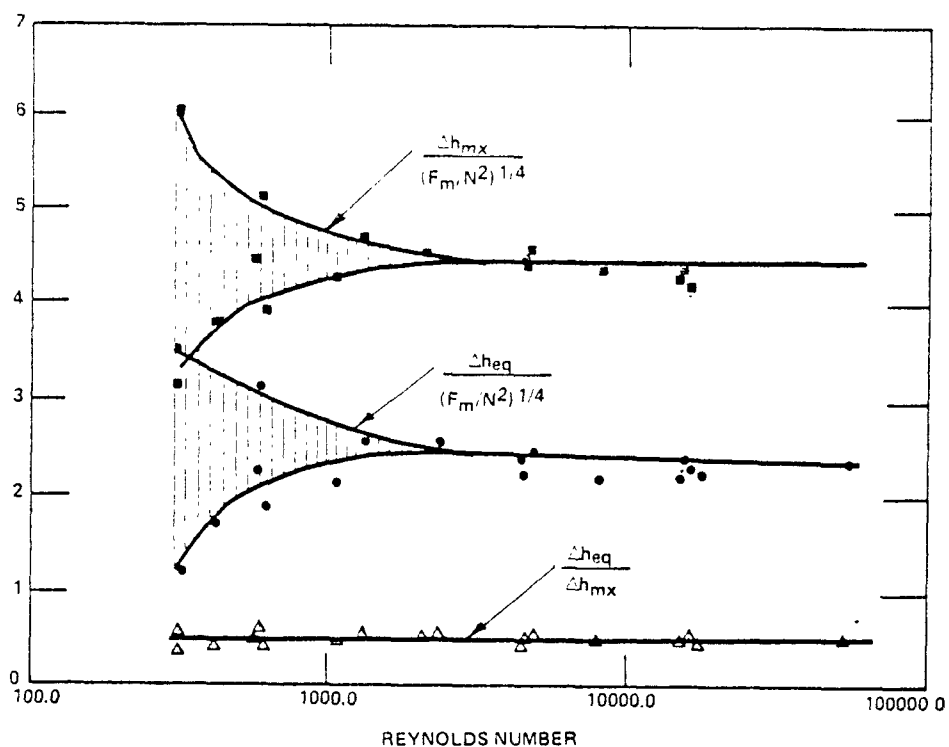
The data of Ricou and Spalding (1961), which suggested $Re_c=15,000$, was applicable to momentum-dominated jets in calm surroundings. Most investigators would agree that for a bent-over plume, the critical value may be substantially lower, of the order of 2000, i.e., a value that is well-established for the maintenance of turbulent flow in a pipe. This is equivalent to saying that the plume behavior is independent of Reynolds number provided that the effluent flow is fully turbulent at the stack exit. Lin, et al. (1974) have taken this one step further. They tripped the flow to ensure that the effluent was fully turbulent at the stack exit at a Re of 530 by placing an orifice with opening $D/2$ inside the stack and located $3D$ from the exit. Their data for (1) the terminal rise of a buoyant plume in a calm and stably-stratified environment and (2) the trajectory of a buoyant plume in a stably-stratified crosswind

compared reasonably well with other laboratory and field data. Hocot, et al. (1973) used a similar technique. Liu and Lin (1975), however, indicate that the placement of the orifice relative to the top of the stack was critical at a stack Re of 200. If the distance was smaller than required, the effluent flow was governed by the orifice diameter and not the stack diameter; if larger, the flow tripped by the orifice would laminarize before it reached the stack exit.

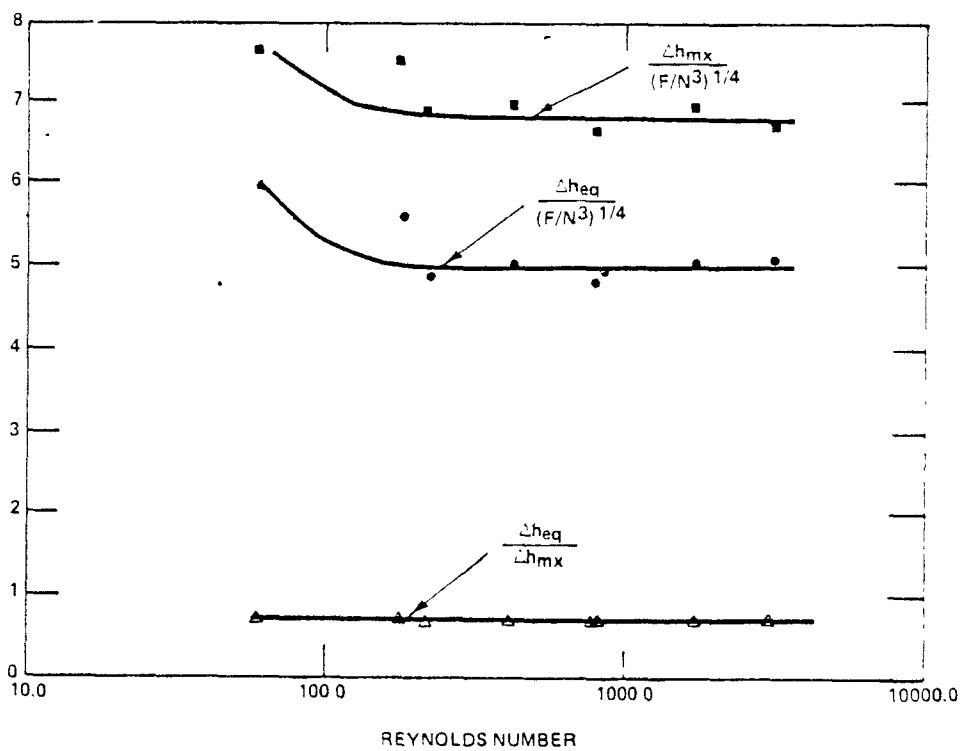
Briggs and Snyder (1979) showed a critical Reynolds number of 2000 for jets and 200 for buoyant plumes in a calm, stably stratified salt water tank (see Figure 9) for $M=0.06$, where M is a dimensionless source momentum parameter; $M=\rho_s W_s N/g\Delta\rho$, and N is the Brunt-Väisälä frequency characterizing the density stratification. It was argued on theoretical grounds that the critical Reynolds number for a buoyant plume is proportional to $M^{-1/2}$. Below these critical values, the plumes were laminar at the stack exit with resulting rises too high. A few attempts at tripping the flow inside the stack yielded unpredictable results.

Experiments with buoyant plumes in neutrally stable crosswinds, conducted by Hoult and Weil (1972), show: (1) at a Reynolds number greater than 300, the plume appears to be fully turbulent everywhere; at lower Reynolds numbers, the plume becomes turbulent only some distance downstream of the exit (there was apparently no tripping of the flow inside the stack), (2) ignoring scatter in the data, no dependence of far field plume trajectory on Reynolds number was observed for Reynolds numbers between 28 and 2800, (3) the vertical plume width was substantially reduced close to the stack exit (within 10 stack diameters downwind) for Reynolds numbers below 300.

It is difficult to reconcile the results of the various sets of experiments. There are numerous possible reasons why the critical Reynolds numbers



(a) Neutrally buoyant plumes



(b) Buoyant plumes

Figure 9. Variation of plume rise with Reynolds number.

are different. The effluent flows differ (momentum-dominated versus buoyancy dominated), the stratification of the ambient fluids differ (neutral versus stable stratification), and in one case the jet issued into a calm environment whereas in the other two, the plumes were bent over by a crosswind. The two-order-of-magnitude difference in critical Reynolds number, however, is difficult to explain. It is evident that a basic systematic study needs to be undertaken to establish that Reynolds number (perhaps different ones for different sets of conditions) above which the rise and spread of model plumes is independent of Reynolds number.

3.1.2 Summary and Recommendations on Modeling Near-Field Plumes

In summary, to model the near-field rise of a buoyant plume from a stack, is recommended that:

1. The effluent Reynolds number be as large as possible.
 - (a) Fix the effluent Reynolds number to be as large as possible, preferably greater than 15,000.
 - (b) If it is necessary to reduce the effluent Reynolds number below 2000, it may be necessary to trip the flow to ensure a fully turbulent exhaust.
 - (c) If it is desired to reduce the effluent Reynolds number below 300, it will be necessary to do some experimentation to determine under what conditions the plume will simulate the behavior of a plume in the field.
2. The set of parameters to be matched (equal in model and prototype) is either
 - (a) For a scale ratio less than about 400, matching of all the following parameters is generally possible and certainly adequate:

$$\frac{W_s}{U}, \frac{\rho_s}{\rho_a}, \left(\frac{W_s}{gD\Delta\rho/\rho_s} \right)^{1/2}.$$

- (b) For a scale ratio greater than about 400, it is generally not possible to match ρ_s/ρ_a and it is probably safe to ignore it. It will then be essential to match:

$$\frac{\rho_s W_s^2}{\rho_a U^2}, \frac{W_s}{(gD\Delta\rho/\rho_s)^{1/2}}.$$

Notice that in Condition 2a, the choice of the reference density in the Froude number does not matter; both will be matched. In Condition 2b, however, it is important to match the Froude number based on effluent density. Since there is only one possible reference length in this problem, the stack diameter, it determines the scale ratio, and geometric scaling is implicit, i.e., all lengths should be referenced to the stack diameter. Other lengths that may be important are the stack wall thickness and the stack height. Obviously these lengths should be scaled with the stack diameter. Also in Condition 2b, it should be cautioned that if $\Delta\rho/\rho_s$ is made very large, the initial entrainment mechanism may be altered due to "impedance mismatch".

These recommendations are subject to change pending future work.

3.1.3 Far-Field Plume Behavior

The previous section reviewed the criteria to be met for modeling plumes close to the top of the stack. With one exception, the use of the ambient density as the reference in the definition of the Froude number, these same criteria also apply to modeling plumes far downwind of the stack. It is obvious, however, that this implies an even greater reduction in scale (larger geographical area to be modeled), and even those criteria will be difficult if not impossible to satisfy. The question to be answered in this section, then, is whether further compromises can be made without making the results unduly suspect.

As an example, suppose we wish to model a power plant in complex terrain, where the scale reduction factor is 1:5000. Typical conditions from the plant operations record might be $T_s=400^\circ\text{K}$, $T_a=300^\circ\text{K}$, $W_s=25\text{m/s}$, $U=10\text{m/s}$, $D_s=4\text{m}$. Suppose we try to match conditions 2b from the previous section, basically the momentum ratio, the stack Froude number (with ambient density reference), and a minimum Reynolds number, using pure methane as the model effluent ($\rho_s/\rho_a=0.56$) in a wind tunnel. The model stack diameter would be 0.8mm. The Froude number of the full scale effluent is 8, which implies a model effluent speed of 0.46m/s. These conditions yield a stack Reynolds number of

$$\text{Re}_s = \frac{W_s D}{\nu} = \frac{46\text{cm/s} \times 0.08\text{cm}}{.16\text{cm}^2/\text{s}} = 23 ,$$

considerably below the value recommended in the previous section.

There are several directions available at this point. Notice that the problem was not created because of the matching of the momentum ratio, although that requirement may later cause problems in obtaining a minimum Reynolds number based on the roughness of the underlying terrain (see Section 3.2). The problem was caused because of the matching of Froude numbers. This problem has been attacked in a variety of ways.

3.1.3.1 Ignoring the Minimum Reynolds Number

Ludwig and Skinner (1976) ignored the minimum Reynolds number requirement; thus, their plumes were laminar in the immediate vicinity of the stack (see Figure 10). Discussion in their report admitted that the rise of an initially laminar plume would exceed that of an initially turbulent plume because the turbulent one mixes more rapidly with the ambient air. They felt, however, that this



Figure 10. Laminar plume caused by low Reynolds number effluent (from Ludwig and Skinner, 1976).

was not a serious limitation in their model because their initial plume rise was quite small before atmospheric turbulence began to dominate the mixing process. It is evident from Figure 10, however, that the scale of the atmospheric turbulence is considerably larger than the initial plume diameter, so that the plume trajectory is highly contorted, but little real mixing of effluent with ambient air occurs for many stack heights downstream. If the effluent plume were turbulent, it would be diluted very rapidly (within a few stack diameters) by ambient air. The resulting plume rise could be substantially different in the two cases, depending on the precise effluent parameters. Ludwig and Skinner did not feel that tripping of the flow within the stacks was possible because the stack diameters ranged from 0.25 to 1.3 mm. Liu and Lin (1975), however, were able to use a sapphire nozzle of 0.18 mm dia. to trip the flow in their stack. As mentioned in Section 3.1.1, the size and placement of the orifice is evidently critical and will require special experimentation.

3.1.3.2 Raising the Stack Height

Pacy (1971) ignored the plume buoyancy, per se, but instead extended the stack and bent-over the top such that the effluent was emitted at the same elevation as that calculated from plume rise formulas. This technique has the advantage that flow Reynolds numbers can be made as large as desirable. The disadvantages, however, are obvious. Since the plume rise is a function of wind speed, there is a contribution to vertical dispersion due to both longitudinal and vertical fluctuations in the wind speed that cannot be simulated via this method. Also, the physical stack height in the model must be changed to simulate different wind speeds. But the most serious limitation is that the complex trajectory of the plume, which may be the most useful information obtained from the model, cannot be obtained using this method. It is frequently desired to determine whether a plume goes over the top, is diverted around, or impacts on the surface of a hill. If the plume is emitted into a different mean streamline, its resulting trajectory could be entirely different. Adding momentum to the effluent to obtain the same rise as for a buoyant plume is objectionable for similar reasons. This technique, however, might be acceptable under certain circumstances; for example, if the problem were to determine concentrations on an isolated hill far downwind of the source (beyond the point of maximum plume rise), then it might be acceptable to inject the plume at its terminal rise height. An additional problem is that one must presume to know the plume rise. This may be acceptable for stable flows, but is an unsettled matter for neutral and unstable flows.

3.1.2.3 Distorting the Stack Diameter

Briggs (1969) equation for the trajectory of a plume possessing both initial momentum and buoyancy, valid only for downwind distances considerably smaller than that to the point of maximum rise is rewritten here in a different form:

$$\left(\frac{\Delta h}{H_s}\right)^3 = 2.3 \left(\frac{\rho_s W_s^2}{\rho_a U^2} \cdot \frac{D^2}{4H_s^2} \right) \left(\frac{x}{H_s} \right) + 1.8 \left(\frac{g D^2 W_s \Delta \rho}{4 \rho_a U^3 H_s} \right) \left(\frac{x}{H_s} \right)^2 \quad (3.5)$$

$$= 2.3 \left(\frac{l_m}{H_s} \right)^2 \left(\frac{x}{H_s} \right) + 1.8 \left(\frac{l_B}{H_s} \right) \left(\frac{x}{H_s} \right)^2, \quad (3.6)$$

where l_m is a momentum length scale and l_B is a buoyancy length scale, defined by Briggs (1975) as

$$l_m = \frac{1}{2} \left(\frac{\rho_s}{\rho_a} \right)^{1/2} \frac{W_s}{U} D \quad (3.7)$$

and
$$l_B = \frac{D^2}{94} \frac{W_s}{U^3} \frac{\Delta \rho}{\rho_a}. \quad (3.8)$$

A physical interpretation of these length scales is that they represent the initial radius of curvature of the plume due to momentum and buoyancy respectively. In our example problem, $l_m = 4.3\text{m}$ and $l_B = 0.25\text{m}$. It is evident from examination of Eq. 3.6 that close to the stack, the first term on the right hand side of this equation will dominate and far from the stack, the second term will dominate. That is, close to the stack, the initial momentum will be important, whereas, ultimately, the buoyancy will dominate.

Hoult (1973) suggested that we ignore the initial momentum, provided only that we avoid stack downwash, and take as our requirement

$$(l_B/H_s)_m = (l_B/H_s)_p, \quad (3.9)$$

where subscripts m and p refer to model and prototype, respectively. He further suggested that Eq. 3.9 could be met by exaggerating the density difference and/or by reducing the effluent speed W_s . Liu and Lin (1976) started at

essentially the same point, but suggested additionally that Eq. 3.9 could be met by exaggerating the stack diameter. They performed an experimental run on a complex terrain model at a scale of 1:10000 using a stack diameter exaggeration factor of 2. Photographs show that the plume was turbulent at the stack exit, even though the effluent Re was only 68, but no experiments were made to validate the use of this method.

It is conceivable from inspection of Eq. 3.5 that, by clever manipulation, we could vary any and all of the parameters ρ_s , ρ_a , W_s , D , or \bar{U} in such a fashion that the coefficients would not be changed, and, therefore, that the plume trajectory would be unchanged, i.e., it would not be necessary to ignore the momentum term--we could include it too. This is equivalent to reducing the momentum and buoyancy lengths by the geometric scale reduction factor. Obviously, however, if we change D , we will also change the plume width at the stack exit ($=D$). This violates our previous requirement of geometric similarity; it may or may not have serious consequences, dependent upon the amount of the exaggeration and on the particular flow field. It is not entirely clear what extraneous effects may be introduced by the manipulation of the other variables.

Basically, the coefficients of the x/H_s terms in Eqs. 3.5 and 3.6 are products of similarity parameters, i.e.,

$$\frac{l_m}{H_s} = \frac{1}{2} \left(\frac{\rho_s W_s^2}{\rho_a U^2} \right)^{1/2} \left(\frac{D}{H_s} \right) \quad (3.10)$$

and

$$\frac{l_B}{H_s} = \left(\frac{1}{Fr_a^2} \right) \left(\frac{D}{H_s} \right) \left(\frac{\rho_s W_s^2}{\rho_a U^2} \right)^{3/2} \left(\frac{\rho_a}{\rho_s} \right)^{3/2} \quad (3.11)$$

If we insist on geometric similarity, then Eq. 3.10 is identical to our previous momentum matching requirement, and Eq. 3.11 is only very slightly different from our previous Froude number matching requirement. There is no reason, a priori, to favor one or the other; the choice will require experimental verification.

In a rather unusual derivation in a recent report, Skinner and Ludwig (1978) have arrived at scaling laws that are essentially equivalent to matching the ratios of momentum and buoyancy length scales to the stack height, i.e., Eqs. 3.10 and 3.11. They also conducted some experimental work showing that "enhanced" scaling (exaggerated density differences) produced the same results as "restricted" scaling (matched density differences), with both tests done in the wind tunnel. Further, they have pointed out the possibility of exaggerating the stack diameter, but they have not conducted tests to verify this.

3.1.4 Summary and Recommendations on Modeling Far-Field Plumes

Most likely more important than the decision on matching the momentum and buoyancy length scales versus diameter exaggeration versus matching of the Froude number and the momentum ratio are the effects of the approach flow, i.e., the stratification and ambient turbulence to which the plume is subjected, as well as the effects of downwash and flow diversion or channeling caused by buildings and terrain. These will be discussed further in later sections. For the present, the recommendation is to avoid a re-turbulent effluent flow and to avoid raising the stack, either physically or through the addition of momentum. Instead, the most advantageous of the methods discussed in Section 3.1.3.3 should be used.

Thus, to model the far-field rise of a buoyant plume from a stack, it is recommended that the modeler:

1. Insure a fully turbulent effluent flow and
2. Either (in order of decreasing "correctness"):
 - a) match $\frac{\rho_s W_s^2}{\rho_a U_s^2}$, $\frac{W_s}{(g D \Delta \rho / \rho_a)^{1/2}}$, and $\frac{D}{H_s}$,
 - b) match l_m/H_s and l_B/H_s ,
 - i) following geometric similarity or
 - ii) exaggerating the stack diameter, but avoiding stack downwash,
 - or c) match l_D/H_s ,
 - i) following geometric similarity or
 - ii) exaggerating the stack diameter, but avoiding stack downwash.

Obviously, if the stack diameter is exaggerated, other lengths are to be referenced to the stack height and not the stack diameter. It is implicit above that the simulated atmospheric boundary layer is matched and that geometric similarity is followed everywhere, with the possible exception of exaggerating the stack diameter as noted. Notice that under conditions 2b and c, that an exaggeration in stack diameter will generally be accompanied by a reduction in the momentum ratio. It must be remembered that the momentum ratio should not be reduced to the point where the plume is downwashed in the wake of the stack.

It is obvious that there are many unresolved problems concerning the modeling of plume rise, in spite of nearly 40 years of such modeling. Because of the lack of basic, systematic studies on these fundamental problems, the above recommendations are tentatively proposed and are subject to change pending future developments.

3.2 THE ATMOSPHERIC BOUNDARY LAYER

In the early wind tunnel studies of flow around buildings (Strom et al., 1957), complex terrain (Strom and Halitsky, 1953), and urban areas (Kalinske et al., 1945), care was taken to insure that the flow approaching the models was uniform and of low turbulence across the wind tunnel test section. Jensen (1958) was the first to suggest that the simulation of the atmospheric boundary layer was important; he was also the first to produce a simulated atmospheric boundary layer approach flow by matching the ratio of the roughness length to the building height between model and prototype. Strong variations in the surface pressure coefficient were observed along with variations in the cavity size and shape downwind from a building with different depths of boundary layers in wind tunnels by Jensen and Frank (1965) and Halitsky (1968). Tan-atichat and Nagib (1974) and Castro and Robins (1975) have shown that the nature, strength, and locations of vortices in the flow pattern around buildings differs markedly with and without a thick boundary layer approach flow. The wind shear and the presence of the ground produce a downward flow on the front face of a building, a reverse flow and an increase in speed upwind of the building, and high winds near the sides as sketched in Figure 11 (Hunt, 1975). It is now generally agreed that a thick boundary layer is essential if similar concentration fields are to be observed downwind of a model.

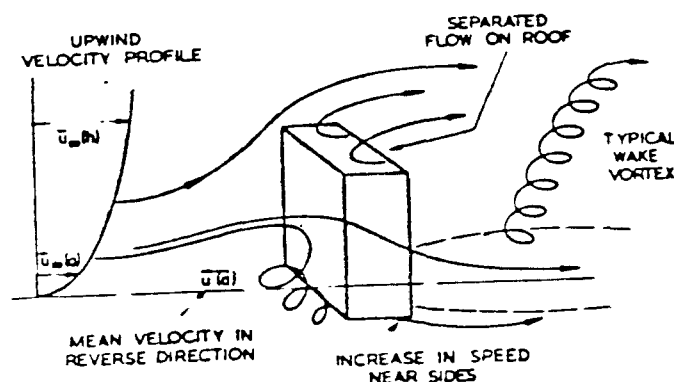


Figure 11. Effects of wind shear on the flow round a building (from Hunt, 1975).

Further, not just any thick boundary layer will do. It must simulate the atmospheric boundary layer structure, including as a minimum, the mean velocity profile and the intensity and spectral distribution of the turbulence. That the simulation of the spectrum is essential is evidenced in a report by Dean (1977). He attempted to duplicate the results of Snyder and Lawson (1976) at the somewhat smaller scale of 1:500 (compared with 1:300). The boundary layer depth was scaled properly and the mean velocity and turbulence profiles were reasonable facsimilies of those of Snyder and Lawson (S&L). However, when measuring concentration profiles in the boundary layer downwind from an isolated stack, he found a vertical plume width over 3 times that of S&L and a maximum concentration 1/9th as large, which was characteristic of Pasquill diffusion category A, highly unstable. A removal of the vortex generators, leaving the roughness strips intact, did not change the velocity or turbulence intensity profiles appreciably, but produced a marked change in the energy spectra, which in turn brought the plume width and maximum concentration to within a few percent of those of S&L, more nearly characteristic of category D, neutral stability.

If the atmospheric boundary layer is to be simulated in a wind tunnel or water channel, it is necessary to decide at some point just what characteristics can and should be matched. If adequate data are available describing the atmospheric boundary layer structure for the specific site to be modeled, it is, of course, more appropriate to use these data. But, generally, sufficient data are not available, so that some model must be chosen. For example, if we want to simulate the dispersion of pollutants from a stack in the atmospheric boundary layer, we need first to answer the question of what the approach flow should look like. What is a typical atmospheric boundary layer depth? What are appropriate parameters that describe atmospheric stability and what are

typical values for these parameters? How do the turbulence spectra vary with stability, height above ground, etc.? It is necessary to establish a goal to be met, say, a simplified analytical description, of the flow in the atmospheric boundary layer. The first part of this section (3.2.1) suggests some goals which the modeler should attempt to achieve. What we attempt to describe is the barotropic planetary boundary layer under steady-state and horizontally homogeneous conditions. The second part (Section 3.2.2) reviews the most promising techniques that have been tried for generating thick, neutral boundary layers simulating the atmospheric boundary layer. The third part (Section 3.2.3) reviews methods which appear promising for simulating stratified boundary layers. Finally, an attempt is made (Section 3.2.4) to summarize the previous sections and to establish guidelines for modeling of the atmospheric boundary layer. Because the discussion of Sections 3.2.1.1 and 3.2.1.3 go into considerable detail, the disinclined reader may wish to skip to the summaries (Section 3.2.1.2 and 3.2.1.4) for the essentials.

3.2.1 Characteristics of the Atmospheric Boundary Layer

The atmospheric boundary layer, alternately referred to as the Ekman layer, the friction layer, or the planetary boundary layer, is concerned with that portion of the atmosphere where the aerodynamic friction due to the motion of the air relative to the earth's surface is of prime importance. Above the boundary layer, the air motion is geostrophic, reflecting a balance between the horizontal pressure gradient and the Coriolis force, and the velocity obtained there is the gradient velocity. The depth of the boundary layer is highly variable, although it is typically between 1/2 and 2 km under neutral conditions. The overall boundary layer may be divided into at least 2 sub-

layers, principally the surface layer, also misnamed the constant stress layer¹, and a transition region above, wherein the shear stress diminishes from the nearly constant value in the surface layer to a near-zero value at the gradient height. The surface layer is typically 10 to 20 percent of the planetary boundary layer. Generally, the mean velocity profile in the surface layer is described by a logarithmic law. Above the surface layer there are numerous analytical expressions for describing the velocity profile. If the entire boundary layer is to be described by one expression, it is common engineering practice to use a power law.

Since Coriolis forces cannot be modeled in an ordinary type of facility, i.e., wind tunnel or water channel, modeling efforts should be restricted to those classes of problems where Coriolis forces are unimportant. As discussed in Section 2.2.1, Coriolis forces may be important under neutral or stably stratified conditions in relatively flat terrain when the length of the model exceeds approximately 5 km. It appears that, if the length scale of the field situation to be modeled is less than 5 km, Coriolis forces may be ignored. Likewise, if the terrain is rugged, so that the flow is highly dominated by local (advective) forces, Coriolis forces may be ignored. This restricted class of flows limits the usefulness of fluid modeling facilities, but there still exists a very large range of problems in which it is not at all unreasonable to ignore these effects.

3.2.1.1 The Adiabatic Boundary Layer

Picking a depth for the adiabatic (neutrally stable) boundary layer is no simple task. After an extensive review of the literature on adiabatic boundary layers, Counihan (1975) concluded that the boundary layer depth is 600m,

1. Strictly speaking, a constant stress layer exists only in a boundary layer with zero pressure gradient, which is seldom the case for the atmospheric boundary layer.

practically independent of wind speed and surface roughness. Davenport's (1963) scheme, which was previously accepted as the "standard" for wind tunnel studies of wind forces on buildings, specified the depth as a function of the roughness length z_0 only, varying from $\delta=300\text{m}$ at $z_0=0.03\text{m}$ to $\delta=600\text{m}$ at $z_0=3\text{m}$. Another popular scheme which is claimed to fit observations quite well is:

$$\delta = cu_*/f_c, \quad (3.12)$$

where δ is the boundary layer depth, u_* is the friction velocity ($=\sqrt{\tau_0/\rho}$), and f_c is the Coriolis parameter $2\omega \sin \phi$, where ω is the earth's rotation rate and ϕ is the latitude. In mid-latitudes, $f_c \sim 10^{-4}\text{sec}^{-1}$. Typical values for c range from 0.2 (Hanna, 1969) to 0.3 (Tennekes, 1973). To determine u_* using this scheme, it is customary to use the geostrophic drag law, which relates the 'drag coefficient' u_*/G to the surface Rossby number $G/f_c z_c$:

$$\ln \frac{G}{f_c z_0} = A + \ln \frac{G}{u_*} + \left(\frac{k^2 G^2}{u_*^2} - B^2 \right)^{1/2}, \quad (3.13a)$$

where G is the geostrophic wind speed (with components U_g and V_g), k is von Kármán's constant (0.4), and A and B are "constants" which differ considerably from one author to the next. From Blackadar and Tennekes (1968), A is about 1.7 and B about 4.7. For the sake of completeness, we also write the expression for the angle α between the surface stress and the geostrophic wind:

$$\sin \alpha = \frac{A}{k} \frac{u_*}{G}. \quad (3.13b)$$

These three schemes for specifying the boundary layer depth are compared in Figure 12, where it may be seen that they yield drastically different results. In view of the uncertainties involved and also because Counihan's (1975)

literature review showed no measurements of depths in excess of 600m, if specific measurements to the contrary are unavailable, the boundary layer should be assumed to be approximately 600m in depth. This value, as well as recommendations that follow, are not in any sense to be taken as absolute. They are recommended in the sense that in the absence of other data, these values are not unreasonable to use as a model. Also, many of Counihan's (1975) as opposed to Davenport's (1963) conclusions are repeated here because they are representative of a wider range of data and they are more thorough in the sense that more kinds of statistics are covered.

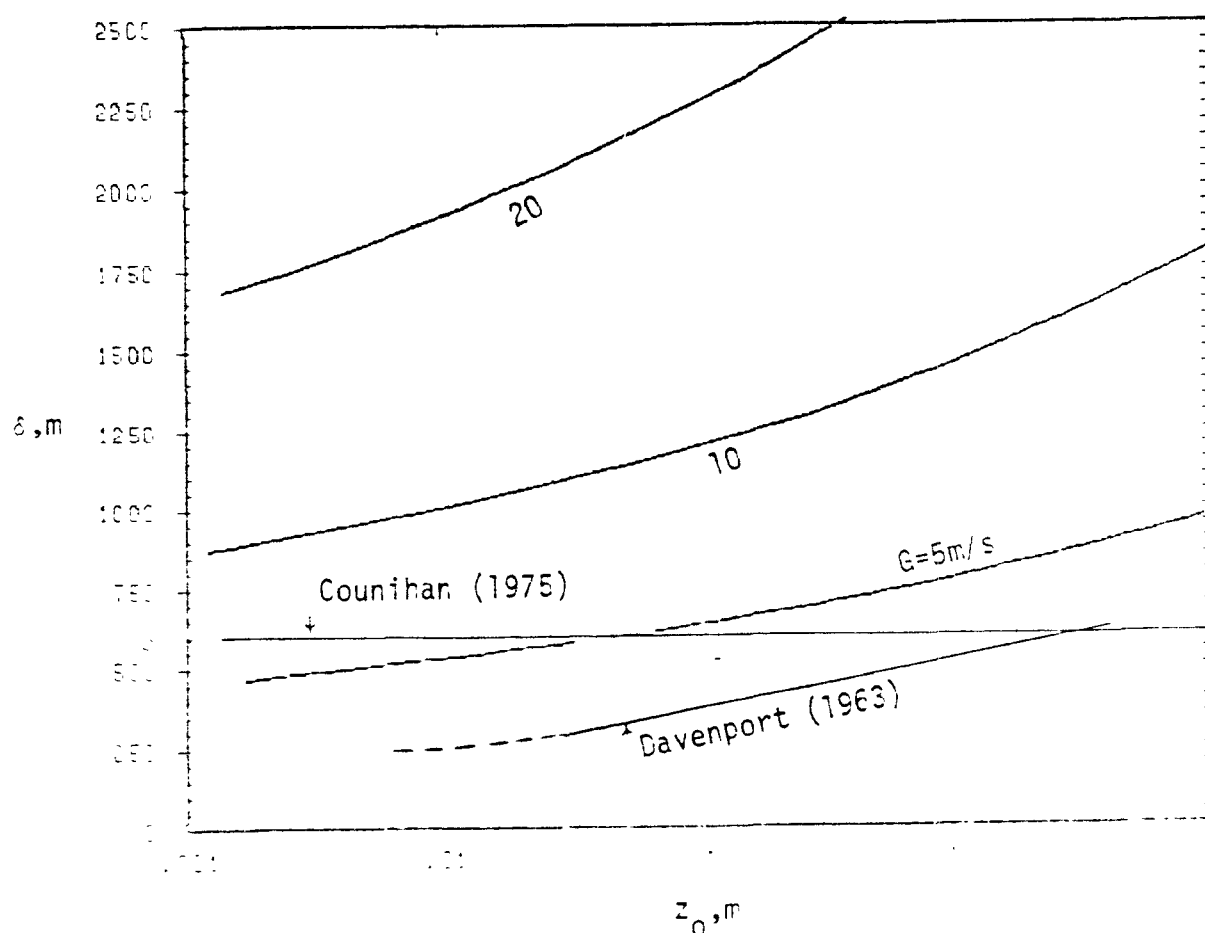


Figure 12: The depth of the adiabatic boundary layer according to the geostrophic drag law compared with other schemes.

The depth of the surface layer, in which the mean velocity profile follows a logarithmic law, and from which the roughness length may be defined, is generally stated to be 10 to 20% of the boundary layer depth. Counihan (1975) suggests a value of 100m as a reasonable average depth for the surface layer. The roughness length z_0 may be derived from the mean velocity profiles in the range $1.5h_r \leq z \leq 0.15\delta$:

$$\frac{U}{u_*} = \frac{1}{k} \ln \frac{z-d}{z_0}, \quad (3.14)$$

where h_r is the height of the roughness elements, and d is the zero plane displacement. The logarithmic profile is well established and has been amply demonstrated in wind tunnel boundary layers and in atmospheric profile studies over ideal sites with roughness varying from smooth ice to trees and buildings. In fact, Thompson (1978) has reported logarithmic wind profiles measured over highly rugged terrain and was able to extrapolate these profiles to obtain a roughness length of 35'. The logarithmic law is, in fact, frequently found to be a close approximation to the velocity profile to heights considerably beyond the "constant stress" layer (Panofsky, 1974).

Typical values of z_0 for various types of surfaces are given in Table 2 (from Simiu and Scanlan, 1978). It should be noted that the values quoted in Table 2 for suburbs, towns, and large cities are exceptionally small. Numerous authors (see Davenport, 1962, or Högström and Högström, 1978, for example) suggest values of 1 to 5m for urban areas. Duchêne-Marullaz (1975) suggested values greater than 2m, but on the assumption that the zero plane displacement d was zero. Secondly, it is well known that z_0 may vary with wind speed over the open ocean and over long grass and trees, but Pasquill (1971) cited evidence of z_0 increasing (as well as d decreasing) with increasing wind speed

over Central London, i.e., large and rigid roughness elements! He suggested that the cause may be due to the more vigorous turbulence scouring the buildings, with the air stream "penetrating" more deeply between buildings, thereby increasing both the inter-building wind speed and the depth of the building contributing effectively to the drag.

The zero plane displacement d may generally be neglected for terrain types where the roughness length is less than about 0.2m. It is suggested by Simiu and Scanlan (1978) that reasonable values of d in cities may be estimated using the formula

$$d = \bar{H} - \frac{z_o}{k} \quad , \quad (3.15)$$

where \bar{H} is the general roof-top level and k is the von Karman constant (0.4).

TABLE 2: Values of Surface Roughness Length (z_0) for Various Types of Surfaces (from Simiu and Scanlan, 1978).

Type of Surface	z_0 (cm)		
Sand	0.01	-	0.1
Sea Surface	0.0003 ^a	-	0.5 ^b
Snow Surface	0.1	-	0.6
Mown Grass (~0.01m)	0.1	-	1
Low Grass, Steppe	1	-	4
Fallow Field	2	-	3
High Grass	4	-	10
Palmetto	10	-	30
Pine Forest (Mean height of trees: 15m; one tree per 10m ² ; $z_d \approx 12m$)	90	-	100
Outskirts of Towns, Suburbs	20	-	40
Centers of Towns	35	-	45
Centers of Large Cities	60	-	80

^aWind speed at 10 m above surface = 1.5 m/sec.

^bWind speed at 10 m above surface > 15 m/sec.

The mean velocity profile throughout the entire depth of the boundary layer is adequately represented by a power law:

$$U/U_\infty = (z/\delta)^P, \quad (3.16)$$

where U_∞ is the mean velocity at the top of the boundary layer of depth δ and

p is the power law index. This form is popular in engineering practice and is highly useful from a practical viewpoint. Davenport (1963) claims that the overall reliability of the power law is at least as good as much more sophisticated expressions and it is recommended here for that reason. It was shown by Davenport to work quite well for high geostrophic winds. It should also work well for light winds as long as the atmosphere is neutral. Even for light winds in the atmosphere, Reynolds numbers are very large. The problem is not that the power law will not work for light winds, but that, especially under light winds, the atmosphere is seldom neutral. Figure 13 shows typical mean wind profiles and Figure 14 shows the variation of p with the roughness length z_0 (from Counihan, 1975). The power law index varies from about 0.1 in exceptionally smooth terrain such as ice to about 0.35 in very rough terrain such as built-up urban areas.

As shown by Counihan, the turbulence intensity at a 30 m elevation follows the same formula as the power law index; their numerical values as functions of roughness length are identical.

$$p = (\sqrt{u^2}/U)_{30m} = 0.24 + 0.096 \log_{10} z_0 + 0.016 (\log_{10} z_0)^2, \quad (3.17)$$

where z_0 is to be specified in meters. The scatter in the Reynolds stress measurements was considerable, and $-\overline{u'w'}/U_\infty^2$ could have been represented by the identical formula (3.17), but Counihan felt that would underestimate the stress in moderately rough terrain. Hence, he proposed, for the surface

$$\text{layer} \quad -\overline{u'w'}/U_\infty^2 = u_*^2/U_\infty^2 = 2.75 \times 10^{-3} + 6 \times 10^{-4} \log_{10} z_0 \quad (3.18)$$

which is also shown in Figure 14. Counihan does not suggest how $\overline{u'w'}$ varies with

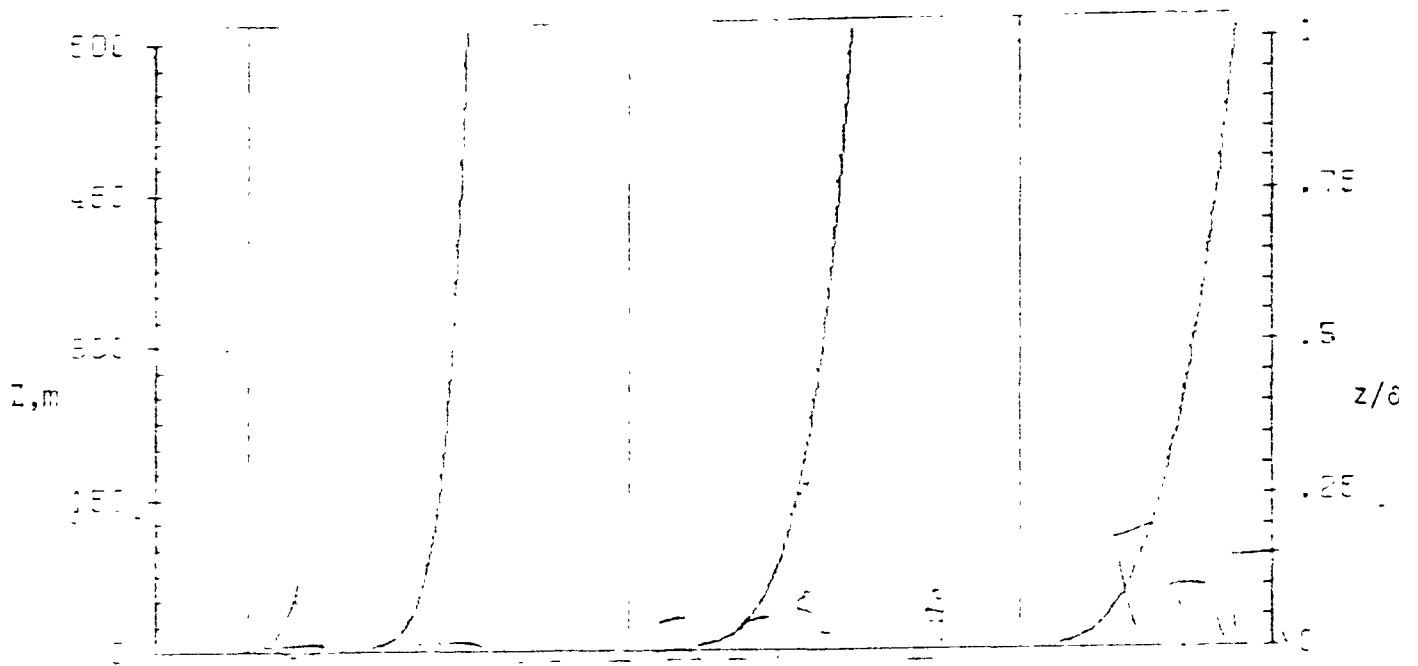


Figure 13: Typical wind profiles over uniform terrain in neutral flow.

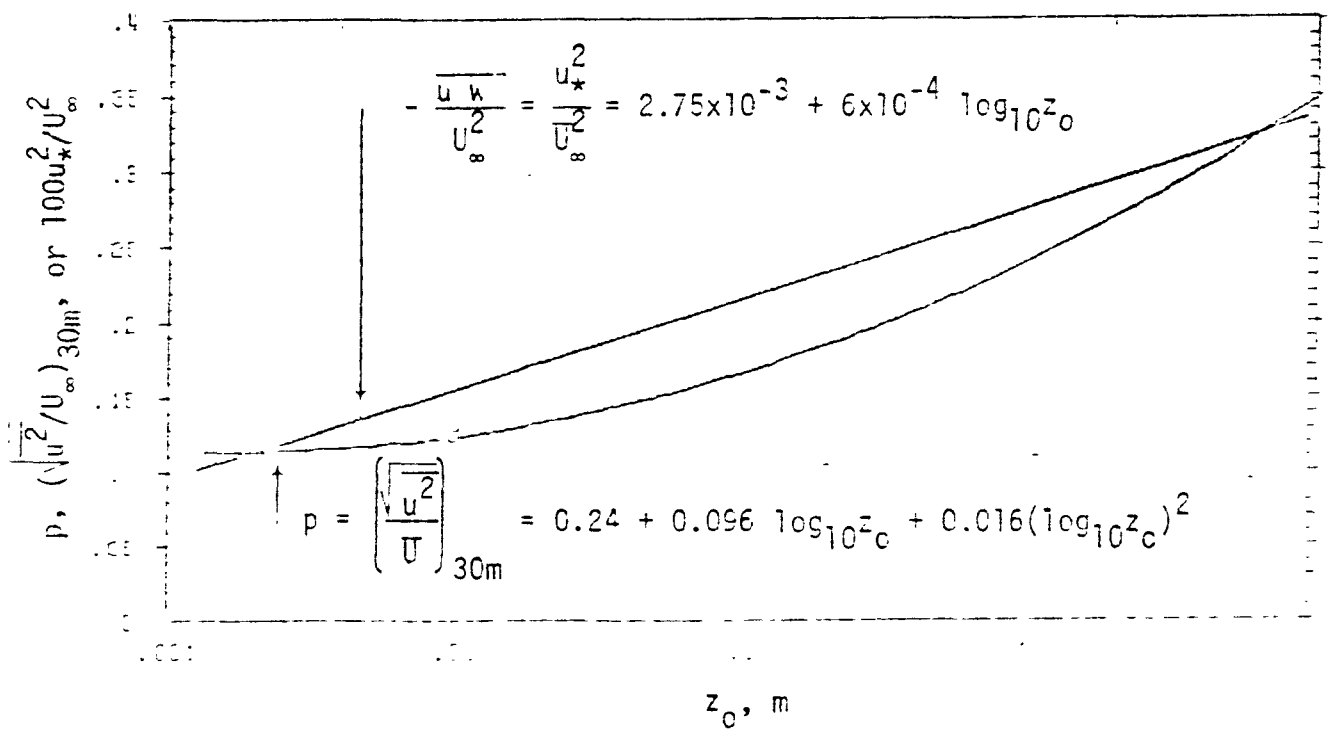


Figure 14: Variation of power law index, turbulence intensity, and Reynolds stress with roughness length in the adiabatic boundary layer (from Counihan, 1975).

height; he implies that Eq. 3.18 gives its "constant" value in the "constant stress" layer. A convenient approximation is a linear decrease with height from its surface value to zero at $z=\delta$.

$$-\overline{uw}(z) = (1-z/\delta)u_*^2 \quad (3.19)$$

Thus, at heights less than 0.1δ , the stress is within 10% of its surface value (see Figure 15).

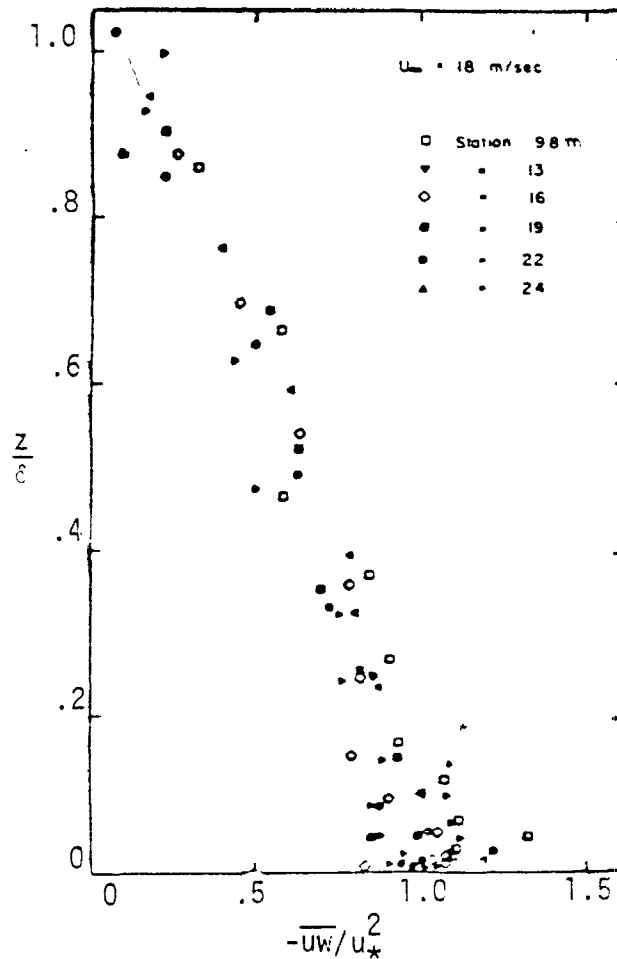


Figure 15. Shear stress distributions measured at various downwind positions in a wind tunnel boundary layer (neutral flow). Data from Zoric and Sandborn (1972).

These figures may be used for model design purposes in a number of ways. In a general type of study, such as diffusion over an urban area, they can be used directly to determine appropriate values for z_0 and p . Or, in a specific study, once U_∞ is chosen, one has only to determine z_0 (by measurement or estimation) and, since p , $\overline{u^2}/U$, and $-\overline{uw}/U_\infty^2$ are principally functions of z_0 , to obtain them from Figure 14. If it is desired to match the wind speed U_1 at a particular height z_1 , say, at the top of a stack, Eq. 3.16 may be rewritten as

$$U_1/U_\infty = (z_1/\varepsilon)^p$$

and the free stream wind speed (gradient wind) may be determined.

The variation of the longitudinal turbulence intensity in the surface layer is given by

$$\sqrt{\overline{u^2}}/\overline{U} = p \ln(30/z_0)/(\ln(z/z_0)) . \quad (3.20)$$

(This formula is slightly different from that of Counihan, but it is consistent with his data and other formulas. Counihan's formulation did not match Eq. 3.17 for the turbulence intensity at $z=30$ m for low values of z_0 and was somewhat ambiguous in the range $0.1 \text{ m} \leq z \leq 5 \text{ m}$.) Above the surface layer ($100 \text{ m} \leq z \leq 600 \text{ m}$), Counihan recommended assuming a turbulence intensity of 0.01 at 600 m and extrapolating to this value from the top of the constant stress layer. Several turbulence intensity profiles using this scheme are plotted in Figure 16. For the lateral and vertical turbulence intensities:

$$\sqrt{\overline{v^2}}/\overline{u^2} = 0.75 ; \sqrt{\overline{w^2}}/\overline{u^2} = 0.5 . \quad (3.21)$$

In spite of very wide scatter in the data and conflicting opinions in the literature, Counihan concluded that the longitudinal integral scale Lu_x

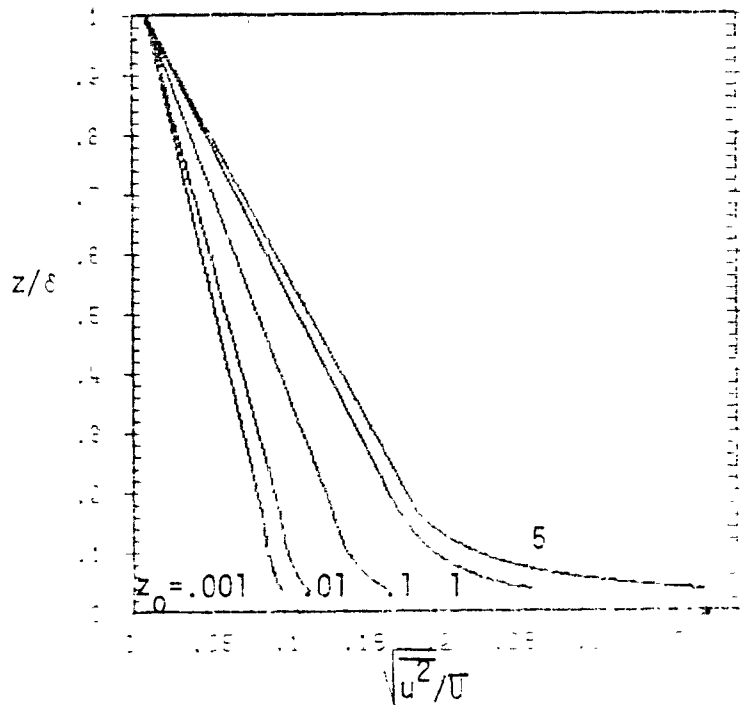


Figure 16. Variation of longitudinal turbulence intensity with height under adiabatic conditions.

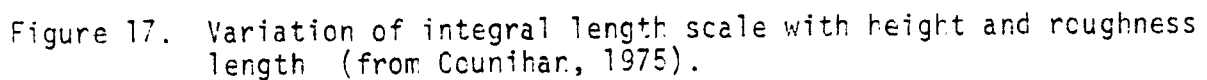
decreased with increase of surface roughness and increased with height up to 200-300 m. Above this level, Lu_x was independent of surface roughness and decreased with height. A summary showing the variation of Lu_x with elevation and roughness length is given in Figure 17. For other integral length scales, Counihan has concluded:

$$\left. \begin{array}{l} Lu_y = 0.3-0.4 Lu_x \\ Lu_z = 0.5-0.6 Lu_x \end{array} \right\} 10m \leq z \leq 240m, \quad (3.22a)$$

$$Lu_y = Lu_z = Lu_x/2 ; 240m \leq z \leq 600m, \quad (3.22b)$$

$$\text{and } Lw_x = 0.4z ; z \leq 100m. \quad (3.22c)$$

For the power spectral densities and the cospectrum of the Reynolds stress, we depart from Counihan and present empirical formulas from Kaimal et al. (1972) which were derived from extensive measurements in Kansas.



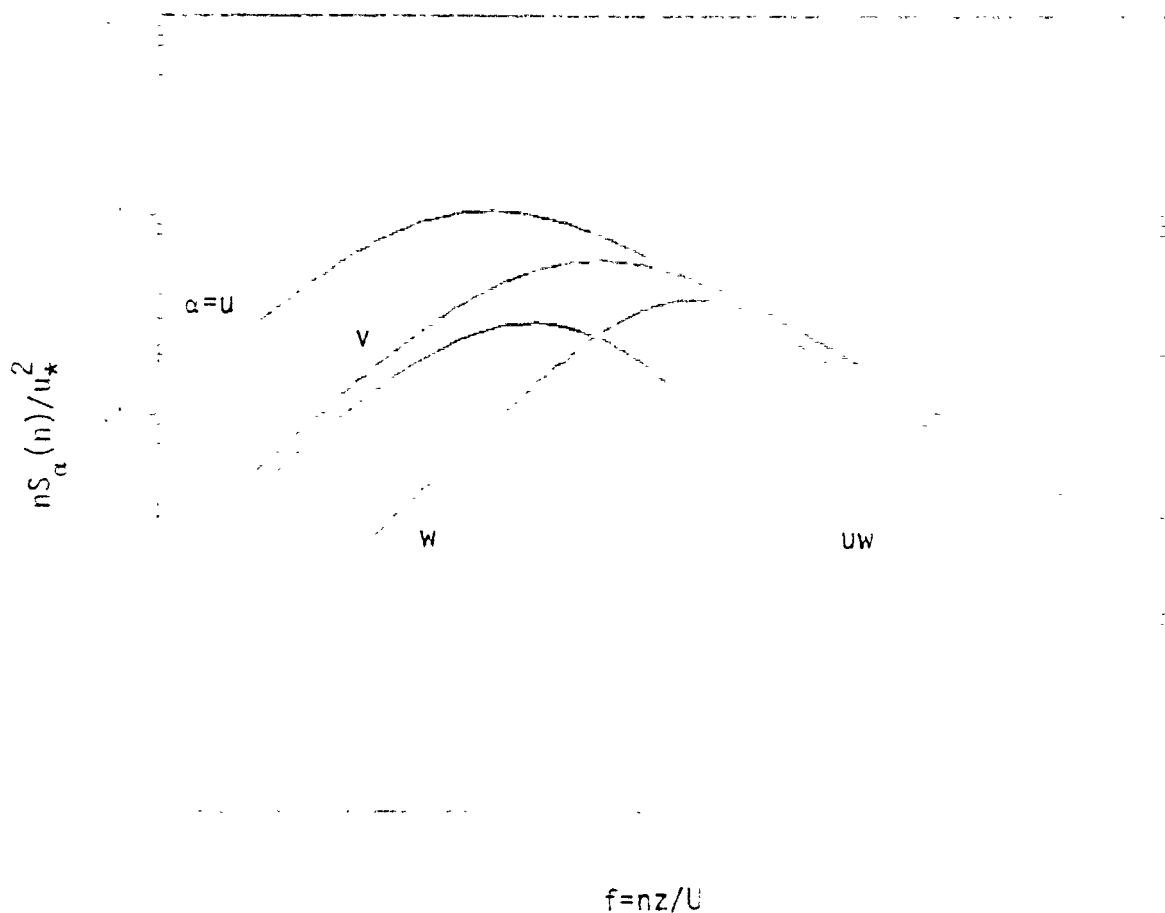


Figure 18. Empirical curves for spectra and cospectrum for neutral conditions (from Kaimal et al., 1972).

neutral atmospheric boundary layer!) This is very unfortunate, because, as was pointed out in the previous section, the larger scales of the turbulence are highly important in simulating diffusion.

3.2.1.2 Summary of the Adiabatic Boundary Layer Structure

If specific site data are available giving adequate information on the structure of the adiabatic boundary layer, it is, of course, most desirable to use those data as the target to simulate in the wind tunnel. If not, as is usually the case, it is recommended that the following model be used. For the sake of conciseness, justifications for the particular choices are

omitted here. The interested reader may consult the previous section and the references given there. Listed here are the main features of the steady state adiabatic boundary layer over horizontally homogeneous terrain (uniform roughness).

1. The depth δ of the boundary layer is 600m, independent of surface roughness and wind speed.
2. The mean velocity profile is logarithmic in the surface layer, which is 100m deep.
3. the roughness length z_0 and the friction velocity u_* may be derived from the mean velocity profile in the range $1.5h_r \leq z \leq 0.15\delta$:

$$\frac{U}{u_*} = 2.5 \ln \frac{z-d}{z_0} ,$$

where h_r is the general height of the roughness elements, and d is the displacement height (neglected for $z_0 < 0.2m$ and given by Eq. 3.15 for $z_0 < 0.2m$). Typical values for z_0 are given in Table 2.

4. The mean velocity profile through the entire depth of the boundary layer is represented by a power law $U/U_\infty = (z/\delta)^p$. The power law index p is a function of z_0 alone and may be obtained from Figure 14 or Eq. 3.17. It varies from 0.1 over smooth ice to 0.35 in built-up urban areas.
5. The Reynolds stress in the surface layer may be calculated as a function of z_0 from Eq. 3.18. Its vertical variation may be approximated as a linear decrease with height from its surface value (Eq. 3.18) to zero at $z=600m$ (Eq. 3.19).

6. The variation of the local longitudinal turbulence intensity with z_0 and elevation is shown in Figure 16. The vertical and lateral turbulence intensities are approximately half and three-quarters, respectively, of the longitudinal turbulence intensity.
7. The variation of the longitudinal integral length scale with z_0 and elevation is shown in Figure 17. Other integral scales may be obtained from Eqs. 3.22.
8. Spectral shapes are given by Eqs. 3.23 and shown in Figure 18.

3.2.1.2 The Diabatic Boundary Layer

In many ways, our knowledge of diabatic boundary layers, at least in the surface layers, is more extensive than that of adiabatic boundary layers. This is so because diabatic boundary layers are far more common and because the change in the surface heat flux is generally slow enough that the surface layer turbulence is able to track it, i.e., the boundary layer is *stationary* long enough that reasonably stable averages are more readily obtainable (Wyngaard, 1975). The depth of the boundary layer is highly dependent upon the stratification. During the day over land, the effective top of the boundary layer may usually be defined as the inversion height, i.e., a layer with stable density stratification exists at some height that is typically in the range of 0.5 to 2 km. On a cloudless night with light winds, the ground cooling generates a strongly stably stratified layer very close to the ground that suppresses the turbulence; the effective boundary layer, then, may be very shallow indeed, as low as a few tens of meters or even meters (Businger and Arya, 1974).

It is convenient at this point to discuss various parameters that characterize the stratification. (This discussion closely follows that of Eusinger, 1973.) The diabatic surface layer differs from the neutral one, of course, because of the presence of the heat flux that creates the stratification that very markedly affects the turbulence structure. This is clearly seen by examination of the turbulent energy budget equation (see, for example, Busch, 1973), where a very important production term appears that is proportional to the heat flux. Another production term is, of course, the mechanical term due to wind shear. Richardson (1920) introduced a stability parameter that represented the ratio, hence, the relative importance of these two production terms:

$$Ri = \frac{g}{\rho} \frac{\partial \theta / \partial z}{(\partial U / \partial z)^2}, \quad (3.24a)$$

where θ is mean potential temperature ($\theta = T + \gamma z$, where T is actual temperature and γ is the adiabatic decrease of temperature with height). This parameter is known as the gradient Richardson number or, simply, Richardson number. In deriving this stability parameter, it was assumed that the eddy transfer coefficients for heat and momentum were equal ($K_h = K_m$). Since this assumption is not quite valid, it is better to leave the flux terms in the form in which they appear in the energy equation, instead of assuming the fluxes are proportional to the gradients of the mean quantities. Hence, we have a flux Richardson number

$$Ri_f = \frac{G}{T} \frac{\overline{w\tau}}{\overline{uw} \partial U / \partial z}, \quad (3.24b)$$

where τ represents temperature fluctuations.

This parameter is rather difficult to determine because of the covariance terms, whereas the determination of Ri involved only the measurement of mean temperature and mean velocity separately as functions of height.

If we differentiate the expression for the logarithmic velocity profile (Eq. 3.14), we obtain $\partial U / \partial z = u_* / kz$. Substituting this expression into the flux Richardson number yields a dimensionless height

$$\frac{z}{L} = - \frac{g}{T} \frac{\overline{w\tau}}{u_*^3} kz$$

where

$$L = - \frac{\tau}{g} \frac{u_*^3}{k \overline{w\tau}} \quad (3.24c)$$

is the Monin-Obukhov (M-O) length. This length is a very useful stability parameter. It contains only constants and fluxes that are approximately constant throughout the surface layer (also called the constant flux layer, analogous to the constant stress layer in the neutral boundary layer). L therefore is a characteristic height that determines the structure of the surface layer. It has been found that many features of the turbulence in the surface layer depend solely upon the dimensionless height z/L . Such dependence is referred to as M-O similarity, which we will return to later in this section.

Another stability parameter is the Ekman-layer equivalent of z/L , i.e., it governs diabatic scaling in the entire boundary layer, much as z/L governs diabatic scaling in the surface layer (Tennekes, 1973).

$$u = \frac{ku_*}{f_c L} \quad (3.24d)$$

A final stability parameter is the Froude number

$$Fr = \frac{U}{\sqrt{gH\Delta\theta/\theta_H}} \quad (3.24e)$$

which was discussed in Section 2.2.4. The Froude number might characterize the stratification in the surface layer or that of the entire boundary layer, depending upon the height H chosen for specifying the velocity and the upper level for the temperature difference. More common in the meteorological literature is the inverse square of this Froude number, which is called the bulk Richardson number

$$Ri_B = \frac{gH\Delta\theta}{\theta_H U^2}.$$

To give the reader a "feel" for the magnitudes of these various stability parameters, we have listed typical values in Table 3. These values are not to be taken as definitions or as absolute in any sense. Particular values depend on the height chosen for specification of the wind speed and temperature and there is not, in any event, a one to one correspondence between the parameters.

With these stability parameters in hand, we will be able to specify many of the features of the diabatic boundary layer (albeit one that is steady and horizontally homogeneous). Let us first quantify our rather qualitative description earlier in this section of the boundary layer depth.

According to Hanna (1969), the formula

$$\delta = \frac{0.75 U_g}{\left(\frac{g}{T} - \frac{\Delta\theta}{\Delta z} \right)^{1/2}}, \quad (3.25a)$$

where $\Delta\theta/\Delta z$ is the average vertical gradient of potential temperature through the boundary layer, agrees well with observed boundary layer thicknesses.

This equation implies that the bulk Richardson number $g\delta\Delta\theta/(TU_g^2)$ equals 0.56

Table 3: Typical Values for the Various Stability Parameters.

Qualitative Description	Pasquill-Gifford Category	L,m	z/L	Pi_f	Pi	Ri_B^a	Fr	u_* ,m/s ^b	
Highly Unstable	A	-5	-2	-5	-2	-0.03	-	-4000	.3
Unstable	B	-10	-1	-2	-1	-0.02	-	-120	.3
Slightly Unstable	C	-20	-0.5	-1	-0.5	-0.01	-	-60	.3
Neutral	D	∞	0	0	0	0	∞	0	.3
Slightly Stable	E	100	0.1	0.07	0.07	0.004	16	12	.3
Stable	F	20	0.5	0.14	0.14	0.02	7	40	.2
Highly Stable	G	10	1	0.17	0.17	0.04	5	40	.1

- (a) The assumed height of the anemometer and upper thermometer was 10 m; the lower thermometer: 2 m. A roughness length of 0.01 m was also assumed in the calculations.
- (b) The friction velocity listed is that value used in calculating u_* .

for all stable boundary layers, i.e., the boundary layer adjusts itself until this criterion is met.

Arya (1977), to the contrary, claims that observations indicate that the bulk Richardson number increases with increasing stratification and may approach a constant (critical) value only under extremely stable conditions. He, Businger and Arya (1974), Wyngaard (1975), Brost and Wyngaard (1978) and others using widely differing theoretical approaches all arrive at the simple form for the height where the stress is some specified small fraction of the surface value:

$$z/L = a u_*^{1/2} \quad \text{or} \quad \delta = a (L u_* / f_c)^{1/2} \quad (3.25b)$$

where a is a constant and $\mu_* = u_* / f_c L$ is a stability parameter related to Eq. 3.24d through $\mu = k_L \mu_*$. The constant a , however, is highly dependent upon the value chosen for the stress criterion. For a 1% stress criterion, Businger and Arya (1974) find $a=0.72$, whereas for 5%, $a=0.4$. The latter value is supported by the second order closure model of Brost and Wyngaard (1978) over a wide range of cooling rates. Comparisons with Wangara data (Arya, 1977) show very large scatter, and that $a=1$ would be a much better fit.

To estimate u_* , the geostrophic drag relation (Eq. 3.13) is used, where the "constants" A and B are functions of the stability parameters. In a critical review, Arya (1977) has suggested

$$A = \ln(\delta/L) - 0.96(\delta/L) + 2.5 \quad (3.26a)$$

and
$$B = 1.15\delta/L + 1.1, \quad (3.26b)$$

where δ is determined from Eq. 3.25b with $a=1$. (This is obviously an iterative procedure in that Eqs. 3.13, 3.25, and 3.26 all involve u_* , which we are attempting to determine.)

Finally, an interpolation formula suggested by Deardorff (1972), i.e.,

$$\delta = \left(\frac{1}{30L} + \frac{f_c}{0.25u_*} + \frac{1}{z_T} \right)^{-1} \quad (3.27)$$

in which z_T is the height of the tropopause, does not suffer from "blowing up" under neutral conditions (where $L \rightarrow \infty$) near the equator (where $f_c \rightarrow 0$);

$\delta \rightarrow 0.25u_*/f_c$ under neutral conditions in mid-latitudes (i.e., Eq. 3.12) and $\delta \rightarrow 30L$ under very stable conditions and/or in low latitudes. Eq. 3.27 yields results comparable to Eq. 3.25b in mid-latitudes (see Figure 19).

The unstable boundary layer is almost always capped by an inversion at some elevation. It is now generally agreed that the height of this boundary

layer is determined by the height of the base of the inversion, i.e., $\delta = z_i$ (Deardorff, 1972, Wyngaard et al., 1974). The height of the inversion base varies from day to day, but its diurnal trend is quite similar. Kaimal et al. (1976) describe their observations in the Minnesota experiments as follows:

"Between sunrise and local noon (1300 CDT) z_i grew rapidly in response to the steadily increasing heat flux (Q_0). The growth of z_i slowed down between 1300 and 1600 CDT as Q_0 reached its maximum value. But as Q_0 decreased through the late afternoon, z_i began to level off to a nearly constant value which it maintained even after Q_0 turned negative."

Even though this convective boundary layer depth changes rather rapidly with time, there is justification for treating its midday structure as if it were in steady state, or at least in a condition of moving equilibrium or quasi-steady state (Kaimal et al., 1976). To predict the height of this boundary layer, Deardorff (1974) and Arya (1977) recommended a rate equation. For purposes of fluid modeling, it is sufficient to pick typical values, i.e., $\delta \approx 1$ to 2 km, as the typical maximum height for the inversion base is 1 to 2 km. Once a boundary layer height is chosen, we can estimate u_{*} from the geostrophic drag relation, Eq. 3.13, where the parameters A and B are functions of the stability parameters δ/L and $f_c \delta/u_{*}$ (Arya, 1977).

$$A = \ln(-\delta/L) + \ln(f_c \delta/u_{*}) + 1.5 \quad (3.28a)$$

$$B = k(f_c \delta/u_{*})^{-1} + 1.8(f_c \delta/u_{*}) \exp(0.2\delta/L) \quad (3.28b)$$

Figure 19 shows predicted boundary layer depths from Eqs. 3.25b and 3.27. It may be seen why the neutral boundary layer depth is so difficult to determine; only slight departures from neutrality effect drastic changes in its depth. Figure 20 shows how the friction velocity u_{*} varies with stability as predicted

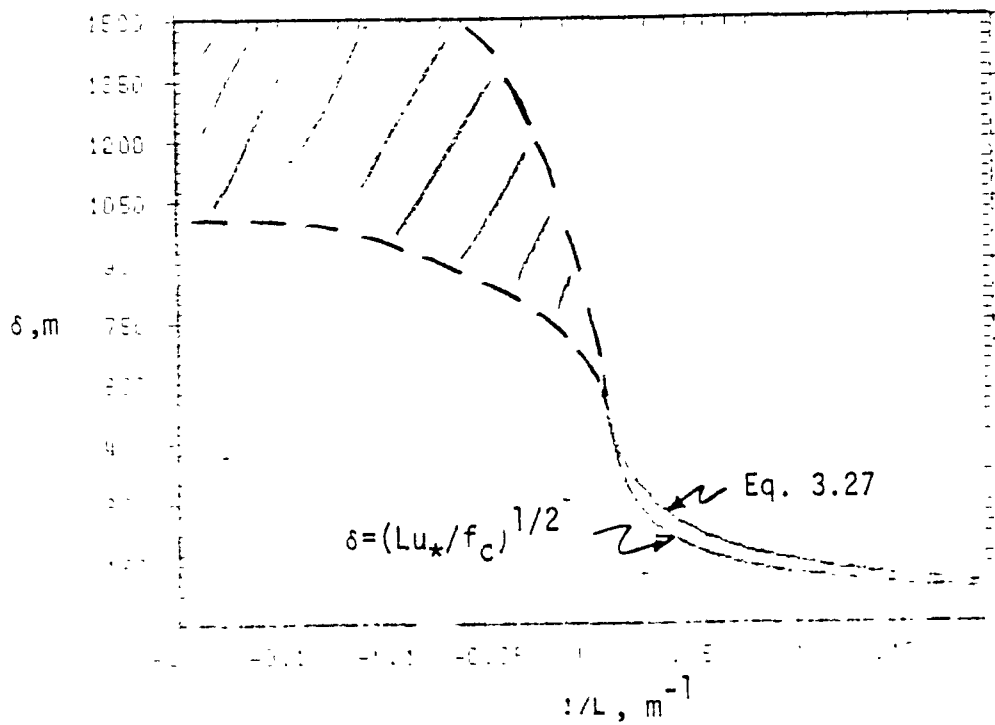


Figure 19. Typical nonadiabatic boundary layer depths from the geostrophic drag relations ($G=10\text{m/s}$, $z_0=0.01\text{m}$, $z_T=10\text{km}$, $f_c \approx 10^{-4}/\text{s}$, $a=1$).

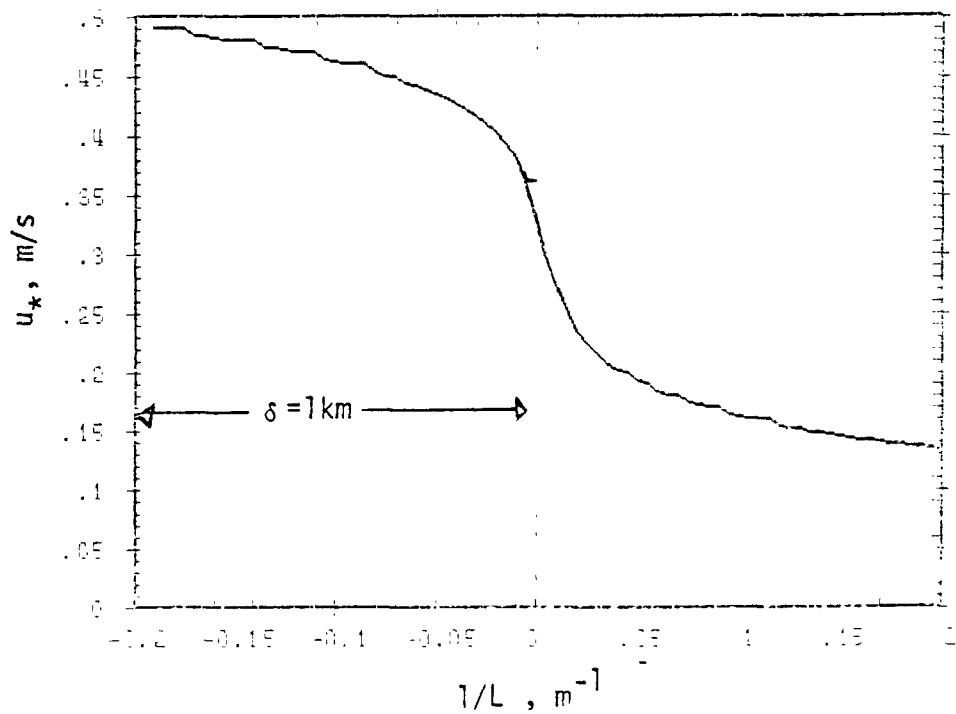


Figure 20. Variation of friction velocity with stability from the geostrophic drag relations (Eqs. 3.13, 3.26, 3.28, $G=10\text{m/s}$, $z_0=0.01\text{m}$, $z_T=10\text{km}$).

from the geostrophic drag relations using Eqs. 3.26 and 3.28.

Regarding the mean wind profile under non-neutral conditions, DeMarrais (1959) has measured the power law index p and has drawn the following general conclusions:

"During the day, when superadiabatic conditions and neutral lapse rates prevail, the values of p vary from 0.1 to 0.3. This variation is principally in proportion to the roughness of the terrain. At night, when stable, isothermal, and inversion conditions exist, the value of p generally varies from 0.2 to 0.8; this variation is proportional to the degree of stability and the roughness of the underlying terrain."

Panofsky et al. (1960) have used a formula due to Ellison (1957) to derive a theoretical relationship for p as a function of z_0 and $1/L$ (L is the M-O length). Irwin (1978a) has, analogously to Panofsky et al., used results of Nickerson and Smiley (1975) to establish a theoretical relationship between p , z_0 and $1/L$. The results, shown in Figure 21, support DeMarrais' (1959) conclusions reasonably well.

Air pollution meteorologists frequently use Pasquill stability classes (or similar groupings) to categorize atmospheric diffusion. Golder (1972) has related the qualitative Pasquill classes to more definitive measures of stability through analysis of a large number of observations at 5 sites. Irwin (1978a) has taken Golder's results relating Pasquill classes to the Monin-Obukhov length and roughness length and overlaid them as shown in Figure 21. Irwin (1978b) has further plotted the variation of p with z_0 where the Pasquill stability class is a parameter (see Figure 22). It may be seen from Figures 21 and 22 that the shape of the wind profile is much more strongly dependent on stability than on the roughness length under stable con-

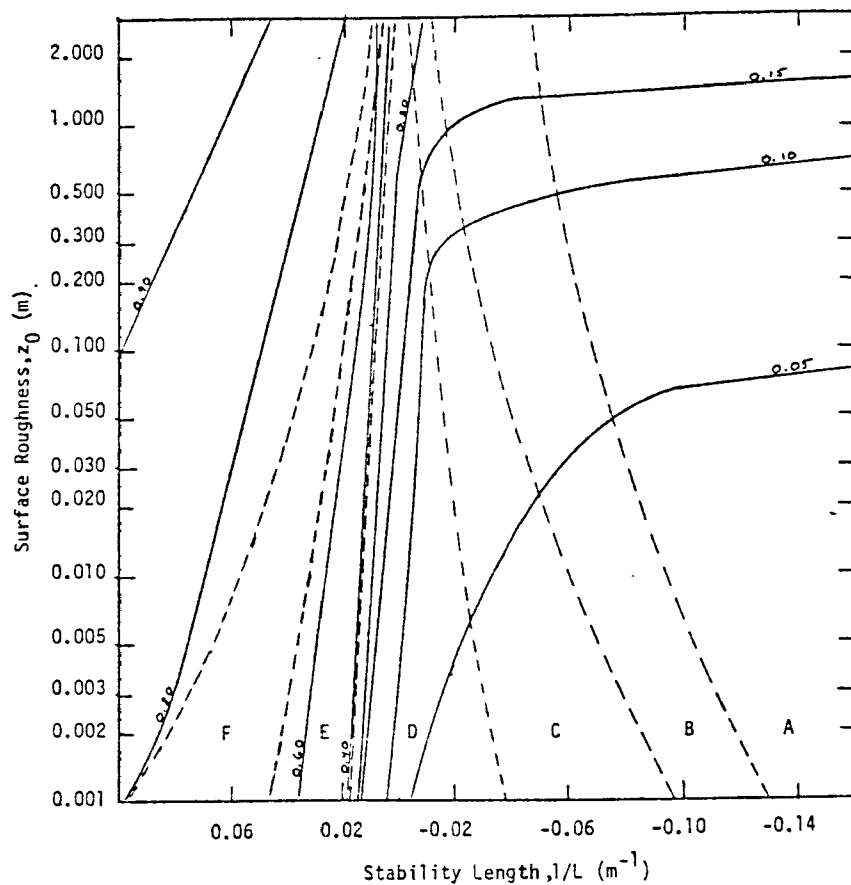


Figure 21. Theoretical variation of the power-law exponent as a function of z_0 and L for z equal to 100m. The dashed curves overplotted are the limits defined by Golder (1972) of the Pasquill stability classes as adapted by Turner (1964) (from Irwin, 1978a).

ditions. It is relatively insensitive to stability but more dependent upon roughness under unstable conditions. Comparisons (and tailoring) of Irwin's results with field data of DeMarrais (1959), Touma (1977) and Izumi (1971) agreed well and explained reported differences in exponent values. His theoretical predictions compare very well with Counihan's (1975) results for neutral conditions, i.e., stability class D (see Figure 22).

In the above discussions, we have largely ignored the influence of the earth's rotation because this feature, in general, cannot be simulated realis-

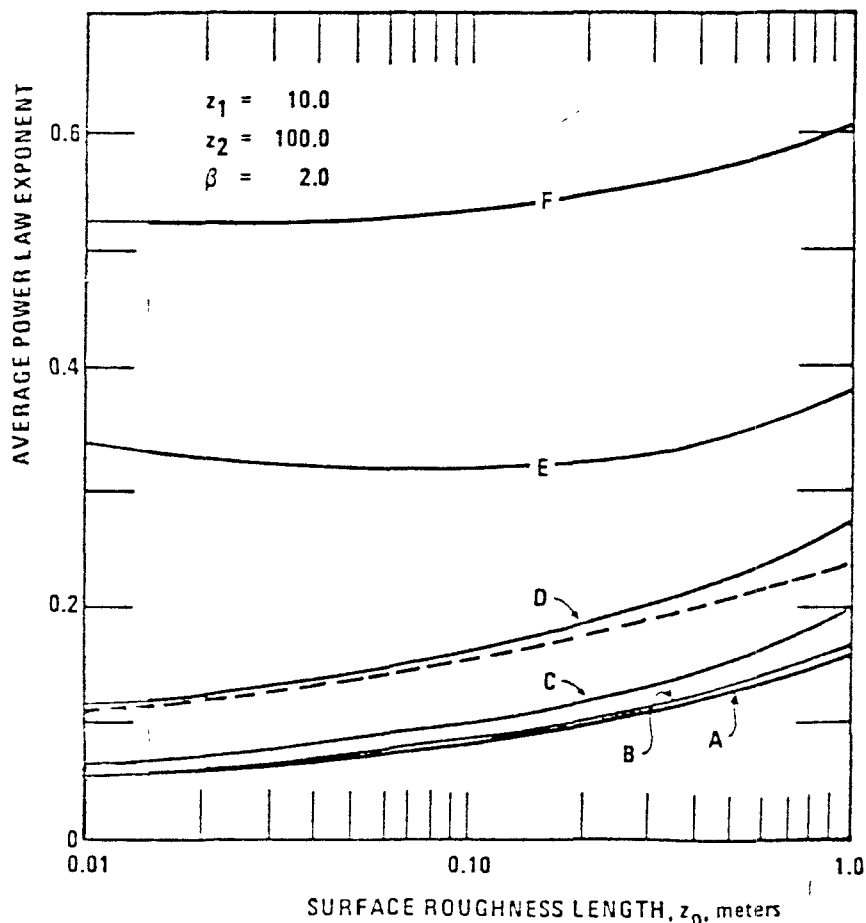


Figure 22. Variation of the power-law exponent p , averaged over layer from 10m to 100m, as a function of surface roughness and Pasquill stability class. Dashed curve is result suggested by Counihan (1975) for adiabatic conditions which should agree with stability class D. (from Irwin, 1978b).

tically in laboratory facilities in any event. On the other hand, many features of the surface layer can be well simulated. Panofsky (1974) has suggested that we further subdivide the Ekman layer (overall boundary layer) into a tower layer, i.e., below 150m or so in neutral or unstable conditions. The surface layer proper extends to approximately 30m, but many of the relationships developed for the surface layer may be extended to the tower layer; whereas the earth's rotation may be important in the tower layer (it was not in the surface layer), the turning of the wind can be ignored. In stable air, this subdivision is useless because significant turning may start at much

lower heights. In the discussion to follow, then, we will discuss in detail various properties of the surface layer that may possibly be extended to the tower layer in neutral and unstable conditions.

It is customary in discussing surface layer profiles and fluxes to define nondimensional vertical gradients of wind speed and potential temperature as

$$\phi_m = \frac{kz}{u_*} \frac{\partial U}{\partial z}, \quad \phi_h = \frac{z}{\theta_*} \frac{\partial \theta}{\partial z} \quad (3.29)$$

where $\theta_* = -\overline{w\theta}/u_*$. It has been found that these nondimensional gradients are functions of z/L only (M-O similarity). In unstable air,

$$\phi_m = (1 - 15z/L)^{-1/4} \quad z/L < 0 \quad (3.30)$$

fits surface observations quite well (Panofsky, 1974). The expression can be integrated to obtain the mean velocity profile (Paulson, 1970):

$$\begin{aligned} U/u_* = (1/k) \left\{ \ln(z/z_0) - 2 \ln \left[\frac{1}{2} (1 + 1/\phi_m) \right] - \ln \left[\frac{1}{2} (1 + 1/\phi_m^2) \right] \right. \\ \left. + 2 \tan^{-1}(1/\phi_m) - \pi/2 \right\}. \end{aligned} \quad (3.31)$$

This formulation is consistent in that under neutral conditions $L \rightarrow \infty$, $\phi_m \rightarrow 1$, and Eq. 3.31 reduces to the familiar log law. Panofsky (1974) showed that $\phi_m = (1 - 15z/L)^{-1/3}$ fit various data sets better than Eq. 3.30 for large values of $|z/L|$.

In stable air

$$\phi_m = 1 + 5z/L, \quad z/L > 0 \quad (3.32)$$

integrates to the familiar log-linear wind profile:

$$U/u_* = (1/k)[\ln z/z_0 + 5z/L]. \quad (3.33)$$

Figure 23 shows typical velocity profiles as predicted by Eqs. 3.31 and 3.33.

The behavior of the nondimensional temperature gradient ϕ_h is somewhat controversial. For simplicity we will here list the forms given by Panofsky (1974)

$$\phi_h = (1-15z/L)^{-1/2}, \text{ for } z/L < 0, \quad (3.34a)$$

and
$$\phi_h = 1+5z/L, \text{ for } z/L > 0. \quad (3.34b)$$

These expressions integrate to

$$(\theta - \theta_0)/\theta_* = \ln(z/z_0) - 2 \ln[(1+1/\phi_h)/2], \text{ for } z/L < 0 \quad (3.35a)$$

$$(\theta - \theta_0)/\theta_* = \ln(z/z_0) + 5z/L, \text{ for } z/L > 0, \quad (3.35b)$$

where θ_0 is the extrapolated temperature for $z=z_c$ (not necessarily the actual surface temperature). Typical temperature profiles as predicted by Eqs. 3.35 are shown in Figure 24. It is useful in interpreting Figure 24 to note that θ_* and $(\theta - \theta_0)$ change sign simultaneously, so that the slopes of the curves are always positive. It is also interesting to note that the limit as $L \rightarrow \infty$ is the same as the limit as $L \rightarrow -\infty$, i.e., a logarithmic temperature distribution, which is not the same as adiabatic, where the potential temperature would be uniform with height. This is an anomaly in the mathematics, because both numerator and denominator of the left hand sides of Eqs. 3.35 approach zero simultaneously as the surface temperature approaches the fluid temperature.

Another useful relationship is that between the gradient Richardson number and z/L :

$$Ri = -z/L \left(\frac{\partial \phi_h}{\partial z} \right)^2 \quad (3.36a)$$

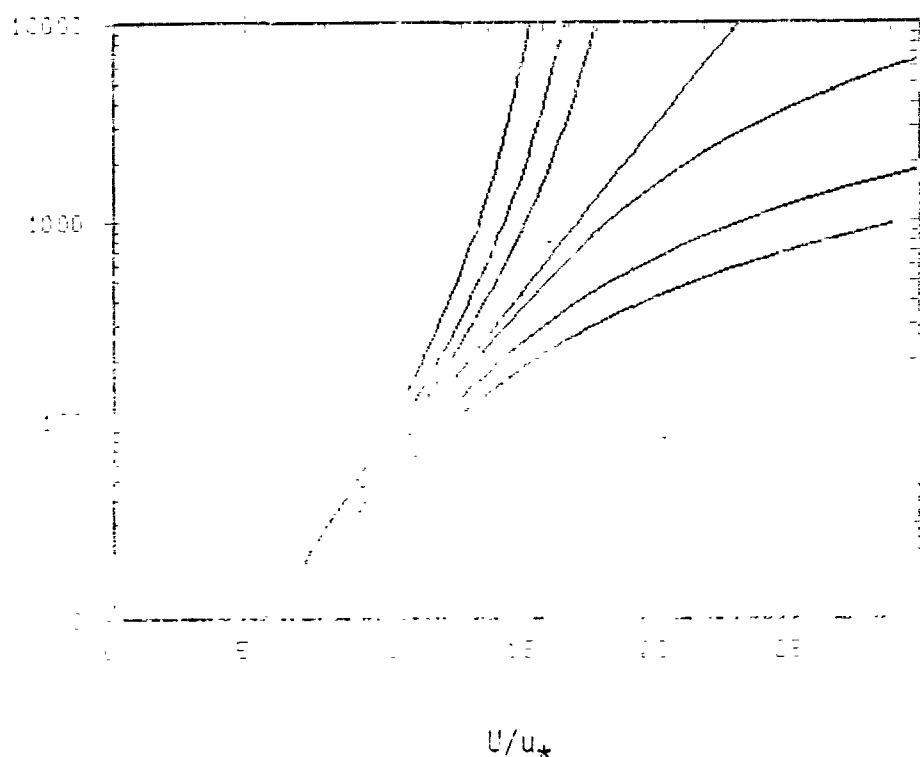


Figure 23. Typical surface layer velocity profiles under nonadiabatic conditions (from Eqs. 3.31 and 3.33 with $z_0=0.01\text{m}$).

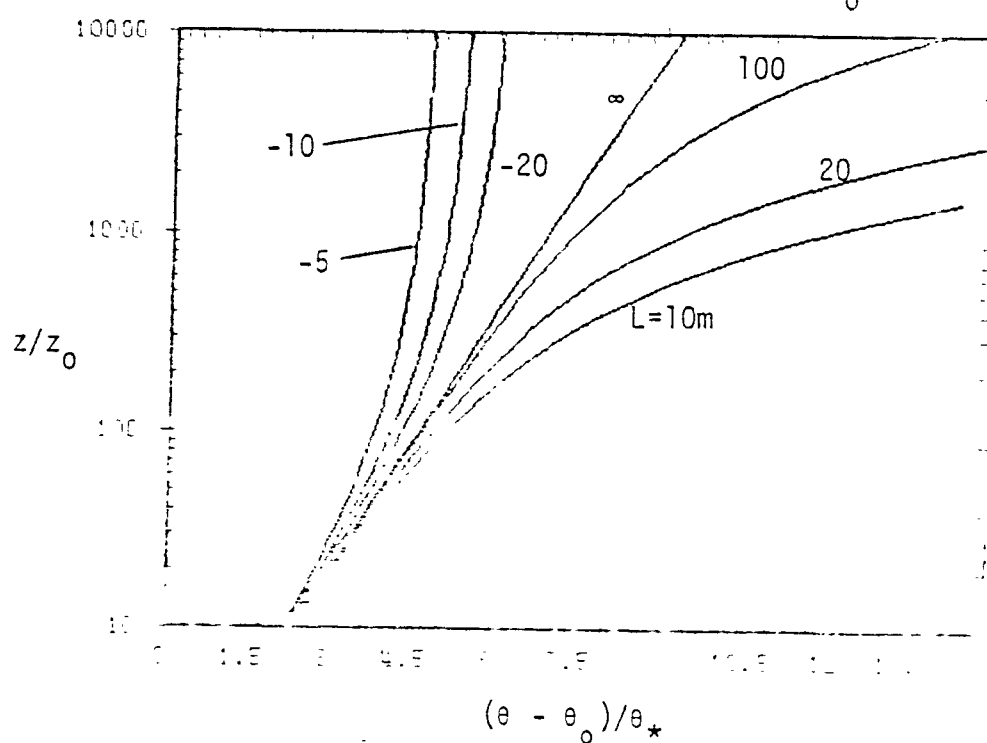


Figure 24. Typical temperature profiles in the surface layer (from Eqs. 3.35 with $z_0=0.01\text{m}$).

or
$$Ri = z/L , \text{ for } z/L < 0 \quad (3.36b)$$

$$Ri = \frac{z/L}{(1+5z/L)} , \text{ for } z/L > 0 . \quad (3.36c)$$

This relationship is shown in Figure 25.

Variances

The variance of the vertical velocity $\sigma_w = \sqrt{w^2}$ follows Monin-Obukhov scaling, so that

$$\sigma_w = u_* \phi_w(z/L) , \quad (3.37a)$$

where ϕ_w is a universal function. According to Panofsky (1974)

$$\phi_w = \begin{cases} \sim 1.25 & \text{for } z/L > -0.3 (\text{including all } z/L > 0) \\ 1.9(-z/L)^{1/3} & \text{for } z/L < -1 \end{cases} . \quad (3.37b)$$

The variance of temperature also follows M-O similarity, so that

$$\sigma_T = \theta_* \phi_\theta(z/L) , \quad (3.38a)$$

where ϕ_θ is also a universal function, which, according to Panofsky (1974)

$$\phi_\rho = \begin{cases} 0.95(-z/L)^{-1/3} & \text{for } z/L < -0.1 \\ 1.8 & \text{for } z/L \geq 0 \end{cases} . \quad (3.38b)$$

ϕ_w and ϕ_θ are shown in Figure 26.

The variances of the horizontal velocity components σ_u and σ_v do not appear at present to follow any discernable pattern and do not obey M-O similarity (but see later discussion in this section of the convective boundary layer). This is evidently due to the low-frequency contributions to these variances that are possibly due to large scale terrain features or circulation systems of large horizontal extent unaccounted for in M-O theory. Part of the problem may also be due to the difficulty in separating fluctuations from means in the original time series, i.e., the "spectral gap" may not be so clearly defined.

Nevertheless, various authors have attempted to force their observations to fit M-O scaling

$$\sigma_u = u_* \phi_u(z/L) , \quad \sigma_v = u_* \phi_v(z/L) . \quad (3.39)$$

The "constants" $\phi_u(0)$ and $\phi_v(0)$ for neutral stratification vary from 1.5 to 3 with "mean" values of 2.5 and 1.9, respectively. Observations of the variation of σ_u and σ_v with height often show little attenuation, but there are notable exceptions where slow and rapid decreases have been observed even in unstable air (see Panofsky, 1974).

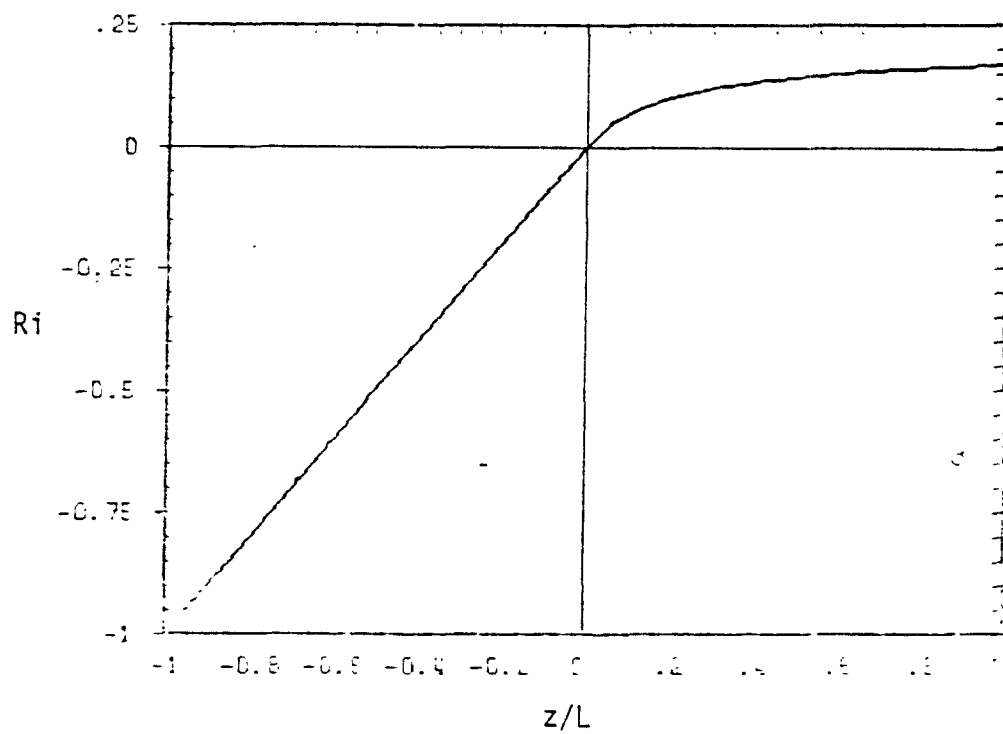


Figure 25. The relationship between Ri and z/L (Eqs. 3.36).

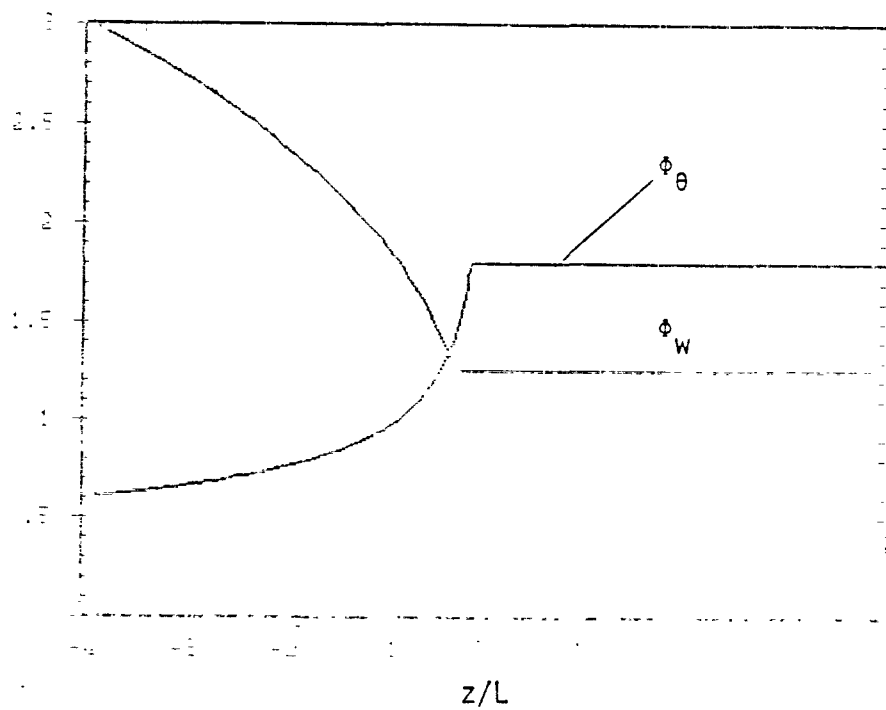


Figure 26. Variation of ϕ_w and ϕ_θ with z/L in the surface layer (Eqs. 3.37 and 3.38).

Birkowski (1975) has derived expressions for Φ_u and Φ_v that fit through the middle of the very wide scatter of the Kansas and Minnesota data. Due to the complexity of the formulas, they are not repeated here, but are shown in Figures 27 and 28.

Spectral forms are taken from Kaimal et al. (1972) and Kaimal (1973). Spectra of vertical velocity and temperature fluctuations were found to be M-0 similar as were the variances, and to have universal forms when appropriately normalized. Hence,

$$\frac{n S_{\alpha}(n)}{\alpha^2} = \frac{0.16 f/f_0}{1+0.16(f/f_0)^{5/3}}, \quad (3.40)$$

where $\alpha=w$ or θ , n is the cyclic frequency (Hz), f is a reduced frequency nz/\bar{U} , and f_0 is the intercept of the inertial subrange spectrum with the $n S_{\alpha}(n)/\alpha^2=1$ line. The normalization of f by f_0 aligns the peaks on the frequency axis, although f_0 is not itself the frequency with maximum energy. Instead,

$$f_{m\alpha} \approx 4 f_{0\alpha}. \quad (3.41)$$

Spectral shapes of longitudinal and lateral velocities were M-0 similar only under stable conditions ($z/L > 0$). The universal spectral shape is shown in Figure 29, and the variation of the peak frequency with z/L is shown in Figure 30.

The integral scales are difficult to evaluate directly from the spectra;

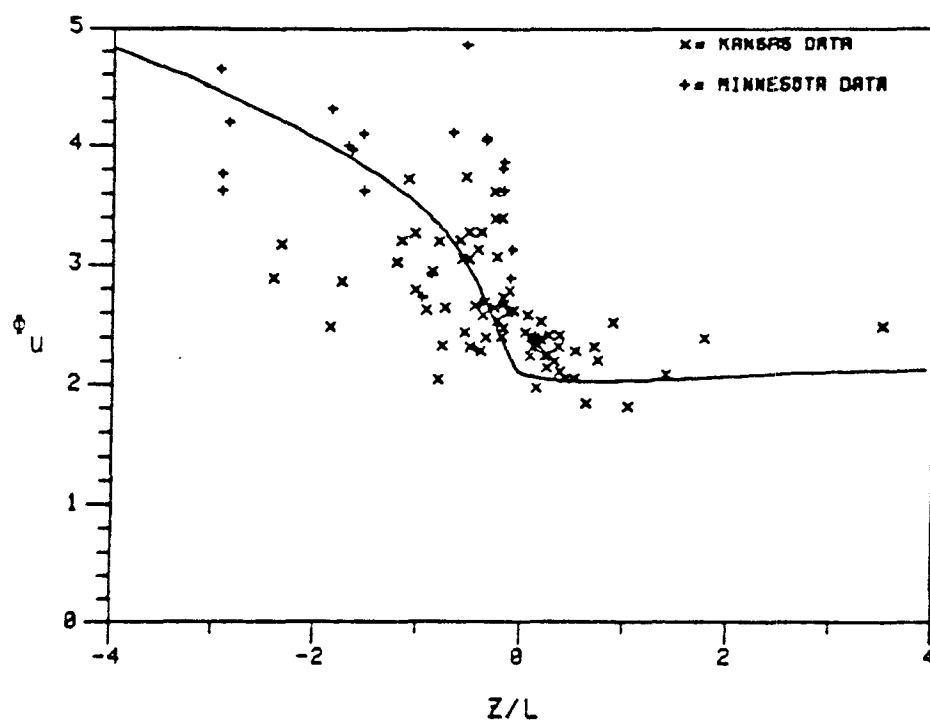


Figure 27. Variation of ϕ_U with z/L in the surface layer (from Binkowski, 1979).

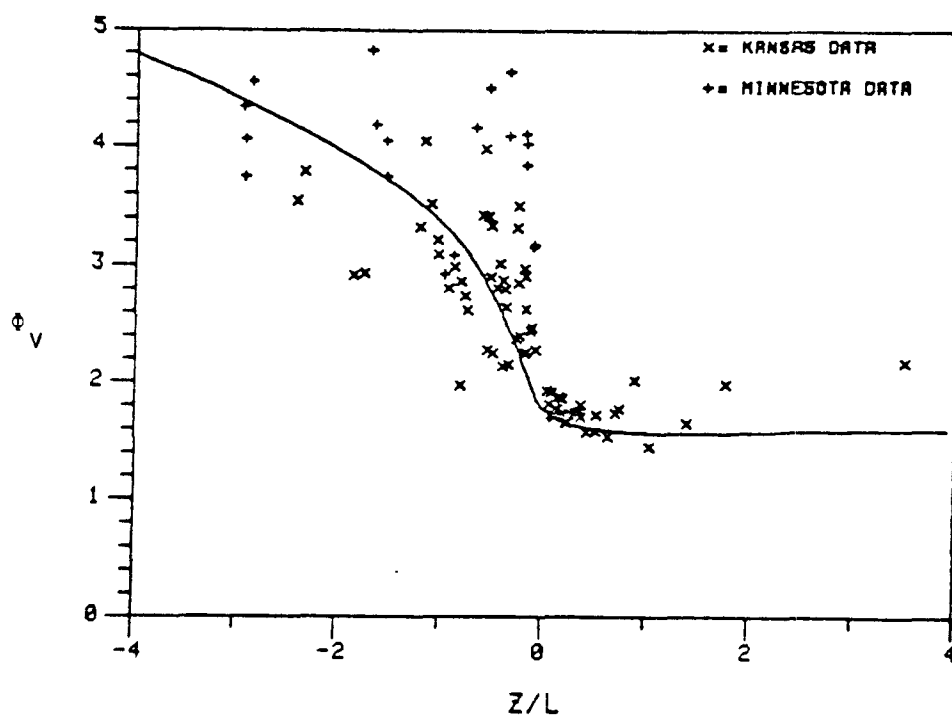


Figure 28. Variation of ϕ_V with z/L (from Binkowski, 1979).

$$\frac{z^{\alpha}}{n S_{\alpha}(n)}$$

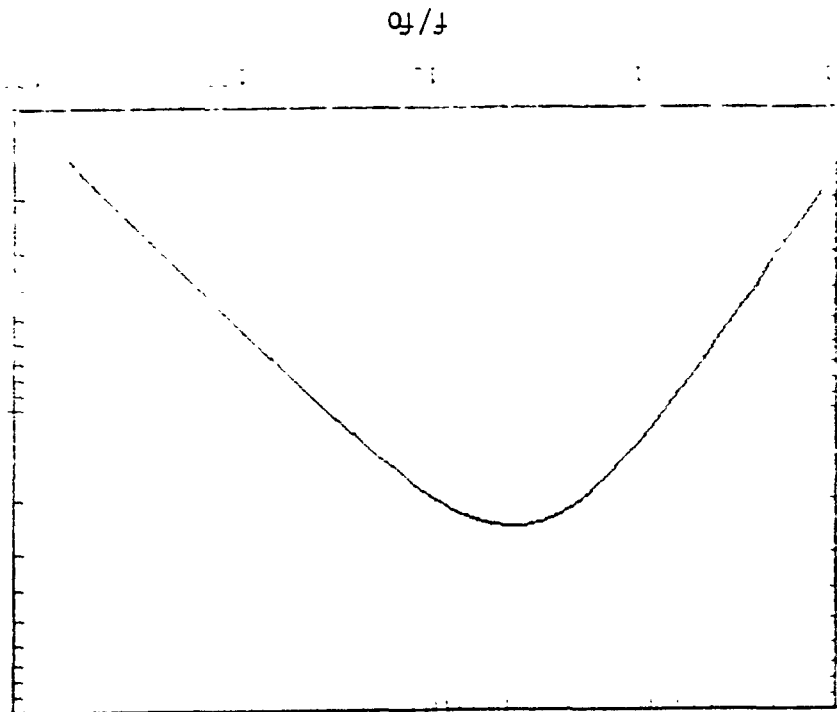


Figure 29. Universal spectral shape (Eq. 3.40).

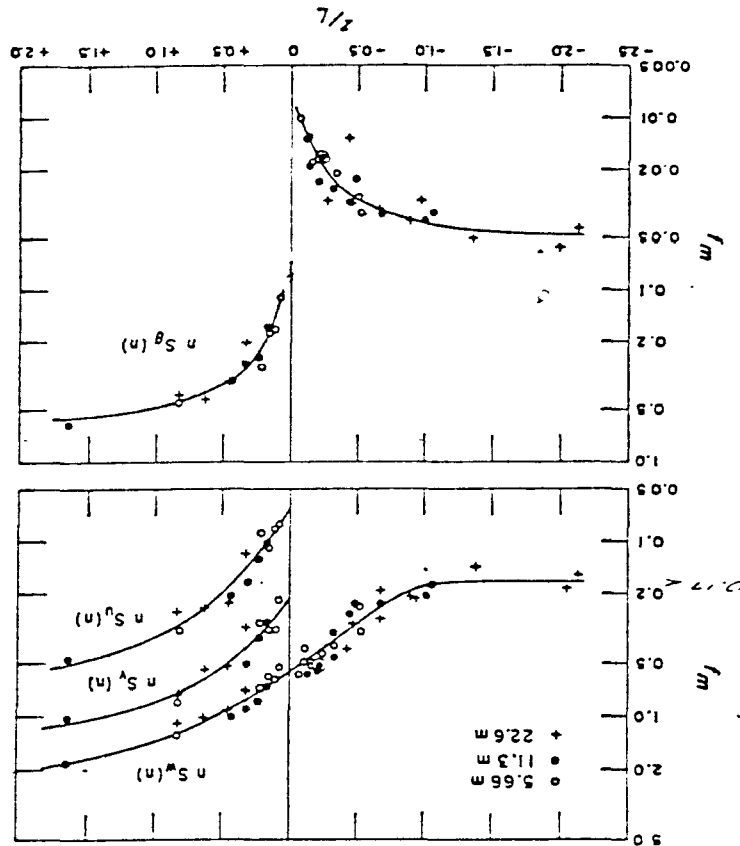


Figure 30. Location of spectral peak for u , v , w and θ plotted against z/L . Curves shown are fitted by eye (from Kaimal, et al., 1972).

a length scale that can be obtained directly is λ_m , the wavelength corresponding to the peak in the logarithmic spectrum $nS(n)$. Using Taylor's hypothesis

$$\lambda_m = U/n_m = z/f_m, \quad (3.42)$$

where n_m and f_m are the cyclic and reduced frequencies at the spectral peaks. This length scale is used extensively (as opposed to the integral scale) in the interpretation of atmospheric spectra. Kaimal (1973) has derived a simple expression relating these two length scales

$$L_{\alpha_X} = 0.041z/f_{0\alpha} = 0.16z/f_{m\alpha} = \lambda_m(\alpha)/2\pi. \quad (3.43)$$

His findings for the variation of these length scales with Richardson number are listed in Table 4.

Table 4. Dimensionless Length Scales as Functions of Ri (0.05 < Ri < 0.2).

Length scale	u	v	w	e
L_c/z	0.082/Ri	0.027/Ri	0.015/Ri	0.049/Ri
$\lambda_m(\alpha)/z$	0.520/Ri	0.173/Ri	0.093/Ri	0.313/Ri

Wamser and Müller (1977) established formulas for $\lambda_m(u)$ and $\lambda_m(v)$ that fit the Kansas data better over the whole stable range ($0 \leq z/L \leq 2$), especially in the very stable range.

$$z/\lambda_m(w) = 0.94(1+2.5(z/L)^{3/5})^{3/2}/(\sigma_w/u_*)^3 \quad (3.44)$$

$$z/\lambda_m(u) = 0.05(1+2.5(z/L)^{3/5})^{3/2} \quad (3.45)$$

They also found these equations were in good agreement with their own data and

with other empirical relationships. No expressions are available for the variation of λ_m in unstable conditions, but values for $\lambda_m(w)$ and $\lambda_m(e)$ may be deduced from Figure 30.

Little is known about the variation of λ_m with roughness. Wamser and Müller (1977) noted that their data showed a decrease in $\lambda_m(w)$ with increasing roughness under neutral and convective conditions, but could not draw any conclusions for stable conditions. They also noted that there was no systematic dependence of $\lambda_m(u)$ on roughness. Higher order statistics such as cospectra and structure parameters are beyond the scope of this review. The interested reader is referred to Wyngaard and Côté (1972) and Wyngaard et al. (1971).

Above the surface layer, the turning of wind with height generally becomes highly important and, therefore, is not amenable to simulation in a laboratory facility. But one case, in fact one that is fairly typical of daytime convective conditions, deserves mention. Kaimal et al. (1976) describe the structure of this "mixed layer" as obtained from their extensive measurements in Minnesota. The surface layer is as described above, but is confined to the height range $z < |L|$. Immediately above the surface layer, they describe a "free convection" layer, where the surface shear stress is no longer important, but the height z continues to be important. The upper level for this free convection layer is approximately $0.1z_i$, where z_i is the height of the base of the lowest inversion, and is also a good measure of the boundary layer depth (typically 1 to 2 km). The remaining 9/10 of the boundary layer, then, is the "mixed layer" where the mean wind is essentially uniform and the wind direction changes little with height. In the "worst case" run, the wind direction varied by only 15° between the surface and the top of the boundary layer; it was typically only a few degrees.

It is conceivable that the entire depth of this convective boundary layer could be simulated in a laboratory facility, albeit at very low Reynolds number. Deardorff and Willis (1974) have done the limiting case of pure convection (no wind) and Schon et al. (1974) have done an unstable boundary layer, but without a capping inversion. That the two approaches can be merged appears promising.

For details of the boundary layer structure (variances, scaling, spectra, etc.), the reader is referred to the papers by Kaimal et al. (1976), Kaimal (1978), and Panofsky et al. (1977). The latter authors show, for example, by using observations from several data sets over uniform surfaces, that ϕ_u and ϕ_v depend not upon z/L , but instead upon z_i/L . Also, there were no significant differences between the lateral and longitudinal components. Their expression fitted to the horizontal velocity data is

$$\phi_H = (12 - 0.5z_i/L)^{1/3}, \quad -400 < z_i/L < 0. \quad (3.46)$$

At the same time, they showed that the vertical velocity was M-O similar and well-fitted by

$$\phi_w = 1.3(1 - 3z/L)^{1/3}, \quad -7 < z/L < 0, \quad (3.47)$$

which is 8% higher than our previous estimate (Eq. 3.37b) for $z/L = -1$, and decreases to 3% higher for $|z/L| \rightarrow \infty$.

Kaimal (1978) found that the behavior of the u and v spectra in the unstable surface layer could be generalized if different regions of the spectra were expressed in different similarity coordinates. The spectra were divided into 3 regions: an inertial subrange ($\lambda < z$), an energy-containing region ($\lambda > z_i$) and a transition region ($z < \lambda < z_i$). In the inertial subrange, both spectra followed M-O similarity. In the energy-containing region, mixed layer similar-

ity, where z_i was the sole-governing length scale, applied. Interpolation formulas for the transition region were derived. Further, it was shown how these surface layer spectra (including w) evolve with height into their mixed layer forms. As the empirical expressions are complicated and of somewhat limited applicability, the interested reader is referred to the original paper.

3.2.1.4 Summary of the Diabatic Boundary Layer Structure

Listed here are the main features of the steady-state diabatic boundary layer over horizontally homogeneous terrain. Again, if specific site data are available giving, for example, typical strongly stable characteristics of the boundary layer, it is, of course, most desirable to use those data as a target to simulate.

1. The depth of the stable boundary layer may be estimated from Eq. 3.27, where the friction velocity u_* is obtained from the geostrophic drag law (Eq. 3.13), and the "constants" A and B are determined from Eqs. 3.26 (an iterative procedure). It is typically 100m deep. The unstable boundary layer undergoes a diurnal trend with a typical maximum depth between 1 and 2 km.
2. Once the boundary layer depth is chosen, the friction velocity is obtained from the geostrophic drag relation (Eq. 3.13), where the "constants" A and B are obtained from Eqs. 3.26 for stable conditions and Eqs. 3.28 for unstable conditions (again, an iterative procedure). Typically, $u_* = 0.05U_\infty$ in unstable conditions and $u_* = 0.02U_\infty$ in stable conditions.
3. The power law exponent p characterizing the shape of the mean velocity profile over the depth of the boundary layer may be obtained from Figure 21 or 22. In unstable conditions, it is

dependent primarily on the roughness length and essentially independent of the degree of instability, varying in the range of 0.1 to 0.2. Under stable conditions, it is highly dependent upon the degree of stability and essentially independent of the surface roughness, varying in the range of 0.2 to 0.8.

4. In neutral and unstable conditions, the surface layer properties may be extended to a depth of approximately 150m. In stable conditions, the surface layer is only 10 to 20 m in depth. The Monin-Obukhov length L is currently the most popular stability parameter because most of the surface layer properties can be described solely in terms of the dimensionless height z/L (M-O similarity theory). Given L and u_* , we can predict the shapes of the mean velocity profile (Eqs. 3.30, 3.31 and 3.33), the mean temperature profile (Eqs. 3.34 and 3.35), the variance of vertical velocities (Eqs. 3.37), the variance of temperature (Eqs. 3.38), and to a rough approximation, the variances of the lateral and longitudinal velocities (Eqs. 3.39 and Figs. 27 and 28). We can also predict spectral shapes (Eq. 3.40) and scales (Eq. 3.41 through 3.45, Fig. 29 and Table 4).
5. Little is known of the boundary layer characteristics above the surface layer except that generally the turning of the wind with height is important. Flow above the surface layer is thus not usually amenable to simulation in a laboratory facility. One special case, however, is the convective boundary layer. It appears that this entire boundary layer could be simulated in a laboratory facility as the change in wind direction with height

is typically only a few degrees over its typically 1 km depth. For additional details, the reader is referred to the original papers.

We have seen in our review of the atmospheric boundary layer that it is ever changing, it is governed by a large number of parameters, and that its space-time characteristics are difficult to determine. Even the specification of one of the "simplest" characteristics, its depth, is a horrendous problem. We have attempted to assimilate the results of the most recent theories, but they continue to develop and are rapidly modified as new experimental results become available. Even the classical "universal" von Karman constant is questioned (Tennekes and Lumley, 1972). There are few generic boundary layers to emulate or to compare with our wind tunnel simulations. Nevertheless, we have classified typical types and have described the salient characteristics of those classical types as they are known at the present time.

3.2.2 Simulating the Adiabatic Boundary Layer

In the previous sections, we have established at least the main characteristics of the adiabatic and nonadiabatic atmospheric boundary layer. In this section, we will examine several techniques commonly used to simulate the neutral atmospheric boundary layer and note, where possible, how successful these techniques have been. Generally, such techniques have been applied only in wind tunnels although, in principle, they could also be used in water tunnels and towing tanks.

The techniques can be broadly divided into three categories:

1. Long tunnels, in which a thick boundary layer develops naturally over a rough floor (Figure 31). The length of the test section of such a tunnel is typically 30 m.
2. Short tunnels with passive devices, in which the boundary layer is generated by a fence, screens or grids of non-uniform spacing, spires or vortex generators, i.e., stationary devices that retard the mean flow close to the floor and induce vorticity and turbulence into the boundary layer (Figure 32). In order to maintain a non-developing boundary layer, it is essential to "match" the generators with the roughness elements.
3. Short tunnels with active devices, in which the boundary layer is generated by jets directed at angles to the main flow stream at the entrance to the test section (Figure 33). Again, "matched" roughness must line the floor of the test section to obtain a non-developing boundary layer.

Subcategories might include tunnels equipped with machine-driven shutters or flaps or possibly a program-driven variable speed fan. In short tunnels with active devices, it is claimed to be possible, within limits, to vary the turbulence structure independently of the mean velocity profile, but it is not clear that boundary layers with different properties can be in equilibrium with the same surface roughness.

Initially, the long tunnels were touted as superior to short ones with devices for artificially thickening the boundary layers because in them the boundary layers were developed "naturally" over rough ground. The long

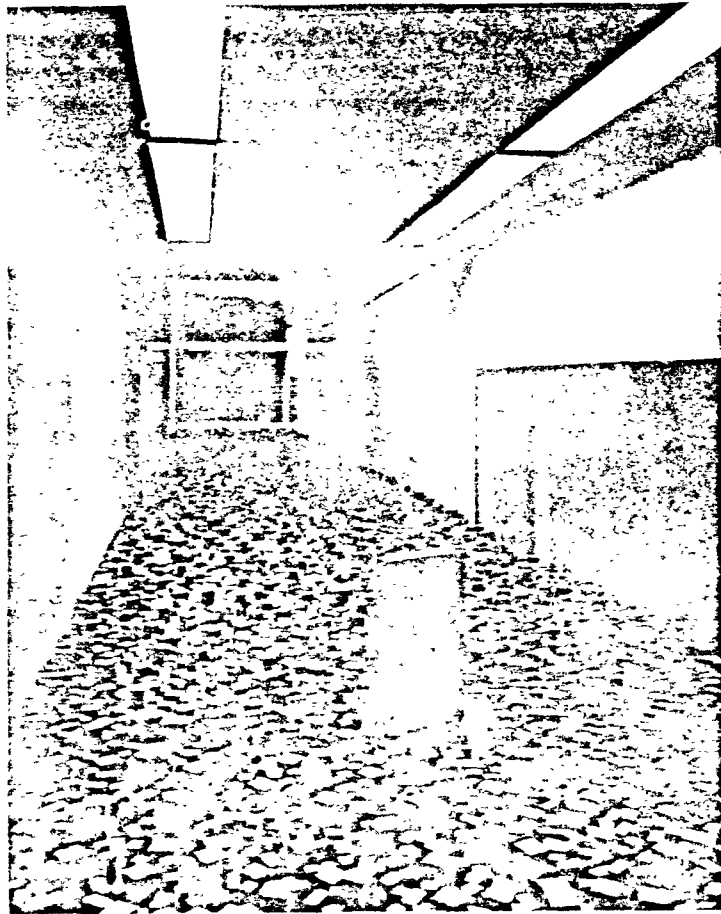


Figure 31. Upstream view of a long wind tunnel (courtesy Boundary Layer Wind Tunnel Laboratory, the University of Western Ontario).

tunnel advocates felt that the grids, jets and vortex generators introduced extraneous turbulence scales and the turbulence dissipated and its structure changed with downstream distance (Cermak and Arya, 1970). The short tunnel enthusiasts, on the other hand, pointed to the developing boundary layer and to the secondary flows caused by the growing sidewall boundary layers as not representing steady and horizontally homogeneous atmospheric boundary layers (Nagib et al., 1974). Recently, however, drag-producing elements have been used in the long tunnels as well, and many techniques for generating

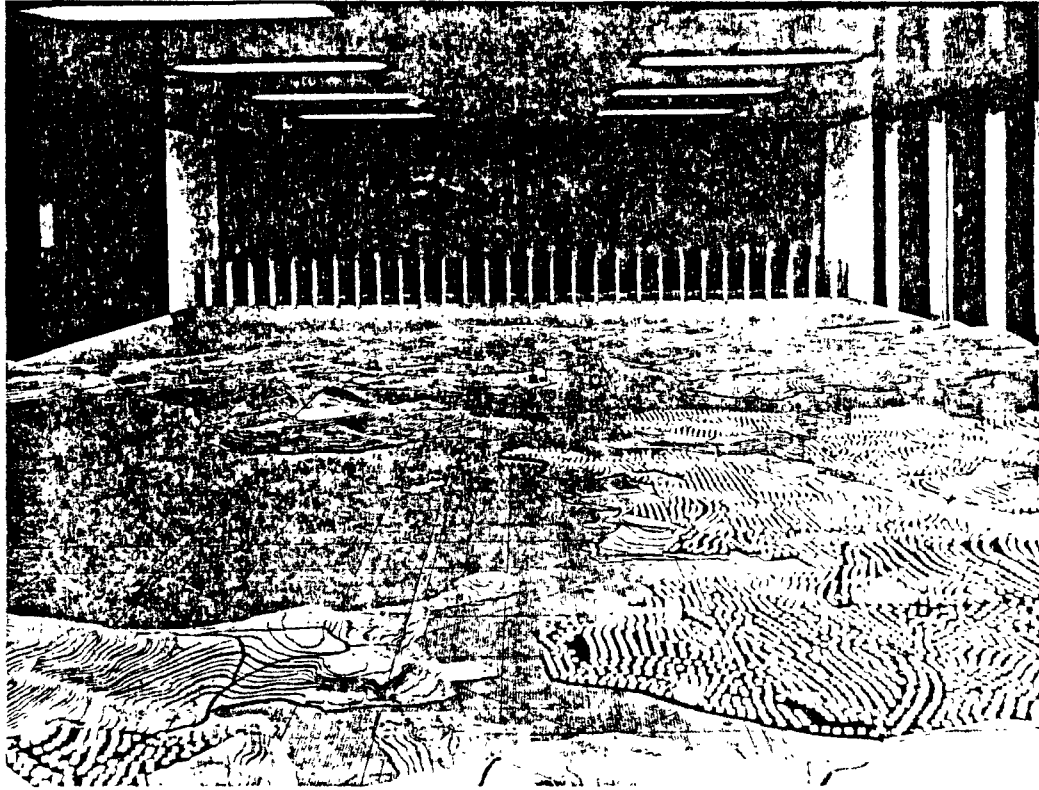


Figure 32. Vortex generators and roughness in a short wind tunnel
(Courtesy of Warren Spring Laboratory, England)

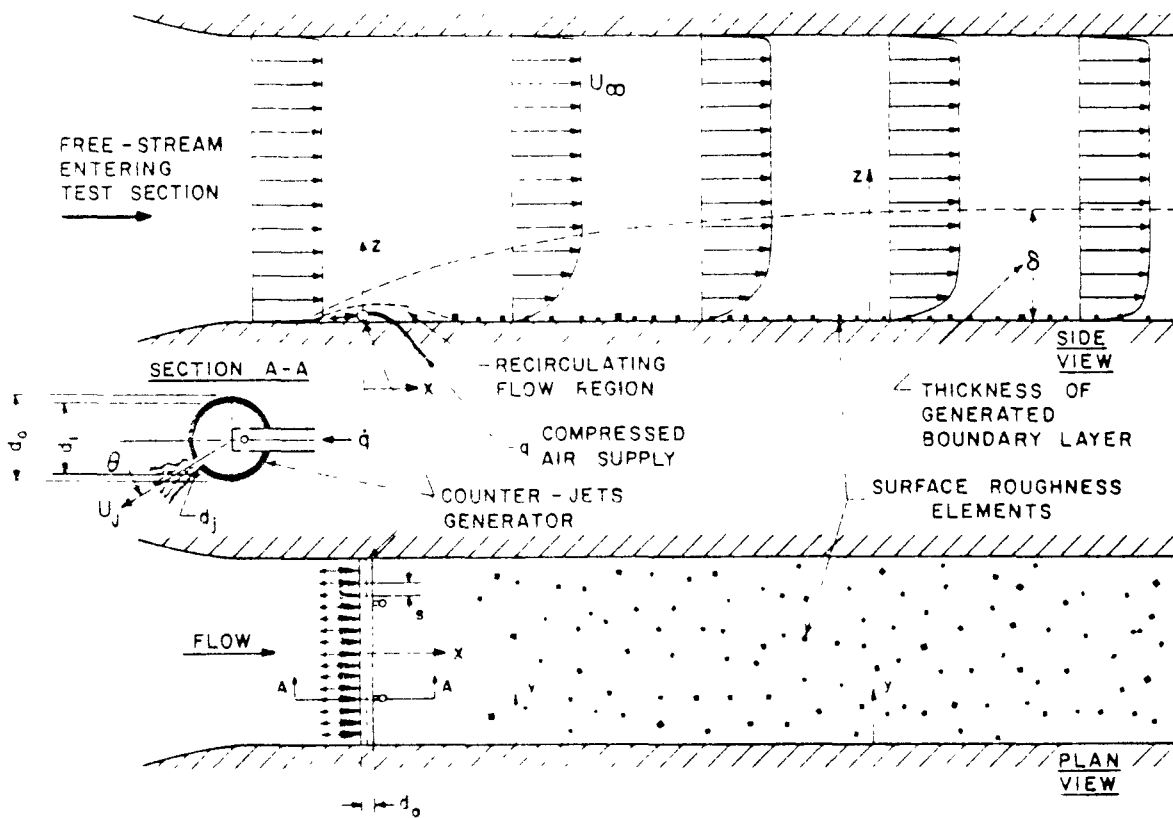


Figure 33. Schematic representation of the counter-jet technique (from Nagib et al., 1974).

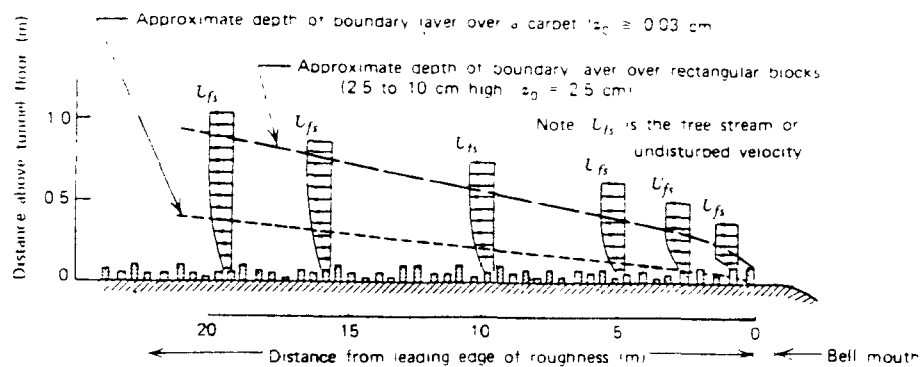


Figure 34. Development of boundary layer in a long wind tunnel (After A.G. Davenport and N. Isyumov, 1968).

thick boundary layers in short lengths of test section have been developed. There is no reason, in principle, why a fully developed layer with unchanging turbulence properties cannot be achieved in short tunnels. An experimentalist must only be clever (or lucky!) enough to determine the proper size, number and arrangement of grids, vortex generators, jets, roughness, etc. to obtain such. Also, some development length is required; current practice indicates that an equilibrium boundary layer may be established in 5 to 10 boundary layer heights, a substantial improvement over the long tunnels. It is not the aim here to favor one system over another, but instead to stress the necessity of adequately measuring the boundary layer, however generated, to be sure that it is laterally homogeneous and non-developing (if that is what is desired) and that it meets the target flow characteristics (which are not, in all cases, of course, those of the atmospheric boundary layer).

Examples of the first category, long tunnels, are the Micro-Meteorological Wind Tunnel at the Colorado State University (CSU) (Plate and Cermak, 1963) and the Boundary Layer Wind Tunnel at the University of Western Ontario (UWO) (Davenport and Isyumov, 1963). Figure 34 illustrates the development of the boundary layer in a long tunnel and how the depth of the boundary layer depends upon the roughness. Because of the growth of the boundary layers, these tunnels generally have adjustable ceilings to control the axial pressure distribution, and the ceiling is adjusted to give a zero pressure gradient along the length of the test section.

Sandborn and Marshall (1965) were the first to show that the turbulence in the boundary layer of the CSU long tunnel exhibited characteristics of the Kolmogoroff local isotropy predictions, i.e., a large separation between the

integral scale and the microscale (see Section 2.2.2.2 and Figure 6) which is characteristic of large Reynolds number turbulence, and is responsible for the $-5/3$ power in the spectral equations (3.23). Their measurements were made over a coarse gravel floor approximately 20 m from the test section entrance with a free stream wind speed of approximately 10 m/sec and boundary layer thickness of about 60cm¹. Whereas this feature is necessary for simulation of wind forces on buildings (see Simiu and Scanlan, 1978), it is regarded as relatively unimportant (but certainly not harmful) for diffusion studies (See Section 2.2.2.2). The results do indicate, however, that the flow Reynolds number may be reduced somewhat without reducing the total turbulent energy or shifting the location of the peak in the energy spectrum significantly (See Figure 7).

Zoric and Sandborn (1972) have shown that profiles of mean velocity nondimensionalized by boundary layer depth are similar beyond 6 m from the entrance (CSU tunnel). Figure 35 shows that they are approximated quite well by a $1/7$ th power law. Figure 36, however, shows that the boundary layer grows nearly linearly and still quite rapidly with downstream distance beyond about 10 m. Zoric (1968) obtained results similar to those of Figures 35 and 36 for freestream velocities between 18 and 30 m/s. Turbulence profiles were strikingly similar in shape to those suggested by Counihan (1975) for very small roughness (see Figure 16). The boundary layers were developed over the smooth wind tunnel floor. Vertical turbulence

1. In fact, under these flow conditions, the turbulent Reynolds number, based on eddy velocity and eddy size, may be estimated to be at most 2000. Tennekes and Lumley (1972) suggest a bare minimum value for an inertial subrange (local isotropy) to exist is 4000. Even though a substantial spectral region with a $-5/3$ slope was measured, it is doubtful that local isotropy existed, i.e., the existence of the $-5/3$ slope is not a critical test of local isotropy.

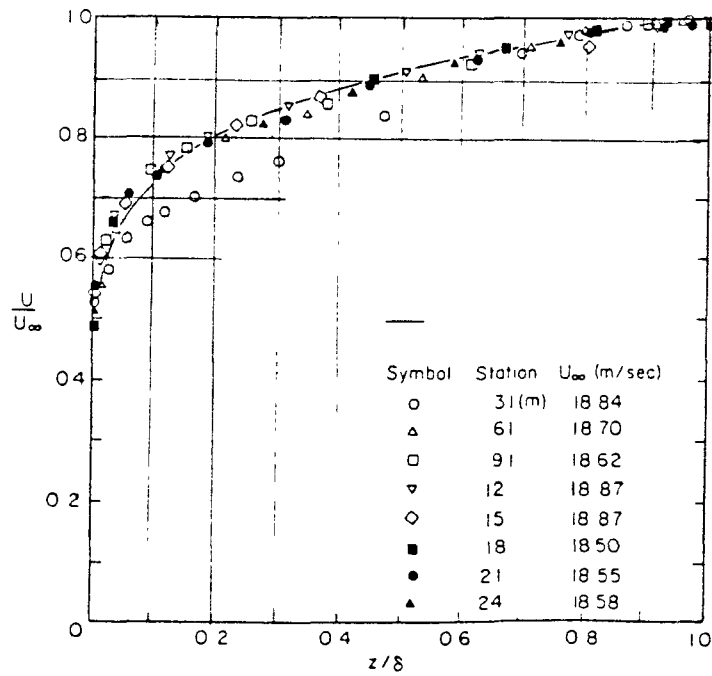


Figure 35. Development of mean velocity profiles along the smooth floor of a long tunnel (from Zoric and Sandborn, 1972).

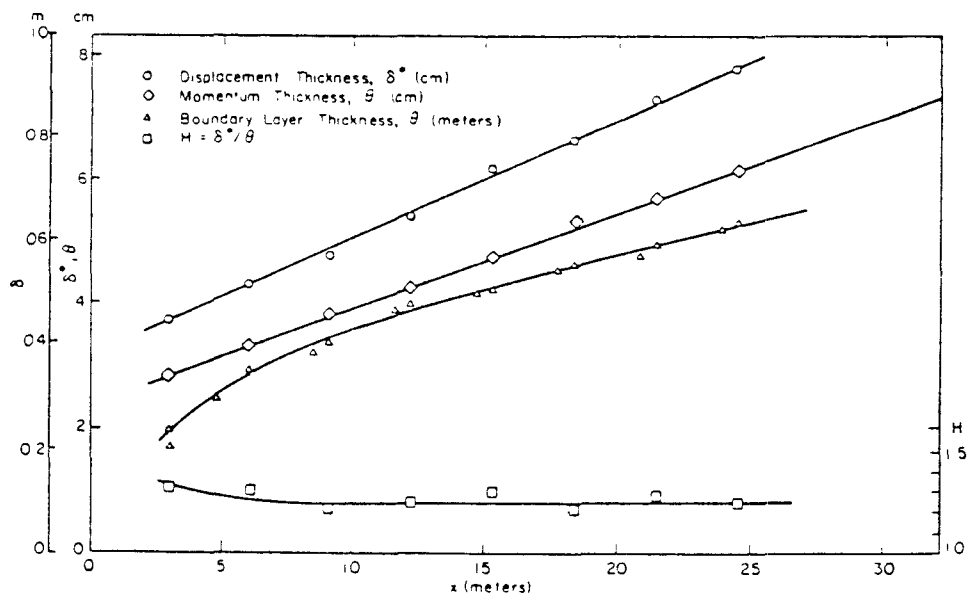


Figure 36. Thickness parameters for boundary layer of Figure 35 (from Zoric and Sandborn, 1972).

intensities were about 50% of the longitudinal intensities close to the ground in accordance with Eq. 3.21, but were typically 70% over the upper 90% of the boundary layer depth.

Surprisingly little has been published along the lines of neutral boundary layer turbulence characteristics over a rough floor that would show, for example, that the flow was laterally homogeneous or how it would compare as a small scale model of the neutral atmospheric boundary layer. Evidently, detailed basic and systematic studies of the turbulence structure in neutral boundary layers have not been made in the long tunnels.

Additionally, the above measurements were made at wind tunnel speeds much in excess of those allowable for modeling buoyant plumes. Isyumov, et al. (1976), for example, suggest typical tunnel wind speeds of 0.5 to 0.7 m/s. They do present one spectrum, reproduced here as Figure 37, that shows the rapid decrease of energy at frequencies in excess of the location of the spectral peak. Also, a relatively large amount of energy at lower frequencies is rather surprising in that significant energy in this part of the spectrum is not generally produced in wind tunnels. Measurements of the spectrum of lateral velocities would ascertain whether this energy is, in fact, due to turbulence or whether it is "pseudo-turbulence", i.e., one-dimensional fluctuations caused, for example, by low frequency oscillations in fan speed.

Low speed boundary layer development characteristics in short tunnels with passive devices are much better documented. The most popular of the passive devices is the barrier/vortex generator/roughness system developed by Counihar (1969). It has been adopted with minor variations at numerous laboratories. Castro et al. (1975) have made

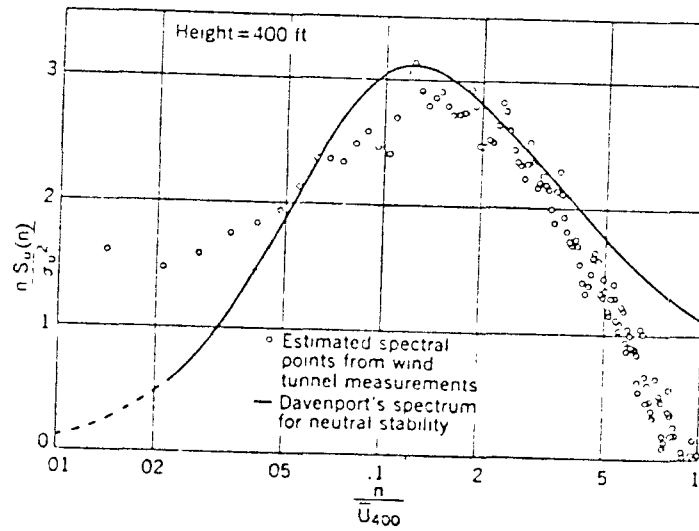


Figure 37. Spectrum of the longitudinal component of velocity (from Isyumov et al., 1976).

extensive measurements of a 2m deep boundary layer developed using Counihan's system, primarily for study of dispersion of chimney emissions in neutral flow. They found that the turbulence in the boundary layer reached a near-equilibrium state in approximately $7\frac{1}{2}$ generator heights (boundary layer heights) downstream. They were able to draw this conclusion because they had measured the various terms in the turbulent energy budget, unfortunately an all too rare measurement. Their conclusions were that the boundary layer thus developed:

1. Had characteristics similar to those of a suburban (or somewhat rougher) layer of 600 m depth and roughness length of 1.3 m at a scale ratio of 1:300, and that departures from equilibrium were unimportant beyond about 5 boundary layer heights. The lower 10 to 20% of the boundary layer could be used beyond about $3\frac{1}{2}\delta$.
2. Was Reynolds number independent for free stream wind speeds in the range of 0.7 to 13 m/s.
3. Appeared to be unaffected by the proximity of the wind tunnel ceiling to the top of the boundary layer. This conclusion was drawn by comparing intermittency distributions with those of "natural" wind tunnel boundary layers.

Moreover, Robins (1978), showed that dispersion in the above wind tunnel boundary layer as well as that in a simulated rural boundary layer was a reasonable model of the full scale process, i.e., it produced concentration patterns approximating Pasquill category C-D atmospheric flows (slightly unstable to neutral), which is normal for such a large roughness length.

1. The present author notes that in some unpublished work, boundary layers developed using Counihan's system were found to be very much dependent upon the proximity of the ceiling, i.e., when the ceiling was several times the height of the vortex generators, even the mean velocity profiles differed drastically from his. The ceiling thus appears essential; indeed, it is an integral part of the simulation system.

Somewhat less-well-documented techniques include the "spires" of Templin (1969) (also quite popular), the "fence" of Ludwig et al. (1971), and the "coffee cups" of Cook (1973). Earlier methods employing graded blockage, grids of rods or slats, etc., have been largely superseded in the Western Hemisphere, but are still quite popular in Japan (Sato, et al., 1974; Ogawa, 1976). Hunt and Fernholz (1975) provided a list of wind tunnels (largely European) used for atmospheric boundary layer simulations and included characteristics of the wind tunnels and relevant measurements of such boundary layers, so that some comparisons of the different techniques may be made.

Short test sections with active devices are also numerous. Schon and Mery (1971) injected air perpendicular to the flow through a porous plate at the entrance to the test section. This system may be thought of as a fluid-mechanical fence, where the fence "height" is adjusted by varying the strength of injected air, but it has the additional potential for injecting gas of different density in order to quickly establish a non-neutral density profile. They have shown that this technique can produce a boundary layer twice as thick as the "natural" one over a smooth floor and that its characteristics are essentially similar. However, this system appears to require a rather long development length compared with Counihan's system (Hunt and Fernholz, 1975). Also, because of the smooth floor, turbulence intensities were somewhat lower than those in even a mildly rough field surface. Mery et al. (1974) have shown that this technique produced dispersion patterns similar to the Brookhaven experiments (Smith and Singer, 1955), but only after "adjusting" their σ_y 's by a factor of 2 to account for an equivalent wind tunnel averaging time (converted to full scale) of

3 minutes compared with atmospheric averaging times of 1 hour. This adjustment technique, however, appears somewhat arbitrary. The small values of the σ_y 's in the wind tunnel were, in the present author's opinion, most likely due to the small turbulence intensities as well as to the lack of large scale lateral fluctuations in velocity.

Nagib et al. (1974) have added some flexibility to the Schon et al. technique, in that the injected air is input through a line of holes in a pipe perpendicular to the flow on the floor at the entrance to the test section. The pipe may be rotated (See Figure 33) to change the jet injection angle and the jet speed may be varied; these, of course, change the boundary layer characteristics. The "counter-jet" technique, it is claimed, avoids the objectionable introduction of extraneous turbulence scales as from vortex generators or grids, but this claim is contested by Cook (1978). Nagib et al. (1974) and Tan-atchat et al. (1974) show that this technique produces reasonable boundary layers with adequate lateral uniformity and that equilibrium is achieved in approximately 4 boundary layer heights. Neither turbulence scales nor diffusive characteristics of this boundary layer has been measured, however.

Other techniques in this third category include the multiple-jet systems of Teunissen (1975) and the "turbulence box" of Nee et al. (1974), but neither of these systems appears to have been developed beyond the initial stages.

3.2.3 Simulating the Diabatic Boundary Layer

Only a few facilities exist for simulating the diabatic boundary layer. The oldest and best-known is the Micrometeorological Wind Tunnel at the Colorado State University (Plate and Cermak, 1963). It has nominal test section dimensions of 1.8 X 1.8 X 27 m and an adjustable ceiling for eliminating the pressure gradient due to growth of the boundary layers. Speeds in the test section may be varied from 0 to 37 m/s. A 12 m length of floor can be heated or cooled and a heat exchanger in the return leg maintains ambient air temperature equilibrium, permitting temperature differences between the cold floor and hot air of about 65°C and between the hot floor and cold air of about 105°C at "moderate" wind speeds. At a speed of about 6 m/s, a boundary layer thickness between 70 and 120 cm can be obtained as the roughness is varied (Cermak and Arya, 1970).

Arya and Plate (1969) have described many characteristics of the stable boundary layer generated in this wind tunnel and have shown that the surface layer characteristics are in excellent agreement with field data when scaling is done according to Monin-Obukhov similarity theory. Their data ranged from neutral to moderately stable ($0 \leq z/L \leq 0.3$) in the lowest 15% of the boundary layer, which was about 70 cm deep. To obtain this range of stabilities, the temperature difference between the cold floor and free stream air was maintained at 40°C while the wind speed was varied from 3 to 9 m/s. Measurements included distributions of mean velocity temperature, turbulence intensities, shear stress, heat flux, and temperature fluctuations. Arya (1975) has presented additional measurements in this stable boundary layer. Thus far, all measurements in stratified boundary layers in the CSU tunnel have been with a smooth floor.

The Fluid Mechanics Laboratory at the Ecole Centrale de Lyon has made extensive measurements of an unstable wind tunnel boundary layer and compared its properties with the atmospheric boundary layer (Schon et al., 1974; Mery et al., 1974; Schon and Mery, 1978). Flow speeds were typically 2 to 4 m/s while the floor temperature was maintained 50°C above ambient. In general, comparisons with the Kansas data (Eusinger et al., 1971; Haugen et al., 1971) were quite satisfactory, but, again, these measurements were made over the smooth wind tunnel floor; longitudinal turbulence intensities exhibited a slight Reynolds number dependence, and the lack of energy in the high frequency portions of the spectra were quite evident, but as noted earlier, this effect is expected to be unimportant in terms of simulating diffusion. The most unstable flow in which diffusion was studied was characterized by a Monin-Obukhov length of -1 m, which, when scaled to the atmosphere, corresponds to -500 to -1000 m, and is indeed only very slightly unstable (See Table 3). Attempts by Rey (1977) in adding a rough floor to this unstable boundary layer showed substantial changes in the boundary layer structure with roughness.

3.2.4 Summary on Simulating the Atmospheric Boundary Layer

The point of the previous two sections (3.2.2 and 3.2.3) was to cite evidence of our ability to simulate at least the main features of the lower portion of the atmospheric boundary layer in wind tunnels. No attempt was made to include in detail all of the various techniques that have been used, as that is beyond the scope of this guideline. The point is only to show that it can and indeed has been done through various schemes.

Adequate simulations of the neutral atmospheric boundary layer have been obtained using short tunnels with either active or passive devices and long tunnels. Strengths and weaknesses of the three types, as far as their ability

to produce adequate boundary layers is concerned, appear to be evenly balanced. Hence, no one technique or system is recommended over any other. (However, see further discussion in Chapter 4). Due to the large number of permutations and combinations and to the possible large changes in boundary layer structure with seemingly small changes in configuration, however, it is imperative that, whatever technique is used, the boundary layer characteristics are adequately documented.

Simulations of diabatic boundary layers have been accomplished using wind tunnels with heated and cooled floors, but present technology allows only small deviations from neutrality, i.e., mildly stable or mildly unstable. Also, because roughness elements on the floor would reduce heat transfer even further, essentially all measurements to date have been made over smooth wind tunnel floors. As we have seen in Figure 22, the inability to use a rough surface could be important, at least for unstable flows and large roughness lengths.

Adequate documentation of the boundary layer characteristics should include, as a minimum:

1. Several vertical profiles of mean velocity, turbulence intensity (3 components), and Reynolds stress throughout the region of interest to establish that the boundary layer is non-developing (or at least very slowly developing), and is similar to the target atmospheric boundary layer (z_0, d, u_*).
2. Lateral surveys of mean velocity and turbulence structure at various elevations to ascertain the two-dimensionality of the boundary layer.
3. Spectral measurements of the turbulence to determine that the integral scales and the shape of the spectra are appropriate.

4. Dispersive characteristics of the boundary layer (in the absence of a model) to determine that the concentration patterns are reasonably similar to those expected in the target atmosphere, e.g., the appropriate Pasquill category.

Perhaps the most critical test of the boundary layer is the measurement of its dispersive characteristics to determine whether appropriate concentration patterns result. This point cannot be over-emphasized. Wind tunnels are generally extremely difficult to operate at low wind speeds ($<1\text{ m/s}$) because they are designed to operate efficiently at their maximum speeds. At these low speeds, the screens and honeycombs designed to reduce turbulence, swirl and external disturbances are completely ineffective; seemingly minor temperature variations across the test section (or elsewhere) or air leakage through holes or seams in the tunnel sidewalls will easily cause secondary flows that are difficult to cope with. Also, measurements of the flow structure are exceedingly difficult with conventional instrumentation. But the measurement of the concentration field downwind of a point source in the boundary layer in the absence of hills, buildings, etc., will quickly and easily expose defects and problems and will determine whether or not the boundary layer is a suitable one for continued study.

3.3 FLOW AROUND BUILDINGS

We discuss here guidelines to be followed in modeling flow around buildings, e.g., in order to determine a necessary height for a stack on a power plant to avoid downwash of the plume in the wake of the plant. The class of problems covered includes single or small groups of buildings, primarily isolated ones in a rural environment, i.e. scale reductions in the range of 1:200 to 1:1000. It is evident from preceding sections that the building must be immersed in an appropriate boundary layer. Geometrical scaling implies that the ratio of the building height to boundary layer height must be matched and, of course, that all length scales be reduced by this same ratio. A minimum building Reynolds number criterion must be met as discussed in Section 2.2.2.2 and further elaborated here. Finally, the effluent plume behavior must be modeled as discussed in Section 3.1.

3.3.1 Discussion

Geometrical scales that come to mind are stack height H_s and diameter D , building height H , boundary layer depth δ , roughness length z_0 , and, if stratified, Monin-Obukhov length L . There are, of course, many other length scales and geometric scaling requires that all lengths be reduced by the same ratio. However, this brings up the question of how much detail is required, i.e., is it necessary to include in the scale model a particular protuberance, say, from the roof of the building? The answer, of course, depends upon the size and shape of the protuberance; it is a question of whether or not the obstacle has a separated wake. Some guidance may be obtained from Goldstein (1965), where it is stated that provided the size ϵ of the

protuberance is such that $\epsilon u_* / \nu \leq 4$, it will have little effect on the flow in a turbulent boundary layer on a flat plate. Hence, protuberances smaller than $\epsilon = 4\nu/u_*$ need not be reproduced in the model.

A closely related but more demanding problem is as follows. A given surface is aerodynamically smooth when the Reynolds number is below a certain value; it is rough when Re exceeds this value. Hence, all surfaces are rough when the Reynolds number is sufficiently large. Because field values of Reynolds numbers are almost always very large, we may assume that surfaces of typical buildings are aerodynamically rough. As we reduce sizes of buildings to fit into our wind tunnel, we also reduce the Reynolds numbers, so that the surfaces become aerodynamically smooth. Hence, locations of separation points, the drag coefficient, and the general character of the flow along the model surface will be affected.

Again, from Goldstein (1965), if $Re_c = \epsilon u_* / \nu \leq 100$, these flow phenomena will be independent of Reynolds number. These results indicate that small details need not be reproduced and, indeed, that model surfaces should be roughened to the point that the critical Reynolds number is at least 100.

Crude estimates will suffice here and an example will help to clarify the procedure. Suppose our model building has a height of 20 cm, and in order to model the buoyancy in the plume, we have reduced the wind speed to 1 m/s. The friction velocity is typically $0.05 U_\infty$, so that size of roughness elements with which to cover the surface of the model building is

$$\epsilon = (100) (0.15 \text{ cm}^2/\text{s}) / 5 \text{ cm/s} = 3 \text{ cm}.$$

This is, in general, an unacceptably large roughness size as we should probably also restrict $\epsilon/H < 30$. We must either increase the size of the model or the wind speed or rationalize as to why a smaller value Re_c is acceptable. There are, in fact, numerous reasons why considerably lower values may be acceptable: (a) the exterior flow is, after all, highly turbulent, (b) the building shape is quite unlike a long flat plate from which the criterion was derived; it has a bluff leading edge and a strongly oscillating wake, and (c) the u_* value that should be used is the one for the boundary layer on the building surface rather than that of the approach flow; the former is likely to be larger. In the absence of more supportive data, we will take the geometric mean of the two extremes (4 and 100) as our criterion:

$$\epsilon u_* / \nu = 20$$

which is to be interpreted both as the minimum size of protuberances that must be reproduced in the model and as the size of the roughness elements with which to cover the model.

Regarding the minimum building Reynolds number $U_H H / \nu$ for the flow structure to be Reynolds number independent, a precise answer will depend upon the geometrical shape, the surface roughness, etc. Only a few systematic studies have been made on Reynolds number independence relating to atmospheric modeling, but none of these mentioned effects of model surface roughness. It may be inferred that the model surface was aerodynamically smooth. Golden (1961) measured the concentration patterns above the roof of model cubes in a wind tunnel. Buoyant and neutrally buoyant effluents were discharged into the air stream from a flush vent in the center of the cube. Two sizes of cubes were used to vary the Reynolds number from 1000 to 94,000. The nondimensional concentration isopleths above the cubes showed only

slight variations over the entire range of Reynolds numbers with neutrally buoyant effluent and with an effluent-to-free-stream velocity ratio of unity. However, the maximum concentration on the roof itself was found to vary strongly with Reynolds numbers less than 11,000, but to be invariant with Reynolds numbers between 11,000 and 94,000. Thus, a critical Reynolds number may be defined, which, with this type of geometry, appears to be 11,000.

Golden's value for the critical Reynolds number for flow around cubes is frequently cited in the fluid modeling literature on building downwash problems. Whereas Golden's value was established for a smooth surfaced cube facing a uniform approach flow of very low turbulence intensity, it is applied "across-the-board" to all shapes and orientations of buildings, in all types of approach flow boundary layers, and without regard to the building surface roughness, all of which will affect the critical Reynolds number. Also, Golden's value was established through the measurement of concentrations at only one point on the roof of the cube, as opposed to measurements of, say, the concentration fields in the wakes. Far too much confidence seems to have been placed in his result. It is probably conservative as the shear and high turbulence in an approach boundary layer as well as a rough building surface are likely to reduce the critical Reynolds number. Also, as pointed out by Halitsky (1968) lower values are probably acceptable if measurements are restricted to regions away from the building surface. Hence, a critical Reynolds number of 11,000 is a useful and probably conservative value for model design purposes, but tests to establish Reynolds number independence should be an integral part of any model study until such time that firmer values are established.

A study by Smith (1951) may also be regarded as a test of Reynolds number independence. He investigated the size of the wake created by both model and prototype sharp-edged buildings. He assumed that the flow was independent of Reynolds number effects if the ratio of the length of the cavity region to the building height was the same in both model and prototype. In the prototype tests, he found this ratio to be constant for Reynolds numbers (based upon an appropriate characteristic length) between about 2×10^4 and 2×10^6 . Moreover, in the model tests, he found the ratio to be constant for various block models over a range of Reynolds numbers from 2×10^4 to 2×10^5 .

Critical Reynolds numbers for other geometrical shapes remain to be determined. A study by Halitsky et al. (1963) on a reactor shell (a hemisphere fitted on a vertical cylinder) indicated a critical Reynolds number greater than 79,000. The separation point, and, hence, the pressure distribution for rounded buildings is affected by the Reynolds number. Generally speaking, the more streamlined is the object, the larger is the critical Reynolds number. It is quite likely that with rough surfaces, critical Reynolds numbers for streamlined objects may be reduced substantially, and systematic studies need to be done in this area.

Suppose there is another building upstream of our example power plant; is it necessary to incorporate this building into our wind tunnel model? Some guidance is provided by Hunt (1974), who reviewed experimental results of several investigators and showed that the velocity deficit in the wakes of cubes and cylinders is given by

$$\frac{\Delta U_{mx}}{U(h)} \approx \frac{A}{(x/h)^{3/2}}$$

downwind of the separation bubble, where ΔU_{mx} is the maximum mean velocity deficit created by the obstacle, h is the height of the obstacle, x is the distance downstream of the obstacle, and A is a constant which is dependent upon the building shape, orientation, boundary layer thickness, and surface roughness. Typically, $A = 2.5$, although it may vary from that by a factor of 2. Hence, if we require that the velocity be within 3% of its undisturbed value, then a cubical building as high as $x/20$ must be included upstream of our power plant. This result, however, is dependent upon the aspect ratio; a building with its width much greater than its height, for example, would require inclusion if its height were greater than $x/100$ (See Section 3.4).

The ratio of the cross-sectional area of a model to the cross-sectional area of the wind tunnel is referred to as "blockage", β . It is easy to show, through the principle of mass continuity, that the average speed-up S (increase in velocity) of the air stream through the plane intersecting the model is equal to the inverse of the blockage ratio, i.e., $S = 1/\beta$. Of course, in the atmosphere, there are no sidewalls or roof to restrict the divergence of the flow around the model, so that the average speed-up is zero. Wind tunnels with adjustable ceilings can compensate to some extent by locally raising the height of the ceiling above the model itself (with gentle slopes upwind and downwind of the model). In fact, the average speed-up can be reduced to zero by raising the ceiling such that the additional cross-sectional area of the tunnel is exactly equal to the cross-sectional area of the model, but it is obvious that this is not a perfect "fix", as that would require local expansion of the sidewalls at the same time.

Some unpublished measurements by the present author on the flow over a two-dimensional ridge sheds light on this problem. Measurements of velocity profiles above the crest of the ridge were made with a flat (unadjusted) ceiling where the blockage caused by the ridge was 10%. The ceiling height was then adjusted until longitudinal surveys of velocity at an elevation 5 hill heights above the tunnel floor showed a nonaccelerating flow. Vertical profiles of mean velocity were similar in shape to those measured with the flat ceiling, but the magnitude of the wind speed was lower by 10% everywhere above the crest (see Figure 38) with little change in the root-mean-square values of the longitudinal or vertical fluctuating velocities (turbulence). It is apparent (but by no means proven) that blockage would reduce the vertical width of a plume by approximately 10% as it traversed the ridge, but, because its centerline would be 10% closer to the ridge crest, resulting surface concentrations upstream of the crest would be essentially unchanged. However, because the flow acceleration changes the pressure distribution around the model, which will in turn affect the location of the separation point, the effects downstream of the crest are not apparent. Blockage "corrections" for conventional aeronautical wind tunnel models is a highly involved engineering science problem. "Rules of thumb" indicate a limit of 5% blockage in the ordinary wind tunnel and somewhat higher, perhaps 10%, in a tunnel with an adjustable ceiling.

3.3.2 Recommendations

To model the flow and dispersion around individual or small groups of buildings, it is recommended that:

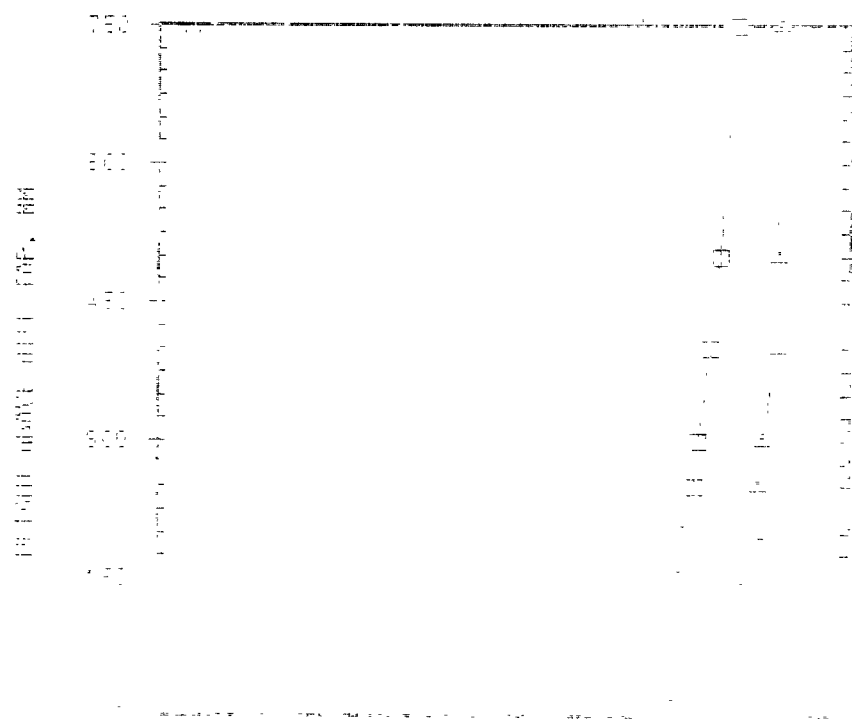


Figure 38. Velocity profiles above crest of triangular ridge indicating effect of blockage (Δ flat ceiling, 10% blockage; \square raised ceiling, nonaccelerating free stream flow).

1. The building be immersed in an appropriate boundary layer, the main features of which include matching of the ratios of roughness length, boundary layer depth and, if stratified, the Monin-Obukhov length to building height.
2. The effluent plume be modeled as discussed in Section 3.1.
3. Reynolds number independence tests be conducted as an integral part of the model study. For design purposes, a minimum building Reynolds number $U_p H/\nu = 11,000$ appears to be conservative.
4. The surface of the building be covered with gravel of size ϵ such that $\epsilon u_* / \nu = 100$. If this results in excessive roughness, i.e., $\epsilon/H > 30$, compromises may be made, but in no case should $\epsilon u_* / \nu$ be less than 20.
5. Another building or major obstruction upstream of the test building be included if its height exceeds 1/20th of its distance from the test building. This recommendation applies to a roughly cubical obstacle. An obstruction whose crosswind dimension is large compared to its height must be included if its height is greater than $1/100^{\text{th}}$ of its distance upstream (see text).
6. Blockage caused by a model be limited to 5% in an ordinary wind tunnel and to 10% in a tunnel with an adjustable ceiling.

3.4 FLOW OVER HILLY TERRAIN

Guidelines for modeling neutral flow over hilly terrain are essentially similar to those for modeling that around buildings; hence, only a few of the unique features of terrain will be discussed in this section. Differences occur primarily because terrain is generally much more streamlined than are buildings and because the roughness is generally more patchy. Whereas separation of the flow from a building surface will almost always occur at a sharp corner, the separation point for a hill with a rounded top may fluctuate in position with time, and may occur on the downwind slope of the hill, or for a hill with low slope, may be absent entirely. Also, the stratification in the approach flow can drastically change the nature as well as the location of the separation and may enhance or eliminate separation entirely (see Hunt and Snyder, 1979).

We will first discuss neutral flow, emphasizing the differences between modeling the flow around hills and that around buildings. Because stratified flows are so different from neutral flows, they will be discussed in a separate section. The two sections are summarized with a set of recommendations.

3.4.1 Neutral Flow

In the field, the ridge Reynolds number based on a ridge height of 75 m and wind speed of only 3 m/s is 10^7 . For these very large Reynolds numbers, at least for a ridge with moderate slopes, separation is certain to occur near the apex, even for a ridge with a smooth rounded top (see Scorer, 1968, p. 113). The Reynolds number for this model mountain ridge would lie between 10^4 and 10^5 , much smaller than the full scale Re. It is possible to trip the flow at the apex (as done by Huber et al., 1976) or to roughen the surface, so that the point of separation on the model will occur at its apex and similarity of the two flow patterns will be achieved.

Appropriate roughening of the surface, as outlined below, is the "safest" of the two techniques, because proper placement of a trip requires foreknowledge or possibly unwarranted presumptions of the location (or indeed existence) of separation.

Concerning the minimum size of protuberances that must be reproduced in the model and also the size of the roughness elements that cover the model to make the flow independent of the Reynolds number, we apply the same criterion as established for buildings, namely $\epsilon = 20\nu/u_* \cong 400 \nu/U_\infty$. This may in some instances conflict with Jensen's criterion that h/z_0 be matched between model and prototype, but the minimum Reynolds number is regarded as more important.

A common practice in constructing terrain models is to trace individual contour lines from enlarged geographic maps onto plywood or styrofoam, then to cut them out and stack them to form "stepped" terrain models. Some laboratories then fill in or smooth out these irregularities, while others use rather large steps and do not smooth them. One laboratory, in fact, proposed to fill in and smooth the model, then to add randomly spaced blocks to simulate surface roughness. Application of the criterion in the previous paragraph shows both the desired step size and the roughness element size. It is not necessary to fill in the steps if the step size is chosen appropriately at the beginning; the steps double, to some extent, as roughness elements, although it is most likely better to densely cover the model surface with gravel of about the same diameter as the step size.

How much terrain is it necessary to include in the model upwind of a power plant? For a two-dimensional ridge, Counihan et al. (1974) have shown that the maximum deficit of mean velocity in the wake, normalized by

the mean velocity at the height of the hill, decays as

$$\frac{\Delta U_{mx}}{U(h)} \approx \frac{B}{x/h},$$

where ΔU_{mx} is the difference in mean velocity created by the hill, h is the hill height, x is distance downstream of hill, and B is a constant dependent upon surface roughness and hill shape. Typically, $B=3.0$. Hence, if we insist that the mean velocity be within 3% of its undisturbed value (i.e., its value in the absence of the ridge), then all upwind ridges with heights as large as $x/100$ should be included in the model. In actual practice, one should study the topographic maps of the area surrounding the plant, locate prominent ridges upstream, then determine the height of each ridge and its distance from the plant. If its height is greater than $x/100$, all terrain between the ridge and the plant should be included. If $h < x/100$, it is probably justifiable to neglect it. This may appear as a stringent requirement, since a 10 cm high model ridge would require a 10 m fetch, but the turbulence decays even more slowly, i.e., $\Delta(\overline{u^2})^{1/2}/U(h) \approx (x/h)^{-3/4}$ (Hunt, 1974).

For three dimensional hills, we may estimate from Hansen et al. (1975), who found for the wake of a rectangular block:

$$\frac{\Delta U}{U_\infty} \approx \left(\frac{2}{x/h}\right)^{3/2}.$$

Hence, the amount of fetch required is much less; a hill of 10 cm height would require a fetch of only 1.7 m for a 3% velocity deficit. Both of these formulas were derived on the basis of a simulated atmospheric boundary layer approach flow. Hence, the indicated fetch is necessary upwind of the plant and an appropriate equilibrium must be developed upstream of that, i.e.,

the formulas do not indicate the fetch required for the development of the boundary layer.

The choice of a boundary layer depth for very rugged terrain is a difficult task. Our choice of 600m (Section 3.2.1.2) is obviously absurd if the heights of the hills themselves are of the same magnitude. One indication from the literature is from Thompson (1978), who examined wind profiles obtained from pilot balloons over complex terrain in southwestern Virginia. The average boundary layer depth, Thompson concluded, was about 800 m, or 4 hill heights under moderate to high wind speed neutral conditions.. As mentioned in Section 3.2.1.1, he also observed a logarithmic wind profile with a z_0 of 35 m.

3.4.2 Stratified Flow

We have discussed in depth the stable boundary layer in Section 3.2.1.4. It was shown that under strongly stable conditions, the boundary layer is very shallow, typically less than 100 m. Frequently, pollutant sources discharge their effluent at much higher elevations, i.e., above the stable boundary layer, where the plume may be transported long distances with little or no dispersion (e.g., see cover photograph of AMS, 1979). Further, results of Godowitch et al. (1979) indicate that extremely shallow stable boundary layers under quite deep surface-based temperature inversions are typical at sunrise at a rural site outside St. Louis, MO. The average depth of the nocturnal inversion, for example, was 325 m (\pm 90 m standard deviation). The average temperature gradient was $1.4^{\circ}\text{C}/100\text{m}$. Under these conditions, it is evident that simulation of the stable boundary layer beneath an elevated source is relatively unimportant. Far more important is the simulation of the stability above the boundary layer because, as shown by Lin et al. (1974),

Hunt and Snyder (1979) and Snyder et al. (1979), the stability determines the essential structure of the flow, i.e., whether plumes will impinge on the hill surface or travel over the hill top, the size and location of hydraulic jumps, etc.

Under strongly stable conditions, the flow is constrained to move in essentially horizontal planes. If a three-dimensional hill is placed in the flow field, streamlines below the hill top will pass round the sides of the hill and not over the top. If a two-dimensional hill is placed across the flow field, the fluid obviously cannot pass round the sides and, because it has insufficient kinetic energy, it cannot pass over the top of the hill (see Section 2.2.4). Thus, upstream blocking of the flow below the hill top will occur. The point is that the modeler must be very careful in determining the amount of terrain to duplicate in the model. An example is shown in Figure 39, where a portion of a three-dimensional hill is turned into a two-dimensional one by an inappropriate choice of the area to be modeled. Under strongly stable conditions, the combination of the hill and tunnel sidewalls would result in upstream blocking of the flow beneath the hill top, whereas, with a wider tunnel or smaller scale model, the flow would be diverted around the sides of the hill as would certainly occur in the atmosphere.

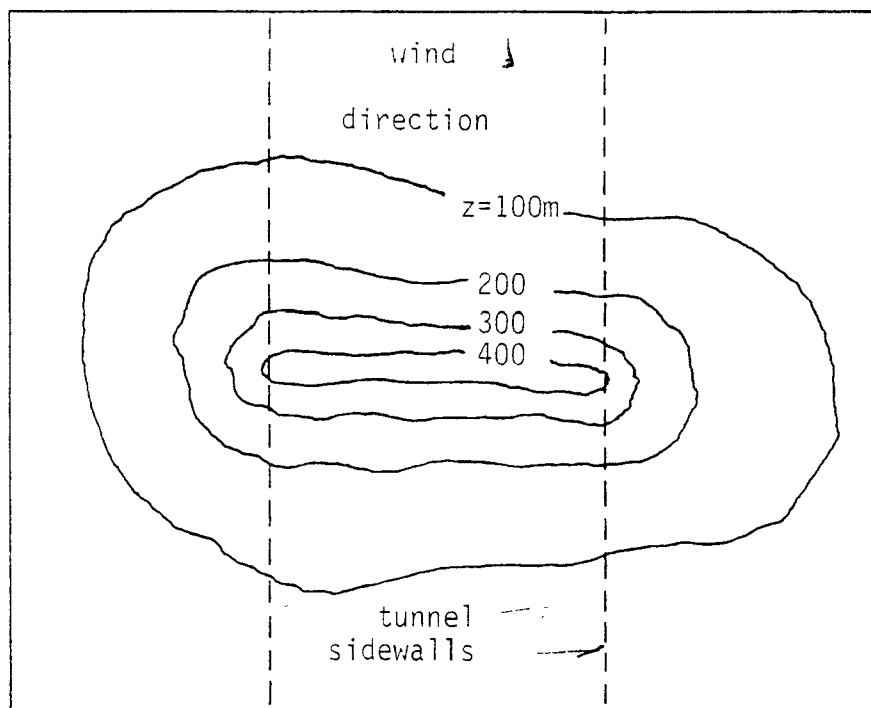


Figure 39. Contour map of three-dimensional hill showing inappropriate choice of area to be modeled.

Similar extensions of this type of reasoning apply to valleys and ridges angled diagonally across the flow stream. It is impossible to give firm and fixed rules for determining the appropriate area of terrain to model because the flow field must be known a priori. However, detailed study of topographic maps of the area and the application of common sense will avoid most pitfalls.

As Scorer has pointed out, laboratory studies of stratified flows tend to overemphasize the effect of stratification in the approach flow; local heating and cooling of hill surfaces are equally, perhaps more, important. The effects of anabatic and katabatic winds are not only local, but may have large effects on the flow structure by inhibiting or enhancing separation (Scorer, 1968, p. 113; Brighton, 1978). There have been some attempts to simulate heating of terrain surfaces, but more to simulate fumigation of elevated plumes than anabatic or katabatic winds (Liu and Lin, 1976). Little is known of the proper similarity criteria to be applied to thermally-driven flows. Any comparison between field and model experiments, where such thermally generated winds are absent, must be made with great caution.

3.4.3 Recommendations

Recommendations for modeling flow and dispersion over hilly terrain in neutral stability are essentially similar to those for modeling flow around buildings. It is recommended that:

1. The terrain be immersed in a simulated atmospheric boundary layer, matching the ratios of roughness length and boundary layer depth to hill height.
2. The effluent plume be modeled as discussed in Section 3.1.
3. Reynolds number tests be conducted as an integral part of the study.

4. The surface of the model be covered with gravel of size ϵ such that $20 \leq \epsilon u_* / \nu \leq 100$. The step size in "stepped" terrain models should also be of order ϵ .
5. An upstream ridge be included in the model if its height exceeds 1/100th of its distance upstream from the test portion of the model. A three-dimensional hill should be included if its height exceeds 1/20th of its distance upwind.
6. Blockage be limited to 5% for an ordinary wind tunnel and to 10% in a tunnel with an adjustable ceiling.

Additionally, in modeling dispersion from elevated sources in strongly stably-stratified flow over hilly terrain it is suggested that:

7. The simulation of the stable boundary layer, per se, is relatively unimportant. More important is matching of the Froude number based on the hill height and the density difference between the base and top of the hill.
8. Topographic maps of the area to be modeled should be studied carefully to insure that an appropriate area is modeled (see text).

Finally, laboratory models to simulate anabatic and katabatic winds must be considered as exploratory in nature at the present time.

3.5 RELATING MEASUREMENTS TO THE FIELD

Since buoyancy in a plume may be modeled using light gas as opposed to temperature, the concentration measured in a model facility may be related to that in the field through the nondimensional concentration $X = CUH^2/Q$, where

C = mass concentration of pollutant (ML^{-3}),

U = wind speed (LT^{-1}),

H = characteristic length (L),

and Q = pollutant emission rate (MT^{-1} , e.g., grams of SO_2 /second).

The relation between model and field concentrations is thus

$$C_f = C_m \left(\frac{U_m}{U_f} \right) \left(\frac{H_m}{H_f} \right)^2 \left(\frac{Q_f}{Q_m} \right).$$

Note that both C and Q are measured in mass units. More frequently, C and Q are measured in volume units, in which case, they must be evaluated at ambient (not stack) temperature, including Q_f (Robins, 1975). An example may help to clarify the procedure. Suppose we model a buoyant plume with a mixture of helium, air and methane as indicated in the following table:

Property	Field	Model
Reference wind speed	10m/s	1m/s
Stack height	50m	50cm
Stack diameter	5m	5cm
Effluent speed	20m/s	2m/s
Pollutant emission rate	500g/s(SO_2)	1g/s(CH_4)
Effluent temperature	117°C	20°C
Ambient temperature	20°C	20°C
Effluent specific gravity	.75	.75

At some point downwind of the source in the wind tunnel, we might measure a model concentration of 100ppm (parts CH_4 per million parts air, by volume), and the problem is to relate this to a field concentration value. First, the model volume concentration must be converted to a mass concentration (relevant densities at 20°C are air: $1.29\text{g}/\ell$; CH_4 : $0.74\text{g}/\ell$; SO_2 : $2.95\text{g}/\ell$):

$$C_m = \left(\frac{100 \ell \text{ CH}_4}{10^6 \ell \text{ air}} \right) \left(\frac{1 \ell \text{ air}}{1.29\text{g air}} \right) \left(\frac{0.74\text{gCH}_4}{1 \ell \text{ CH}_4} \right) = \frac{57 \times 10^{-6} \text{gCH}_4}{\text{g air}}.$$

Hence, the field mass concentration will be:

$$\begin{aligned} C_f &= \left(\frac{57 \times 10^{-6} \text{gCH}_4}{\text{g air}} \right) \left(\frac{1\text{m/s}}{10\text{m/s}} \right) \left(\frac{0.5\text{m}}{50\text{m}} \right)^2 \left(\frac{500\text{gSO}_2/\text{s}}{1\text{gCH}_4/\text{s}} \right) \\ &= 0.285 \times 10^{-6} \text{gSO}_2/\text{g air}. \end{aligned}$$

Converting this mass concentration to volume concentration yields:

$$\begin{aligned} C_f &= \left(\frac{0.285 \times 10^{-6} \text{gSO}_2}{\text{g air}} \right) \left(\frac{1.29 \text{ air}}{1 \ell \text{ air}} \right) \left(\frac{1 \ell \text{ SO}_2}{2.95\text{gSO}_2} \right) \\ &= 0.125 \times 10^{-6} \ell \text{ SO}_2/\ell \text{ air} = 0.125\text{ppm SO}_2. \end{aligned}$$

To summarize, the relation between model and field concentrations in this example is

$$\begin{aligned} 1 \text{ ppm SO}_2 &\rightarrow 800 \text{ ppm CH}_4 \\ \text{or } 1 \text{ g SO}_2/\text{g air} &\rightarrow 200\text{g CH}_4/\text{g air}. \end{aligned}$$

Whereas it is tempting to bypass some of the above steps by using volume emission rates, shortcuts are not recommended. It is important to note that all densities were specified and used at ambient temperature, i.e., 20°C .

Regarding the comparison of model results with field results, it is

well-known that in the field the averaging time has a definite effect on the measured concentrations. This is not the case in model tests. (This discussion is taken largely from Ludwig, 1974). The model results correspond to short-time-averaged field measurements, taken over not more than 10 or 15 minutes in most cases. Briefly, what is involved here is the following. The energy spectrum of wind gusts in the atmosphere generally shows a null, or near null, in the frequency range of 1 to 3 cycles per hour (the "spectral gap" discussed in Section 2.2.2.2). Thus, it is possible to separate the spectrum into two parts and to deal with the phenomena associated with each part separately. The high-frequency portion, related to the roughness of the surface and the turbulence around obstructions is well-simulated in a wind tunnel. The low-frequency portion, related to the meandering of the wind, diurnal fluctuations, passage of weather systems, etc., cannot be simulated in a wind tunnel. However, a correction for meandering of the wind can be applied, if desired, to derive longer term averages (Pino, 1968; Isyumov, et al., 1976). Model averaging times, on the other hand, are chosen to provide data that are repeatable to within some specified accuracy, as discussed later. However, as noted above, the data so obtained will correspond to field data measured while the wind direction is essentially steady, which is generally not more than 10 to 15 minutes. Shorter term averages obtained from the model can be related to the short term fluctuations in the atmosphere, and instrumentation is being developed to accomplish this (Fackrell, 1978).

3.6 AVERAGING TIME AND SAMPLING RATES IN THE LABORATORY

Because the flow is turbulent, essentially all of the quantities we attempt to measure will fluctuate in time. Generally, we will deal with a fluctuating electrical signal from a transducer, and it is not the precise

value at any particular instant of time that is of interest, but rather the average values and the statistics of the fluctuations. It is necessary at some point to determine how long an averaging period is required to obtain a stable average. Frequently, it is convenient to digitize an analog signal (sample it and convert the analog voltage to digital form). Sampling at too high a rate is a waste of resources; sampling at too low a rate may not allow us to obtain the desired information and, in fact, may lead to incorrect answers. Hence, it is also necessary to determine an appropriate sampling rate.

To determine an appropriate averaging time for measuring the mean of a fluctuating quantity $F(t)$ in a wind tunnel, it is useful to consider the turbulence as a Gaussian process. (Whereas turbulence is not a Gaussian process, experience has shown that this assumption leads to quite reasonable estimates of the errors involved.) The variance σ^2 of the difference between the ensemble (true) average and the average obtained by integration over time T is (Lumley and Panofsky, 1964):

$$\sigma^2 = \frac{\overline{f^2} I}{T},$$

where $\overline{f^2}$ is the ensemble variance of F about its ensemble mean, $f = F - \bar{F}$ and I is the integral scale of F . The fractional error ϵ , then, is given by

$$\epsilon^2 = \frac{\sigma^2}{\bar{F}^2} = \frac{\overline{f^2} I}{\bar{F}^2 T}.$$

If, for example, it is desired to measure the turbulent energy $\overline{u^2}$, it may be shown, using the assumption that u has a Gaussian distribution, that

$$\epsilon^2 = 4I/T.$$

To obtain a conservative estimate of the error, it is convenient to

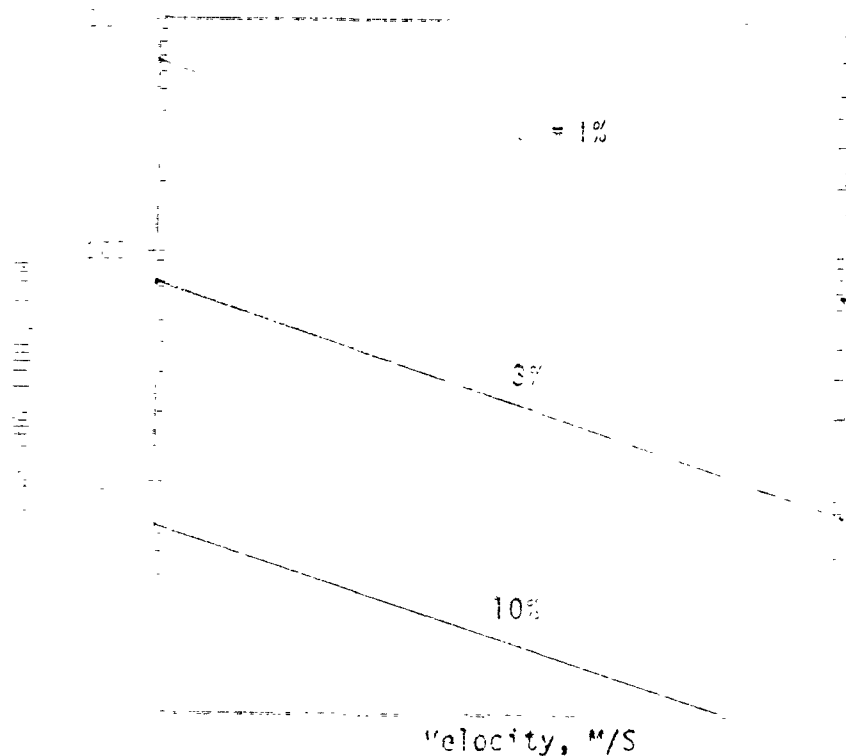


Figure 40. Averaging time requirements for wind tunnel measurements.

estimate a maximum integral scale as δ/U_∞ , where δ is the boundary layer depth and U is the free stream velocity; the required averaging time is then

$$T = 4\delta/U_\infty \epsilon^2 .$$

This relationship is shown in Figure 40 for a typical boundary layer depth of 1m. For a wind tunnel speed of 4m/s and a desired accuracy of 10%, a two-minute averaging time is required. It is readily observed that much higher accuracies at such low wind speeds are impractical, as an accuracy of 1% would require an averaging time of over 3 hours.

To estimate averaging times required for measuring other quantities (besides turbulent energy), respective integral scales must be known and numerical factors are generally larger; however, experience has shown that

$\tau = 4\delta/U_0 \epsilon^2$ is a reasonably good estimate of the averaging time required for making all of the common measurements (mean velocity, turbulence intensity, concentration, etc.). Higher order moments require considerably longer averaging times.

To estimate an appropriate sampling rate, we begin by drawing from a mathematical theorem (Miller, 1963):

"If a signal $f(t)$ extending from 0 to ∞ contains no frequencies above W cycles per second, then it is completely determined by giving its ordinates at a sequence of points spaced $1/2W$ seconds apart."

Hence, in order not to lose information from our continuous signal through our discrete sampling, it will be essential to determine the highest frequency component in our signal and to sample at twice that rate. The highest frequency of any significance in the turbulence is the Kolmogoroff frequency, $f_d = U/2\pi\lambda$ (see Section 2.2.2.2). Hence, assuming an excellent anemometer (good frequency response and low electrical noise), all information about the turbulent signal may be obtained by sampling at a rate of $2f_d = U/\pi\lambda$. At the slow flow speeds typical of fluid modeling studies ($<10\text{m/s}$), the Kolmogoroff microscale is not likely to be much smaller than 0.5 mm. Hence, a typical sampling rate would be approximately 2 kilohertz at a flow speed of 5m/s. Because of aliasing, lower sampling rates are unwise (for more information, see Lumley and Panofsky, 1964). Of course, if the transducer or amplifier have slower frequency response, it is pointless to sample at twice the Kolmogoroff frequency. A flame ionization detector, for example, has a time constant of approximately 0.5 sec., so that a sampling rate in excess of 4 hertz is not necessary.

4. THE HARDWARE

The choice of air versus water as the fluid medium for modeling of atmospheric flow and diffusion of pollutants will depend on many different factors: the availability of the facility, economics, the type of problem to be studied and the type of information to be obtained, to name a few. The kinematic viscosity of water at normal room temperature is a factor of 15 less than that of air, so that, in principle, a factor of 15 in the Reynolds number may be gained by modeling with water as the medium. However, because water is so much heavier than air, structural and pumping requirements dictate that water facilities be much smaller and run at much lower flow speeds than wind tunnels. Thus, the full potential for obtaining larger Reynolds numbers using water facilities is seldom realized.

If it is essential to obtain very high Reynolds numbers, water has some advantages. Because of its incompressibility, it may be run at high speeds while maintaining low Mach numbers, which is not possible with air. However, a different problem appears with water at high speeds -- cavitation behind obstacles. This may be overcome by maintaining large pressures inside the water tunnel, which then requires heavy steel construction, so that compromises must again be made.

4.1. VISUAL OBSERVATIONS

Smoke and helium filled soap bubbles (for which a generator is now commercially available) are about the only visible tracers for use in air. A very much wider variety of tracer techniques is available for use in water, making flow visualization much easier. These include different colors and densities of dye, hydrogen bubbles, potassium permanganate crystals, shadowgraphs, and neutrally buoyant particles. And because flow speeds are generally low, it is easy to observe and photograph flow patterns in

water. The comparable smoke in a wind tunnel is difficult to regulate either in concentration or specific gravity (oil fog smoke generators are notoriously cantankerous and they occasionally explode!). Smoke is also difficult to observe visually and photographically at flow speeds in excess of 1 to 2 m/s. Titanium tetrachloride is relatively easy to use, but is corrosive, hazardous to handle, and is not easily used as a stack effluent.

The importance of flow visualization should not be underestimated. Much time and effort can be wasted searching for a maximum ground level concentration in complex terrain using a probe and some sort of analyzer, whereas visual observations of smoke or dye would narrow the area to be searched tremendously. Fixed rakes are frequently positioned downwind of a hill to sample the vertical and lateral concentration profiles; but unless it is known a priori about where the plume will be, the data collected will not be highly useful and the experiment may have to be run again. With flow visualization, it is obvious at a glance, for example, whether a plume is going over or around a hill, whereas extensive point-by-point measurements would be required otherwise. Flow visualization can also be of great help in the interpretation and understanding of quantitative data. Hot wire anemometry, in spite of its increased sophistication and reliability in recent years, still cannot tell us the direction of flow (there is a $\pm 180^\circ$ ambiguity) and reverse flows commonly exist downwind of bluff obstacles. Finally, some quantitative results may also be obtained from flow visualization. For example, Hunt and Snyder (1979) used flow visualization to measure the displacement of streamlines by a hill, the surface streamline patterns, the increase of velocity or speed up over the top of the hill, for understanding lee waves, hydraulic jumps, and separated flow regions downwind of the hill, and for extending

Drazin's (1961) theory to determine whether plumes from upwind sources would pass over the top or impact on the surface and pass round the sides of the hill in stratified flow. Also, different colored dyes emitted from different elevations on the hill surface showed oscillations in the wake that were anticorrelated at different elevations; this kind of information would have been difficult to obtain through other means.

4.2 QUANTITATIVE MEASUREMENTS

Quantitative measurements of flow speeds are more difficult in water. Wind tunnel techniques for these measurements have been developed and advanced to a level of high reliability and accuracy (Bradshaw, 1970). For local velocity measurements in wind tunnels, numerous instruments are available: pitot tubes, hot wire-, hot film,- and pulse wire-anemometers. Hot film anemometers are used in water, but require much travail to obtain reliable measurements. At typical low flow speeds used in water, pitot tubes are not very useful. Small propeller anemometers (~ 1 cm dia.) have been developed for special studies in air and water, but are not readily available.

Highly accurate and reliable flame ionization detectors are available for quantitative measurements of pollutant concentrations downwind from a source in a wind tunnel. These instruments are presently the most popular because they have a relatively fast response time (~ 0.5 second), their output is linear with concentration over a very wide range (about 0.5 to 10,000 ppm methane with proper adjustments), and they can be used with any hydrocarbon gas, including methane, ethylene, and butane, which have specific gravities of 0.5, 1 and 2, respectively. Many other tracers and instruments have also been used including sulfur dioxide, carbon monoxide, temperature, smoke (Motycka and Leutheusser, 1972), helium (Isyumov et al., 1976), and radioactive gases (Meroney, 1970), along with corresponding measuring devices. Smoke, temperature,

and helium techniques offer possibilities for the measurement of concentration fluctuations, but are generally limited to the measurement of small dilutions, i.e., 1:100, as compared with the 1:10,000 desired. Fackrell (1978) has developed a "popper valve" to allow the flame ionization detector to be used for the measurement of concentration fluctuations. Salts in conjunction with conductivity meters, acids with pH meters, temperature with thermistors, and dyes with colorimeters and fluorimeters have been used as tracers for quantitative measurements of concentration in water. Except for temperature, these techniques offer a wide range in concentration detectability. The conductivity probes and thermistors can be quite fast response devices. They offer possibilities for the measurement of concentration fluctuations.

4.3 PRODUCING STRATIFICATION

There are two common methods for producing stratification in water. The most common method of producing stable density stratification in water is by slowly filling a tank through distribution tubes on the bottom with thin layers of salt water, each layer increasing in specific gravity (Hunt et al., 1978). The heavier solutions flow under the lighter fluid above, thus lifting it. In view of the very small mass diffusivity of salt in water, an undisturbed stable mass of salt water will remain that way for weeks, even months, before the density gradient is substantially changed by molecular diffusion. Maximum dimensionless density differences are limited to about 20% using common salt (NaCl). Recirculating systems using this technique have been impractical because of the mixing within the pump. However, Odell and Kovaszny (1971) have designed a rotating disk pump that maintains the gradient; this device permits the use of recirculating salt water systems, but, thus far, has been used only for very small channels (~ 10 cm depth).

The second common method for producing stratification in water is by heating and cooling. Frenzen (1963) had produced both stable and unstable stratification in a towing tank using this method. Because of the large heat capacity of water, large amounts of energy are required for heating and cooling to produce significant stratification, so that this method is generally limited to small tanks. Deardorff and Willis (1974) and Liu and Lin (1976) have combined heating and cooling (respectively) with stable salt water stratification to study inversion break-up phenomena.

Air, with its low heat capacity, is comparatively easy to stratify. Provisions must be made, of course, for heating or cooling of the floor of the test section and, if it is a closed return tunnel, for cooling or heating the return flow. In order not to exceed reasonable temperatures in the tunnel (say 100°C), the maximum dimensionless density difference is limited to about 35%. The Micrometeorological Wind Tunnel at the Colorado State University (Cermak, 1975) has a test section 1.8 m square and 27 m long. It has heating and cooling capabilities for maintaining the floor temperature between 1 and 200°C and the ambient air temperature between 5 and 95°C . Calspan (Ludwig and Skinner, 1976) used liquid nitrogen dripped onto aluminum plates upstream of a model in their open return wind tunnel to produce stable stratification. Dry ice has been used in a similar manner (Cermak et al., 1970). The problem with the liquid nitrogen and dry ice is that a stable boundary layer is created at the point of contact, but a growing mixed-layer (elevated inversion) develops downstream because of the air contact with the uncooled tunnel floor or model surface.

4.4 AIR VERSUS WATER

Thus far in this chapter, we have discussed the comparative advantages of using air or water as the fluid medium for modeling studies. There are no "hard and fast" rules for deciding which type of facility is best for a particular study. Two example problems are given below, one of which appears best suited for study in a wind tunnel and the other of which appears best suited for study in a towing tank. However, in principle and -- depending upon the ingenuity and perseverance of the investigator -- in practice, similar information could be obtained from either study in either facility.

Problem 1: We wish to determine the excess ground level concentrations caused by an insufficiently tall chimney next to a power plant in essentially flat terrain.

Method of Solution: A plume from a power plant is generally highly buoyant, so that building downwash probably occurs only in high wind, hence neutral, conditions. The advantages of a wind tunnel over a water channel here are obvious. Thick, simulated neutral atmospheric boundary layers are easily obtained in wind tunnels, whereas the development and testing of such in a water channel would be a cumbersome task. Measurement of the turbulent flow structure in a water channel would be a very difficult task; accessibility to the model would be limited; instrumentation would be more expensive and less reliable; concentration measurements would be more easily obtained in air using hydrocarbons (probably methane in this case) and a flame ionization detector; etc. A large enough Reynolds number can probably be obtained in a wind tunnel even though it is necessary to simulate the buoyant effluent.

Probably the only advantage to using a water channel in this case would be for the ease of flow visualization, but smoke or helium filled soap bubbles would probably be adequate in a wind tunnel.

Problem 2: We wish to determine the maximum ground level concentration (glc) that may occur (at least once per year) on an isolated three-dimensional hill 200 m high downwind of a 100 m high chimney. Typical nocturnal surface-based inversions develop to 400 m depth with temperature gradients of $1.5^{\circ}\text{C}/100\text{m}$ and wind speeds of 2m/s at the 200 m elevation.

Method of Solution: The maximum glc will probably occur during the nocturnal inversion. The boundary layer will be below the plume and, hence, is probably unimportant. The most important parameter is the Froude number based on the hill height and the density difference between the base and top of the hill:

$$F = U/Nh = U/(\rho g \Delta \theta / \theta)^{1/2} = 2/(9.8 \times 200 \times 4/300)^{1/2} = 0.4$$

(Notice that potential temperature instead of density has been used in calculating the Froude number.) This problem is rather easily studied in a towing tank of 1 m depth where the stratification is obtained using a continuous gradient of salt water (s.g. = 1.0 at the top and 1.2 at the bottom, yielding $N=1.3\text{rad/s}$). The required towing speed for a hill of height 0.2m would be $U=FNh=10\text{cm/s}$, which is a reasonable towing speed for a water channel and yields a Reynolds number $Uh/\nu=20,000$.

This type of flow has not yet (at least, to the author's knowledge) been obtained in a wind tunnel, but rough calculations will easily illustrate the difficulties. The maximum temperature difference that could be generated is on the order of 100°C . Let us suppose that the model hill height is also 20 cm in the wind tunnel and that the 100°C temperature difference is imposed over a

40 cm depth, so that $N=2.9$. The required tunnel speed is thus 23 cm/s, which is exceedingly difficult to maintain, control, and measure in any wind tunnel, especially when the temperature varies so drastically. The Reynolds number would be only 4600 (although it is most likely unimportant in this case, since the flow will definitely not be turbulent).

4.5 SUMMARY

The ease and convenience of operating wind tunnels and associated measuring equipment and the ability to adequately simulate the neutral atmospheric boundary layer make the wind tunnel far superior to the water tunnel for small scale studies where buoyancy is relatively unimportant. However, the inability of the wind tunnel to achieve adequate buoyancy or stratification and adequate Reynolds numbers simultaneously make the towing tank indispensable for the study of elevated plume dispersion in stably-stratified flow in complex terrain. Somewhere in the middle, where the interest is in low-level dispersion in mildly stratified flows, the two types of facilities have essentially equal capabilities.

5. CONCLUDING REMARKS

The problem with simulating the neutral boundary layer is that the atmosphere is very seldom neutral. There is "always" an inversion at some height with surface heating or cooling from below. Perhaps, occasionally, the atmosphere is truly neutral for a few minutes around sunrise or sunset, but such a state cannot be considered stationary because it lasts only a few tens of minutes (Kaimal, et al., 1976) and, because the surface heat flux is changing so rapidly, the turbulence cannot track it (Wyngaard, 1973). Perhaps our only hope is cloudy, high wind, conditions, but "cloudy" implies a temperature inversion (at the base of the clouds), so this cannot be truly neutral either.

One might rightly ask at this point: "Why bother with wind tunnel modeling? We can't simulate the rotational effects, and even if we restrict ourselves to cases where rotational effects are relatively unimportant, the type of flow that we have some chance of simulating well, the neutral surface layer, hardly ever exists in the atmosphere." Panofsky (1974) rather summarily dismissed wind tunnel modeling because of our inability to simulate the turning of wind with height. The answer is "fluid modeling is heuristic." We have the ability to control the flow and to independently adjust specific parameters. To paraphrase Corrsin (1961a), a wind tunnel is, in effect, an analog computer and, compared with digital computers (numerical models), it has the advantages of "near-infinitesimal" resolution and "near-infinite" memory. The inability to achieve large Reynolds number turbulence limits the size of the dissipative eddies. In many ways, this situation is analogous to numerical fluid-dynamic models wherein

the small-scale turbulence is "parameterized." Whereas we have difficulty in simulating the large scale eddies, we are no worse off than the numerical modelers and we need not make any second-order closure "assumptions." Nor must we deal with an inviscid potential flow that cannot separate from any body, let alone a sharp corner. The point is that we need to understand the characteristics of the flow we generate and to understand how changing those characteristics changes the result. We must also recognize the limitations of our facilities and interpret the results accordingly--with caution.

There are two basic categories of fluid modeling studies: (1) The "generic" study wherein idealized obstacles and terrain are used with idealized flows in an attempt to obtain basic physical understanding of the flow and diffusion mechanisms, and (2) the engineering "case" study wherein the miniature scaled model of a specific building or hill is constructed and a specific decision is to be made based upon the results of the tests, i.e., the necessary stack height or the siting of a plant. Advances in the basic understanding obtained from the generic studies will ultimately reduce the need for case studies, but the present state-of-the-art falls far short of eliminating this need.

There are many "doubting Thomases" concerning the applicability of fluid modeling studies to the real atmosphere; yet those same "doubting Thomases" do not hesitate to apply potential flow models with constant eddy diffusivities in order to predict surface concentrations on hills under all types of stratified flow conditions. Frequently, they appear to be unaware that many of the underlying physical ideas and even many of "constants" used directly in their models were obtained from laboratory experiments. A fluid modeling study, after all, employs a real fluid, and if a mathematical model is to be applied to the atmosphere, it should also be applicable to a fluid model, e.g., by eliminating

or adjusting that portion of the model dealing with rotational effects, by reducing the Reynolds number, etc. If a mathematical model cannot simulate the results of an idealized laboratory experiment, what hopes does it have of being applicable to the atmosphere? The point is that fluid models should be used to bridge-the-gap between the mathematical model and its application to the field.

A well-designed and carefully executed fluid modeling study will yield valid and useful information - information that can be applied to real environmental problems - - with just as much and generally more credibility than any current mathematical models.

Cermak, J.E. and Arya, S.P.S., 1970: Problems of Atmospheric Shear Flows and Their Laboratory Simulation. *Boundary Layer Meteorol.*, v. 1, p. 40-60.

Cermak, J.E., Drigill, M.M. and Grant, L.O., 1970: Laboratory Simulation of Atmospheric Motion and Transport over Complex Topography as Related to Cloud Seeding Operations. Second Nat. Conf. on Wea. Mod., Apr. 6-9, Santa Barbara, CA.

Cermak, J.E. and Feterich, J., 1966: Simulation of Wind Fields over Point Arguello, Calif. by Wind Tunnel Flow over a Topographic Model. Rpt. to Navy under Contract N123-61756-34351A(PMP), Color. State Univ., Ft. Collins, CO. Nov.

Cermak, J.E., Sandborn, V.A., Plate, E.J., Binder, G.H., Chuang, H., Meroney, R.N. and Ito, S., 1966: Simulation of Atmospheric Motion by Wind Tunnel Flow Rpt. to Army under Grant DA-AMD-28-043-629. Fluid Mech. Prog., Colo. State Univ., May, 1966.

Choudhury, P. and Cermak, J.E., 1971: Simulation of Flow and Diffusion over an Urban Canopy. Paper Pres. at Conf. on Air Poll. Meteorol., Raleigh, NC, Apr. 5-9, p. 128-131.

Cioffi, H.J., 1973: On Simulating the Lower Third of the Urban Adiabatic Boundary Layer in a Wind Tunnel. *Atmos. Envir.*, v. 7, no. 7, July, p. 691-706.

Cioffi, H.J., 1978: Wind Tunnel Simulation of the Adiabatic Atmospheric Boundary Layer by Roughness, Barrier and Mixing-Layer Methods. *J. Indus. Aerol.*, v. 3, p. 157-75.

Cornish, G., 1953: Remarks on Turbulent Heat Transfer. *Proc. Iowa Thermodyn. Symp.*, State Univ. of Iowa, April 27-28, p. 5-38.

Cornish, G., 1951a: Turbulent Flow. *Am. Scientist*, v. 49, no. 3, p. 309-325, Sept.

Cornish, G., 1951b: Theories of Turbulent Dispersion, *Mechanique de la Turbulence*, Marseille, France.

Cornish, G., 1963: Turbulence: Experimental Methods. *Handbuch Der Physik. Encyclopedia of Physics*, edited by S. Flugge (Freiburg, v. VIII/2.

Cornish, G., 1964: Further Generalization of Onsager's Cascade Model for Turbulent Spectra. *Phys. of Fluids*, v. 7, no. 9, p. 1156-59.

Counihan, J.. 1966: An Improved Method of Simulating an Atmospheric Boundary Layer in a Wind Tunnel. Atmos. Envir., v. 3, p. 197-214.

Counihan, J.. 1975: Adiabatic Atmospheric Boundary Layers: A Review and Analysis of Data from the Period 1960-1972. Atmos. Envir., v. 9, no. 10, p. 871-885. Oct.

Counihan, J., Hunt, J.C.R. and Jackson, P.S.. 1974: Wakes behind Two-Dimensional Surface Obstacles in Turbulent Boundary Layers. J. Fluid Mech., v. 64, pt. 3, p. 529-53, Sept.

Deardorff, G.W.. 1969: Diffusion in a Ekman Layer. J. Atmos. Sci., v. 26, no. 3, May, p. 414-26.

Deardorff, G.W.. 1963: The Relationship of Wind Structure to Wind Loading. Paper 2, Proc. Conf. on Wind Effects on Blags. and Structures. Nat. Phys. Lab., June. HMSO, London, 1965, p. 54-102.

Deardorff, G.W. and Isyumov, N.. 1968: The Application of the Boundary Layer Wind Tunnel to the Prediction of Wind Loading. Proc. Int. Res. Sem. Wind Effects on Buildings and Structures, Ottawa, Can., v. 1, p. 201-22.

Dean, W.. 1977: Gas Pollution Discharge from Boiler Stacks (A Wind Tunnel Study). Dept. Arch. Sci., Univ. of Sydney, Australia, Oct.

Deardorff, J.W.. 1972: Numerical Investigation of Neutral and Unstable Planetary Boundary Layers. J. Atmos. Sci., v. 29, p. 91-115.

Deardorff, J.W.. 1974: Three-dimensional Numerical Study of the Height and Mean Structure of a Heated Planetary Boundary Layer. Boundary Layer Meteorol., v. 7, p. 81-105.

Deardorff, J.W. and Willis, G.E.. 1974: Computer and Laboratory Modeling of the Vertical Diffusion of Nonbuoyant Particles in the Mixed Layer. Adv. Geophys., v. 18, p. 187-200.

DeLannoy, G.A.. 1959: Wind-Speed Profiles at Brookhaven National Laboratory. J. Meteorol., v. 16, p. 181-190. April.

Drazen, P.G.. 1961: On the Steady Flow of a Fluid of Variable Density Past an Obstacle. Tellus, III, no. 3, p. 239-251.

Ducene-Monville, P.. 1976: Full-Scale Measurements of Atmospheric Turbulence in a Suburban Area. Proc. 4th Int. Conf. on Wind Effects on Bldgs. and Structures. Cambridge Univ. Press., p. 23-31.

Ellison, T.H.. 1957: Turbulent Transport of Heat and Momentum from an Infinite Rough Plane. J. Fluid Mech., v. 3, p. 456-66.

Fackrell, J.E.. 1978: Measuring Turbulent Concentration Fluctuations with the Popper Valve. Cent. Elect. Gen. Bd. Research Memo. R/11/1971. London. Jan., 37s.

Fady, L.. 1971: Dispersion and Diffusion of Effluents Emitted by the Conemaugh and Seward Power Plants in the Vicinity of Johnstown, PA.. Unpublished Rpt., Institute for Meteorol. Research and Dev., Magny-Les-Hameaux, France, Oct.

Franzen, P.. 1963: A Laboratory Investigation of the Lagrangian Autocorrelation Function in a Stratified Fluid. Argonne Nat. Lab. Rpt. ANL-6734. Argonne, IL. Nov., 166p.

Fulady, J.I., Simpson, C.L. and Hinds, W.T.. 1964: Prediction of Environmental Exposures from Sources near the Ground Based on Hanford Experimental Data. J. Appl. Meteorol., v.3, 761-70.

Goodrich, J.M., Ching, J.K.S. and Clark, J.F.. 1979: Dissipation of the Nocturnal Inversion Layer at an Urban and Rural Site in St. Louis, MO., 4th Symp. on Turb., Diff. and Air Poll., Jan. 15-18, Reno, NV. Am. Meteorol. Soc., Boston, MA., p. 418-20.

Golden, J. 1961: Scale Model Techniques, M. S. Thesis, College of Engr., New York Univ., May.

Golden, D.. 1972: Relations among Stability Parameters in the Surface Layer. Boundary Layer Meteorol., v. 3, no. 1, p. 47-58.

Goldstein, S.. 1955: Modern Developments in Fluid Dynamics. Dover, NY. 702p.

Holitsky, J.. 1969: Gas Diffusion Near Buildings. Meteorol. and Atomic Energy, p. 221-55., Sect. 5-5.

Holitsky, J., Golden, J., Holpern, P. and Wu, P.. 1963: Wind Tunnel Tests of Gas Diffusion from a Leak in the Shell of a Nuclear Power Reactor and from a Heating Stack. Geophys. Sci. Lab. Rpt. 63-2. Dept of Meteorol. and Ocean., New York Univ.

Hanna, S.P.. 1969: The Thickness of the Planetary Boundary Layer. Atmos. Environ., v. 3, no. 5, p. 519-36. Sept.

Hansen, A.C., Peterka, J.A. and Cermak, J.E.. 1975: Wind-Tunnel Measurements in the Wake of a Simple Structure in a Simulated Atmospheric Flow. NASA CP-2540. April. 45p.

Harris, P.I.. 1968: Measurement of Wind Structure at Heights up to 598 ft. above Ground Level. Symp. Wind Effects on Buildings and Structures. Loughborough Univ. Tech. (Dept. of Transport Technology).

Haugen, D.A., Ismail, J.C. and Bradley, E.F.. 1971: An Experimental Study of Reynolds Stress and Heat Flux in the Atmospheric Surface Layer. Quart. J. Roy Meteorol. Soc., v. 97, p. 158-80. Jan.

Hidy, G.M.. 1967: Adventures in Atmospheric Simulation. Bull. Am. Meteorol. Soc., v. 48, no. 3, p. 143-61. March.

Hino, M.. 1968: Maximum Ground-Level Concentration and Sampling Time. Atmos. Environ., v. 2, p. 149-65.

Hinze, J.C.. 1975: Turbulence. 2nd ed.. McGraw Hill. NY.

Hogstrom, R.S. and Hogstrom, U.. 1978: A Practical Method for Determining Wind Frequency Distributions for the First 200m from Routine Meteorological Data. J. Appl. Meteorol., v. 17, p. 942-54.

Hogstrom, U.. 1964: An Experimental Study on Atmospheric Diffusion. Tellus., v. 16, p. 325-51.

Homma, M.. 1969: Main Research Activities on Air Pollution. Central Res. Inst. of Elec. Power Industry. (Japan). Sept.. unpublished.

Hoot, T.G., Maroney, R.N. and Peterka, J.A.. 1973: Wind Tunnel Tests of Negatively Buoyant Plumes. Env. Prot. Agcy. Rpt. No. EPA-650/3-74-003. 94p.. Oct.

Hoult, D.P.. 1973: Simulation of Buoyant Pollutants in the Atmospheric Boundary Layer. Flow Studies in Air and Water Pollution. Am. Soc. Mech. Engrg., NY, NY.

Hoult, D.P., O'Fed, S.P., Touchton, G.L. and Ketterer, P.J.. 1977: Turbulent Plume in a Turbulent Cross Flow: Comparison of Wind Tunnel Tests with Field Observations. J. Air Poll. Cont. Assoc., v. 27, no. 1, p. 56-60. Jan.

Holtt, J.P. and Weil, J.C.. 1972: Turbulent Plume in a Laminar Cross Flow. Atmos. Environ., v. 6, no. 8, p. 513-32, Aug.

Huber, A.H., Snyder, W.H., Thompson, P.S., and Lawson, P.E. Jr., 1976: Stack Placement in the Lee of a Mountain Ridge: A Wind Tunnel Study. Envir. Prot. Agcy. Rept. No. EPA-600/4-76-047, Res. Tri. Pk. NC., Sept., 48p.

Huber, A.H., Snyder, W.H., Thompson, P.S., and Lawson, P.E. Jr., 1979: The Effects of a Skat Building on Short Stack Effluents. Envir. Prot. Agcy. Rpt. in preparation. Res. Tri. Pk., NC.

Hunt, J.C.P., 1974: Vortices behind Buildings. Paper pres. to Atmos. Envir. Comm. of Aero. Res. Council, London, Oct. 23, ARC Rept. 35291, Atmos. 229, 23p.

Hunt, J.C.P., 1975: Fundamental Studies of Wind Flow Near Buildings. Models and Systems in Arch. and Bldg., LUBFS Conf. Proc. no. 2, Construction Press, Ltd., Lancaster, England.

Hunt, J.C.P. and Fernholz, H., 1975: Wind-Tunnel Simulation of the Atmospheric Boundary Layer: A Report on Euromech 50. J. Fluid Mech., v. 70, pt. 3, p. 543-56.

Hunt, J.C.P. and Snyder, W.H., 1979: Experiments on Stably and Neutrally Stratified Flows of a Model Three-Dimensional Hill. J. Fluid Mech. (to appear).

Hunt, J.C.P., Snyder, W.H., and Lawson, P.E. Jr., 1978: Flow Structure and Turbulent Diffusion around a Three-Dimensional Hill: Fluid Modeling Study on Effects of Stratification: Part I: Flow Structure. Envir. Prot. Agcy. Rpt. No. EPA 600/4-78-041, Res. Tri. Pk., NC, 84p., July.

Inwin, J.G., 1978: Dispersion Estimate Suggestion No. 6. Unpublished Note. Envir. Appl. Branch, Meteor. and Assess. Div., Envir. Prot. Agcy., Res. Tri. Pk., NC.

Inwin, J.G., 1979: A Theoretical Variation of the Wind Profile Power-Law Exponent as a Function of Surface Roughness and Stability. Atmos. Envir., v. 13, no. 1, p. 191-4.

Izajumov, M., Jendali, T. and Davenport, A.G., 1976: Model Studies and the Prediction of Full Scale Levels of Stack Gas Concentration. J. Air Poll. Control Assoc., v. 26, no. 10, p. 954-64, Oct.

Izumi, Y., 1971: Kansas 1968 Field Program Data Report, AFOSPL-72-0041, Air Force Cambridge Research Lab. (LYB), LG Hanscom Field, Bedford, MA.

Jensen, H., 1958: The Model-Law for Phenomena in a Natural Wind. Ingeniøren. Int. Ed., v. 2, no. 4.

Jensen, H. and Franch, H., 1963: Model-Scale Tests in Turbulent Wind. Pt. I: Phenomena Dependent on the Wind Speed. Danish Technical Press, Copenhagen.

Kaimal, J.C., 1973: Turbulence Spectra, Length Scales and Structure Parameters in the Stable Surface Layer. Boundary Layer Meteorol., v. 4, p. 289-328.

Kaimal, J.C., 1975: Horizontal Velocity Spectra in an Unstable Surface Layer. J. Atmos. Sci., v. 32, p. 18-24, Jan.

Kaimal, J.C., Wyngaard, J.C., Haugen, D.A., Cote, O.R., Izumi, Y., Caughey, S.J. and Reading, C.J., 1976: Turbulence Structure in the Convective Boundary Layer. J. Atmos. Sci., v. 33, no. 11, p. 2152-69, Nov.

Kaimal, J.C., Wyngaard, J.C., Izumi, Y. and Cote, O.R., 1972: Spectral Characteristics of Surface Layer Turbulence. Quart. J. Roy. Meteorol. Soc., v. 98, no. 417, p. 563-89, July.

Klincksie, A.A., Jensen, P.A. and Schadt, C.F., 1945: Wind Tunnel Studies of Gas Diffusion in a Typical Japanese District and Correlation of Wind Tunnel Studies with Field Measurements of Gas Diffusion. OPRD, NDRC, Div. 10 Informal Rpt. No. 10-34-48 and 49a, available from Lib. of Congress.

Lange de Feriet, J., 1939: Les Fonctions Aleatoires Stationnaires et la Theorie Statistique de la Turbulence Homogene. Ann. Soc. Sci. Bru., v. 59, p. 145.

Kistler, A.L. and Vrebalovich, T., 1966: Grid Turbulence at Large Reynolds Numbers. J. Fluid Mech., v. 26, pt. 1, p. 37-47.

Kolmogoroff, A.N., 1941: The Local Structure of Turbulence in Incompressible Viscous Fluid for Very Large Reynolds Number, Compt Rend (Doklady), Acad. Sci. U.P.S.S., v. 30, p. 301-5.

Lin, J.T., Liu, H.T., Pao, J.H., Lilly, D.K., Israeli, H. and Orszag, S.A., 1974: Laboratory and Numerical Simulation of Plume Dispersion in Stably Stratified Flow over Complex Terrain, Envir. Prot. Agency, Rpt. No. EPA-600/4-74-044, 75p., Nov.

Lin, J.T. and Lin, J.T., 1975: Laboratory Simulation of Plume Dispersion from a Lead Smelter in Glover, Missouri, in Neutral and Stable Atmosphere. Envir. Prot. Agcy. Rep. No. EPA-460 3-75-026, 53p., April.

Lin, J.T. and Lin, J.T., 1975: Plume Dispersion in Stably Stratified Flow over Complex Terrain: Phase I. Envir. Prot. Agcy. Rep. No. EPA-600 4-75-022, 53p., May.

Lin, J.T., 1974: Atmospheric Simulation Facility: Technical Supplement. Environ. Monit. Rep. No. 11p.

Lin, J.T. and Skinner, G.T., 1975: Wind Tunnel Modeling Study of the Dispersion of Pollutants in Southern Allegheny County, Pa., Envir. Prot. Agcy. Rep. No. EPA-600 3-75-019, 123p., Feb.

Lin, J.T. and Sreenivasan, T.R., 1969: On the Laboratory Simulation of Flow with Atmospheric Turbulence. Cornell Univ. Lab. Rep. No. C-2747-9-1, 141p., May.

Lin, J.T., Sreenivasan, T.R. and Skinner, G.T., 1971: Laboratory Modeling of the Atmospheric Boundary Layer with Emphasis on Diffusion. Cornell Univ. Lab. Rep. No. C-2747-9-2, July, 89p.

Looney, J.P., 1971: Kinematic Tools in Turbulence. Academic Press.

Looney, J.P. and Portilla, J. A., 1964: The Structure of Atmospheric Turbulence. International No. 236a

Looney, J.P., Looney, J.P. and Sreenivasan, T.R., 1967: On the Feasibility of Modeling Small Scale Atmospheric Motions. Cornell Univ. Lab. Rep. No. C-2747-9-3, 1967, 141p., May.

Martini, R., 1970: Gaseous Plume Diffusion about Isolated Structures of the City of Rome. Rep. No. CERN-70-PM129. Month also AEC Rep. No. CERN-70-PM-129, Rome Univ. of Studies, Rome, Italy.

Martini, R., 1967: Recherches sur la Simulation de la Diffusion des Gases dans l'Atmosphere. In Etudes de la Diffusion des Gases, No. 4, p. 327-47.

Martini, R., Sreenivasan, T.R. and Solari, J., 1974: Comparison of Thermally Neutral and Unstable Shear Flow in the Wind Tunnel and the Atmosphere. Adv. Geophys., 1974, Vol. 17, 1-47.

Miller, R.S., 1967: Engineering Mathematics. Dover, NY, 417p.

Monin, A.S. and Obukhov, A.M., 1954: Basic Laws of Turbulent Mixing in the Ground Layer of the Atmosphere. Geophys. Inst. Acad. Sci., U.S.S.R., 24, p. 163-87.

Motyka, J. and Leutheuser, H.J., 1972: Concentration Meter for Wind Tunnel Studies of Gaseous Dispersion. Atmos. Envir., v. 6, no. 12, Dec., p. 911-16.

Nagib, H.M., Morfordin, M.W., Jung, J.T. and Tan-Aitchat, J., 1974: On Modeling of Atmospheric Surface Layers by the Counter-Jet Technique. AIAA Paper No. 74-533, AIAA 9th Aerodynamic Testing Conf., Bethesda, MD., Jul 8-10, 1974.

Nee, M.W., Szulc, A.P., Jung, K., Cheung, F.B. and Liu, W.H., 1974: The Simulation of the Atmospheric Surface Layer in the Notre Dame Atmospheric Wind Tunnel. Pres. at 67th Ann. Mtg. of ASCE, Denver, Paper 74-213, June 9-13, 1974.

Nemoto, S., 1968: Similarity between Natural Local Wind in the Atmosphere and Model Wind in a Wind Tunnel. Papers in Meteorol. and Geophys., v. 18, no. 2, p. 131-230.

Nicherson, E.C. and Smiley, W.E., 1975: Surface Layer and Energy Budget Parameterizations for Mesoscale Models. J. Appl. Meteorol., v. 14, p. 397-300.

Odell, G.M. and Kozachenko, L.S.G., 1971: A New Type of Water Channel with Density Stratification. J. Fluid Mech., v. 50, pt. 3, p. 535-43, March.

Ogawa, Y., 1976: A New Wind Tunnel for the Simulation of Atmospheric Diffusion. 68th Ann. Mtg. of the ASCE, June 27-July 1, Portland, Oregon, pp. 76-17.07.

Orlandini, T.J. and Smith, D.P., 1971: Precipitation in the Wake of Cooling Towers. Atmos. Envir., v. 5, no. 9, p. 751-66, Sept.

Panofsky, H.A., 1974: The Atmospheric Boundary Layer Below 150 Meters. Annual Review of Fluid Mech., v. 6, p. 147-78.

Panofsky, H.A., Blackadar, A.K. and McVehil, G.E., 1960: The Diabatic Wind Profile. Quart. J. Roy. Meteorol. Soc., v. 86, p. 390-6.

Panofsky, H.A., Tennekes, H., Lenschow, D.H. and Wyngaard, J.C., 1977: The Characteristics of Turbulent Velocity Components in the Surface Layer under Convective Conditions. *Boundary Layer Meteorol.*, v. 11, p. 355-61.

Pao, Y. H., 1965: Structure of Turbulent Velocity and Scalar Fields at Large Wavenumbers. *Physics of Fluids*, v. 8, no. 6, p. 1063-75, June.

Pasquill, F., 1962: Some Observed Properties of Medium-Scale Diffusion in the Atmosphere. *Quart. J. Roy. Meteorol. Soc.*, v. 88, p. 78.

Pasquill, F., 1969: The Influence of the Turning of Wind with Height on Crosswind Diffusion. *Phil. Trans. Roy. Soc. London, Ser. A*, v. 265, p. 173-81.

Pasquill, F., 1971: Wind Structure in the Atmospheric Boundary Layer. *Phil. Trans. Roy. Soc.*, v. 269A, p. 439-66.

Paulson, C.A., 1970: The Mathematical Representation of Wind Speed and Temperature Profiles in the Unstable Surface Layer. *J. Appl. Meteorol.*, v. 9, no. 6, p. 857-61, Dec.

Plate, E.J. and Cermak, J.E., 1963: Micrometeorological Wind Tunnel Facility: Description and Characteristics. *Fluid Dynamics and Diffusion Laboratory Report CER63EUP-JEC9*, Colo. State Univ., Feb., 60p.

Ray, C., 1977: Effets du nombre de Prandtl, de la Gravité et de la Fluideité sur les Spectres de Turbulence Cinématique et Scalaires. Ph.D. Dissertation, Université Claude Bernard, Lyon, France, 327p.

Riordan, L.F., 1933: The Supply of Energy from and to Atmospheric Eddies. *Proc. Roy. Soc. London*, v. 197, p. 354-73.

Rizzo, F.F. and Seidling, D.B., 1961: Measurements of Entrainment of Asymmetrical Turbulent Jets. *J. Fluid Mech.*, v. 11, p. 21-32.

Robins, A.G., 1975: Wind Tunnel Modelling of Plume Dispersion. Central Electricity Generating Board, Research Dept., Manohood Engrg. Labs., Mech. Research Memo. No. 236, Dec.

Robins, A.G., 1978: Plume Dispersion from Ground Level Sources in Simulated Atmospheric Boundary Layers. *Atmos. Environ.*, v. 12, no. 5, p. 1033-44.

Saffman, P.G., 1962: The Effect of Wind Shear on Horizontal Spread from an Instantaneous Ground Source. Quart. J. Roy. Meteorol. Soc., v. 88, no. 378, p. 382-93. Oct.

Sandborn, V.A. and Marshall, R.D., 1965: Local Isotropy in Wind Tunnel Turbulence. U.S. Army Research Grant DA-ARO-28-043-64-G-9, Colo. State Univ. Rpt. No. CER-65WAS-RPT 71. 25p., Oct.

Sato, H., Onda, Y. and Saito, T., 1974: Laboratory Simulation of Atmospheric Turbulence: Generation of Arbitrary Velocity Distributions and Model Experiment on Flow around Mt. Fuji. Adv. Geophys., v. 18B, p. 341-51.

Schlichting, H., 1968: Boundary-Layer Theory. McGraw-Hill, NY., 744p.

Schon, J.P. and Mery, P., 1971: A Preliminary Study of the Simulation of Neutral Atmospheric Boundary Layer Using Air Injection in a Wind Tunnel. Atmos. Environ., v. 5, no. 5, p. 299-312. May.

Schon, J.P. and Mery, P., 1978: Physical Simulation of Atmospheric Phenomena in the Planetary Boundary Layer - Wind Tunnel Experiments. Pres. @ Enice, Italy.

Schon, J.P., Rey, C., Mathieu, J. and Mery, P., 1974: Experimental Study of Unstable Stratified Boundary Layers: Comparison with the Structure of the Atmospheric Surface Layer. Proc. 67th Annual Meeting of the APCA, Denver, CO., Paper 74-212, June 9-13. 23p.

Scorer, R.S., 1968: Air Pollution. Pergamon Press., NY., 151p.

Sterlock, P.H. and Stalker, E.A., 1940: The Control of Gases in the Wake of Smoke Stacks. Mech. Engrg., v. 62, p. 455-8.

Simiu, E. and Scanlan, R.H., 1978: Wind Effects on Structures. John Wiley and Sons, NY. 459p.

Skinner, G.T. and Ludwig, G.P., 1978: Physical Modeling of Dispersion in the Atmospheric Boundary Layer. Colspan Rpt. No. 201, Colspan Corp., Buffalo, NY. 31p.

Smith, E.G., 1951: The Feasibility of Using Models for Predetermining Natural Ventilation. Res. Rep. Tex. Engrg. Exp. Stn. 26.

Smith, F.E., 1955: The Role of Wind Shear in Horizontal Diffusion of Ambient Particles. Quart. J. Roy. Meteorol. Soc., v. 81, no. 389, p. 318-29, July.

Smith, M.E. and Singer, I.A., 1955: Sampling Periods in Air Pollution Measurements. Proc. 3rd Nat. Air Pollut. Symp., April 18-20, Pasadena, CA, p. 82-5.

Styder, W.H., Britter, R.E. and Hunt, J.C.P., 1978: A Fluid Modeling Study of the Flow Structure and Plume Impingement on a Three-Dimensional Hill in Stable Stratified Flow. Fifth Int. Conf. on Wind Engr., July 8-14, Paper No. 132, Colo. State Univ., Fort Collins, CO.

Styder, W.H. and Lawson, R.E. Jr., 1978: Determination of a Necessary Height for a Stack Close to a Building - A Wind Tunnel Study. Atmos. Envir., v. 12, no. 9, p. 887-91.

Styder, W.H. and Lumley, J.L., 1971: Some Measurements of Particle Velocity Autocorrelation Functions in a Turbulent Flow. J. Fluid Mech., v. 48, p. 41-71.

Stewart, P.W., 1972: Turbulence. Illustrated Experiments in Fluid Mechanics. Part I. Comm. for Fluid Mech. Films, MIT Press, Cambridge, MA, p. 92-8.

Ström, G.H., Hackman, M. and Haslin, E.J., 1957: Atmospheric Dispersion of Industrial Stack Gases Determined by Concentration Measurements in Scale Model Wind Tunnel Experiments. J. Air Poll. Cont. Assoc., v. 7, no. 3, p. 198-204, Nov.

Ström, G.H. and Halitsky, J., 1953: Topographical Influences on Dispersion of Stack Gases. Combustion, v. 24, no. 12, p. 40-43, June.

Ellen, O.G., 1949: Atmospheric Turbulence. Methuen, London, 111p.

Tannatichat, J. and Nagib, H.N., 1974: Wind Tunnel Simulation of Neutral Atmospheric Surface Layers by the Counter-Jet Technique. Pres. at 67th Annual Mtg. Air Poll. Cont. Assoc., Denver, CO., Paper 74-214, June 9-13, 21p.

Taylor, G.I., 1921: Diffusion by Continuous Movements. Proc. London Math. Soc., v. 20, p. 196-212.

Templin, R.J., 1969: Interim Progress Note on Simulation of Earth's Surface Winds by Artificially Thickened Wind Tunnel Boundary Layers. Lab. Tech. Rpt. LA-22, Nat. Res. Coun. of Canada, Ottawa.

Tanner, H., 1973: Similarity Laws and Scale Relations in Planetary Boundary Layers. Workshop in Micrometeorology, Am. Meteorol. Soc., Boston, MA., p. 177-212.

Tennekes, H. and Lumley, J.L., 1972: A First Course in Turbulence. MIT Press, Cambridge, MA., 300p.

Tennessen, H., 1975: Simulation of the Planetary Boundary Layer in a Multistage Jet Wind Tunnel. Atmos. Envir., v. 9, no. 2, p. 145-75, Feb.

Thompson, R.S., 1978: Note on the Aerodynamic Roughness Length for Complex Terrain. J. Appl. Meteorol., v. 17, no. 9, p. 1402-3, Sept.

Tinno, J.B., 1977: Dependence of the Wind Profile Power Law on Stability for Various Locations. J. Air Poll. Cont. Assoc., v. 27, no. 9, p. 863-6, Sept.

Tiroland, A.F., 1956: The Structure of Turbulent Shear Flow. Cambridge Univ. Press, 315p.

Turner, D.B., 1964: A Diffusion Model for an Urban Area. J. Appl. Meteorol., Feb.

Toldesale, J.B. and Wallington, C.E., 1963: The Effect of Wind Shear and Vertical Diffusion on Horizontal Dispersion. Quart. J. Roy. Meteorol. Soc., v. 89, p. 152-74.

Udagawa, H., Sakata, H., Okamoto, H. and Ide, Y., 1967: Study on Stack Gas Diffusion. Mitsubishi Tech. Bul., no. 52, p. 1-13, Aug.

Van der Hoven, I., 1957: Power Spectrum of Horizontal Wind Speed in the Frequency Range from 0.0007 to 900 Cycles Per Hour, v. 14, J. Meteorol., p. 160-4, April.

Wierse, G. and Muller, H., 1977: On the Spectral Scale of Wind Fluctuations Within and Above the Surface Layer. Quart. J. Roy. Meteorol. Soc., v. 103, p. 721-33.

Wynne, J.C., 1967: An Experimental Investigation of the Small-Scale Structure of Turbulence in a Curved Mixing Layer. Ph.D. Dissertation, Dept. Mech. Engrg., Penn. State Univ., Univ. Park, PA, 105p.

Wanggaard, J.C., 1973: On Surface-Layer Turbulence. Workshop on Micrometeorology. Am. Meteorol. Soc., Boston, MA, p. 101-49.

Wanggaard, J.C., 1975: Modeling the Planetary Boundary Layer - Extension to the Stable Case. Boundary-Layer Meteorol., v. 9, p. 441-60.

Wanggaard, J.C., Arya, S.P.S., and Cote, O.R., 1974: Some Aspects of the Structure of Convective Planetary Boundary Layers. J. Atmos. Sci., v. 31, p. 747-54, April.

Wanggaard, J.C. and Cote, O.R., 1972: Cospectral Similarity in the Atmospheric Surface Layer. Quart. J. Roy. Meteorol. Soc., v. 98, no. 417, p. 530-537, July.

Wanggaard, J.C., Cote, O.R. and Izumi, Y., 1971: Local Free Convection, Similarity, and the Budgets of Shear Stress and Heat Flux. J. Atmos. Sci., v. 28, no. 7, p. 1171-82.

Janis, J. L. and Sandborn, W.A., 1972: Similarity of Large Reynolds Number Boundary Layers. Boundary-Layer Meteorol., v. 2, p. 326-33.

Janis, J.L., 1968: Approach of Turbulent Boundary Layer to Similarity. Ph.D. Dissertation, Colo. State Univ., Ft. Collins, CO., 1968.